APPLICATION OF MACHINE LEARNING ALGORITHMS FOR DETECTION AND TRACKING OF MULTIPLE TARGETS BASED ON EXPERIMENTAL DATA ACQUIRED USING RADAR SENSOR OPERATING IN THE 77 GHz BAND

Thesis

Submitted in partial fulfillment of the requirements for the degree of

DOCTOR OF PHILOSOPHY

by

KUMUDA D K

DEPARTMENT OF ELECTRONICS AND COMMUNICATION ENGINEERING

NATIONAL INSTITUTE OF TECHNOLOGY KARNATAKA,

SURATHKAL, MANGALORE - 575025

JUNE 2024

DECLARATION

by the Ph.D. Research Scholar

I hereby declare that the Research Thesis entitled **APPLICATION OF MACHINE LEARNING ALGORITHMS FOR DETECTION AND TRACKING OF MULTIPLE TARGETS BASED ON EXPERIMENTAL DATA ACQUIRED USING RADAR SENSOR OPERATING IN THE 77 GHz BAND** which is being submitted to the **National Institute of Technology Karnataka, Surathkal** in partial fulfillment of the requirements for the award of the Degree of **Doctor of Philosophy** in **Electronics and Communication Engineering** is a *bonafide report of the research work carried out by me.* The material contained in this Research Thesis has not been submitted to any University or Institution for the award of any degree.

Kumuda

(197EC001, Kumuda D K)

Dept of Electronics and Communication Engg

Place: NITK, Surathkal.

Date: 11/06/2024

CERTIFICATE

This is to *certify* that the Research Thesis entitled **APPLICATION OF MACHINE LEARNING ALGORITHMS FOR DETECTION AND TRACKING OF MULTIPLE TARGETS BASED ON EXPERIMENTAL DATA ACQUIRED USING RADAR SENSOR OPERATING IN THE 77 GHz BAND** submitted by **KUMUDA D K**, (Roll Number: 197EC001) as the record of the research work carried out by her is *accepted as the Research Thesis submission* in partial fulfillment of the requirements for the award of the degree of **Doctor of Philosophy**.

Dr. Pathipati Srihari
Research Guide

Prof. Neelawar Shekar Vittal Shet
Chairman - DRPC

Acknowledgment

First and foremost, I take this opportunity to thank the Lord Almighty for enabling me to work persistently in pursuit of this research work, and for empowering me with the strength and perseverance towards the fruitful accomplishment of the task.

I offer my deepest gratitude to my research supervisor, **Dr. Pathipati Srihari** who has been a constant source of support and encouragement to me. His timely counselling has always guided me technically and morally. His profound knowledge and thorough patience have always been a beacon of light for me throughout my journey. He has been a hands-on advisor who was always ready to help and I have learned a great deal from him.

I would also like to acknowledge the encouragement, guidance and assessments provided by my RPAC members, **Dr. Narendranath S** and **Dr. Krishnamoorthy K**. I would like to take this opportunity to thank my committee members for taking time to provide useful and insightful feedback to improve my thesis. My hearful thanks to **Prof. Linga Reddy Cenkeramaddi**, Department of Information and Communication Technology, University of Agder, Norway, for his valuable advice. My appreciation goes to all my current and former research group members. A special thanks to **Dr. Bethi Pardhasaradhi** for his stimulated discussion throughout my stay at NITK. I convey special thanks to **Mrs. Vandana** and her team, Sri Shashaprayathi Technologies Pvt. Ltd. for their support in conducting experiments. I take this opportunity to thank all the teaching and non-teaching staff and the lab technicians for offering their valuable expertise at all times which has helped me realize the goals of my work at a faster pace. I express my sincere thanks to the evaluators **Prof P H Rao**, IIT Bombay, and **Dr. Pyari Mohan Pradhan**, IIT Roorkee for their valuable comments during the review of my thesis. I convey my special thanks to Doctoral Thesis Assessment Committee (DTAC) Members **Dr. Prabu K**, ECE

Dept, and **Prof. Srinivasa Rao Kola**, MACS Dept, NITK.

I would like to thank the Principal, Director and management of Sree Siddaganga Education Trust, Tumakuru for deputing me to Ph.D at NITK, Surathkal. I particularly thank my fellow scholars who have been a part of my journey and helped me technically and motivated me. Surviving Ph.D. would have been impossible without all my awesome friends. I take this opportunity to genuinely thank all my friends from far and near who have always been with me, never failing to support me and lift me at times of need. I will forever be indebted to them for their invaluable friendship, care, concern and timely interventions.

Throughout the different phases of my Ph.D., the love and support provided by my family know no bounds, I thank them for always having worked behind the scenes for me. Their silent prayers and gentle chiding have moulded me into the person I am today. A special word of thanks to my mother-in-law Daya Thippeswamy, husband Dr. Dhruvakumar T, daughter Dwani and parents for the sacrifices they have made and for always believing in me. I deeply feel that without family members, surely, this research work would not have been possible. I also thank my well wishers, who directly or indirectly supported me.

Place: Surathkal Kumuda D K

Date:

Abstract

Small form factor radar sensors at millimeter wavelengths find numerous applications in the industrial and automotive sectors. These radar sensors provide improved range resolution, good angular resolution, and enhanced Doppler resolution for short-range and ultra short-ranges.

The primary objective of this thesis is to detect and track the targets accurately, when a radar is interfered by another. This research proposes an experimental evaluation of a 77 GHz IWR1642 radar sensor in the presence of a second 77 GHz AWR1642 radar sensor acting as a spot jammer. A real-time experiment is carried out by taking into account five different targets of various radar cross sections, such as a car, a larger size motorcycle, a smaller size motorcycle, a cyclist, and a pedestrian. The collected real-time data is processed using four different constant false alarm rate (CFAR) detectors, CA-CFAR (cell averaging-CFAR), OS-CFAR (order statistics-CFAR), GOCA-CFAR (greatest of cell averaging-CFAR), and SOCA-CFAR (smallest of cell averaging-CFAR).

Furthermore, the data from the above detectors is fed into two different clustering algorithms (DBSCAN (density based spatial clustering of applications with noise) and K-means), followed by the extended Kalman filter (EKF) based tracker with global nearest neighbor data (GNN) association, which provide tracks of various targets with and without the presence of a jammer. Furthermore, four different metrics (1.Tracks reported (TR), 2.Track segments (TS), 3.False tracks (FT), and 4.Track loss (TL)) are used to evaluate the performance of various tracks generated for two clustering algorithms with four detection schemes. The experimental results show that the DBSCAN clustering algorithm outperforms the K-means clustering algorithm for many cases.

In addition, deep learning (DL) based technique is applied for the range Doppler (RD) maps obtained from 77 GHz mmWave sensor. CA-CFAR and OS-CFAR detections are labeled by LABELIMG software, and then these images are processed by you only look once (YOLO) V5 method. The results obtained have been compared with ground truth information for various cases. The results obtained reveals that,

the DL based approach provides good performance in terms of mean absolute average error.

Due to the increased on-road density of mmWave radars, the primary radar mounted on the ego vehicle faces mutual interference. As a result of this, another contribution is made in the thesis to mitigate the mutual interference. To address this interference problem, two novel algorithms are proposed. One of the method is weighted beat signal normalization and the other is clipping followed by a hampel filtering algorithm. Both these approaches are applied on IF (intermediate frequency) signal followed by a traditional detection scheme as a mutual interference mitigation mechanism. Finally, simulated clutter is generated to see the target detection using a novel sigma delta space time adaptive processing ($\Sigma\Delta$ STAP) technique to detect multiple targets in the presence of clutter.

Contents

List of Figures

List of Tables

Abbreviations and Nomenclature

Abbreviations

2-D	Two-Dimensional
3-D	Three-Dimensional
S-D	S-Dimensional
ACC	adaptive cruise control
ADAS	advanced driver assistance system
ADC	analog to digital converter
AJ	absence of jammer
CA-CFAR	cell averaging CFAR
CFAR	constant false alarm rate
CPI	coherent processing interval
CUT	cell under test
CV	Constant Velocity
DBSCAN	density based spatial clustering of applications with noise
DL	deep learning
ED	Euclidean Distance
EKF	Extended Kalman Filter
FFT	fast fourier transform

FMCW	frequency modulated continuous wave
FoV	field of view
FT	false track
GNN	Global Nearest Neighbor
GOCA-CFAR	greatest of cell averaging CFAR
IF	intermediate frequency
KF	Kalman Filter
LNA	low noise amplifier
LO	local oscillator
LOS	line of sight
LPF	low pass filter
MATLAB	MATrix LABoratory
MIMO	multiple input multiple output
ML	machine learning
mmWave	millimeter wave
OS-CFAR	order statistics CFAR
PA	power amplifier
PJ	presence of jammer
SIMO	single input multiple output
SOCA-CFAR	smallest of cell averaging CFAR
SRR	short range radar
STFT	short time fourier transform

TI	Texas Instruments
TL	track loss
TR	tracks reported
TS	track segment
UAV	unmanned air vehicle
USRR	ultra short range radar

Nomenclature

ΔD	Doppler resolution
ΔR	Range resolution
λ	Wavelength of a wave
$\Lambda(\cdot)$	Likelihood function
τ	Round trip time
$\mathbf{F}(\cdot)$	State transition matrix
$\mathbf{G}(\cdot)$	Kalman gain
$\mathbf{H}(\cdot)$	Measuremenet transition matrix
$\mathbf{I}$	Identity matrix
$\mathbf{O}$	zero matrix
$\mathbf{Q}(\cdot)$	Process noise covariance matrix
$\mathbf{R}(\cdot)$	Measurement noise covariance matrix
θ_{res}	Angle resolution
B	Bandwidth
c	Speed of light

d	Distance between two antenna elements
f_c	Carrier frequency
f_d	Doppler frequency
i	Target index
j	Interferers index
M	Number of pulses in one CPI
M_{conf}	Number of measurement frames associated for track conformation
M_{init}	Number of measurement frames associated for track initialization
M_{tent}	Number of measurement frames associated for tentative track
MI	Total number of interferers
N_{conf}	Number of measurement frames for track conformation
N_{init}	Number of measurement frames for track initialization
N_{tent}	Number of measurement frames for tentative track
Nt	Total number of targets
S	Frequency slope
T_r	Duration of one sweep

Chapter 1

Introduction

1.1 Background

1.1.1 mmWave Radar Sensors

Millimeter wave (mmWave) sensor is a type of radar that operates in frequency range of 30 to 300 GHz, which is the millimeter wave region in the electromagnetic spectrum. These mmWave sensor have become popular in recent years because of their ability to provide high range resolution, good angular resolution and even Doppler resolution, making it possible to distinguish between closely spaced objects. Thus, they are widely used by automotive and industrial sectors.

mmWave sensors work by emitting short pulse of electromagnetic radiation and then receives the echo signal that is reflected back from objects in its field of view (FoV). The time delay and frequency shift of the reflected signal is used to estimate distance and velocity of the objects. The main advantage of mmWave sensor is that, they operate in any adverse weather conditions, such as fog, snow, rain, and even in complete dark. Thus, mmWave radar sensors offer powerful tool for sensing and imaging applications, and its use is expected to grow in coming years.

1.1.2 Applications

The automotive radars come in short, mid, and long ranges to facilitate various functionalities like emergency braking assistant (EBA), forward collision warning, parking assistance, blindspot detection, and adaptive cruise control (ACC) [Waldschmidt et al., 2021]. These radars are built on only one chip with low input power. These automotive radars are responsible for providing intermediate pieces of information like

environmental perception [Gao et al., 2019], classification of target [Zhao et al., 2020], tracking [Pardhasaradhi and Cenkeramaddi, 2022], scene imaging [TS et al., 2022], in-cabin driver vital signs [Dayananda et al., 2022], detection of micro and nano objects [Kavya et al., 2022]. In addition, the automotive radar gets fusion activity with other sensors like camera, lidar, and ultrasonic to improve the performance [Vandana et al., 2022].

1.1.3 Research Motivation

Some of the metropolitan cities have already adopted autonomous vehicles, that is vehicles mounted with multiple radar sensors. Each vehicle's radar sensor could interfere with the other radar sensor. A frequency-modulated continuous wave (FMCW) radar operated at mmWave frequency is considered as an automotive radar. As the mmWave radars on-road traffic density increases, it creates problems of mutual interferences. As a result of this mutual interference, the true target detection and tracking get affected. Hence, there is a need to focus on target detection and tracking aspect of the mmWave sensors in the presence of mutual interference. To address this important problem an experimental evaluation is to be carried out in the presence of spot-jammer. Besides, there is necessity to understand the radar sensor performance under these conditions. This is the motivation to carryout the proposed research investigation using real measurements extracted from 77 GHz IWR1642 radar sensor in the presence of another 77 GHz AWR1642 radar sensor. Furthermore, various unsupervised machine learning (ML) methods and deep learning (DL) methods are chosen as efficient approach to detect and track the targets in the presence of spot-jamming.

1.2 Target Detection and Tracking Background

Some Terms

- **Target** a moving or stationary object (Eg: car, pedestrian).
- **Target Detection** is the process of recognising and localising target of interest.
- **Target Tracking** is the process of estimating kinematic parameters (position, azimuth angle, and velocity) of a moving target using sensor measurements.

- **State** is a collection of time varying quantities that represent status of an object, such as position, velocity and acceleration.

1.2.1 CFAR Detection Technique

Constant false alarm rate (CFAR) is one of the widely employed detection technique. Here, detection of target is based on the comparison of power of each resolution cell with a threshold (Th). If the power of resolution cell is greater than the Th indicates the presence of target else target is absent [Nitzberg, 1972]. The general likelihood ratio test decision criterion for Th is denoted by [Richards, 2014]

$$\Lambda(\tilde{r(t)}) \underset{H_1}{\overset{H_0}{\lessgtr}} Th \tag{1.1}$$

where, $\Lambda(\cdot)$ is likelihood ratio test, H_0 and H_1 are hypothesis test represented for the echo signal received is [Richards, 2014], [Srinath et al., 2022]

$$\tilde{r(t)} = \begin{cases} s_t(t-\tau) + s_j(t) + n(t), & \text{under } H_1, \\ s_j(t) + n(t), & \text{under } H_0, \end{cases} \quad t \in T_r \tag{1.2}$$

Decision in favour of the presence of target depends on the interference and on the desired probability of false alarm (P_{fa}). Since interference is not known prior, calculating Th is not easier. Hence, Th in CFAR is calculated from the neighbouring K cells (training or secondary cells) of the cell under test (CUT), and thus the Th is adaptive for desired P_{fa} and is given by [Nitzberg, 1972, Lawrence, 1981]

$$Th = \frac{a}{K} \sum_{i=1}^{K} |\tilde{r}_i|^2 \tag{1.3}$$

where, 'a' is a scaling factor and $\tilde{r}_i$ is the amplitude in the i^{th} training cell. For Th and P_{fa}, probability of detection is given by [Gandhi and Kassam, 1988, Lawrence, 1981]

$$P_d = {P_{fa}}^{\frac{1}{1+X}} \tag{1.4}$$

where, X is signal to noise ration (SNR) given by Lawrence [1981]

$$X = \frac{P^2}{2 * NP} \tag{1.5}$$

where, $\frac{P^2}{2}$ is average signal power while NP is average noise power.

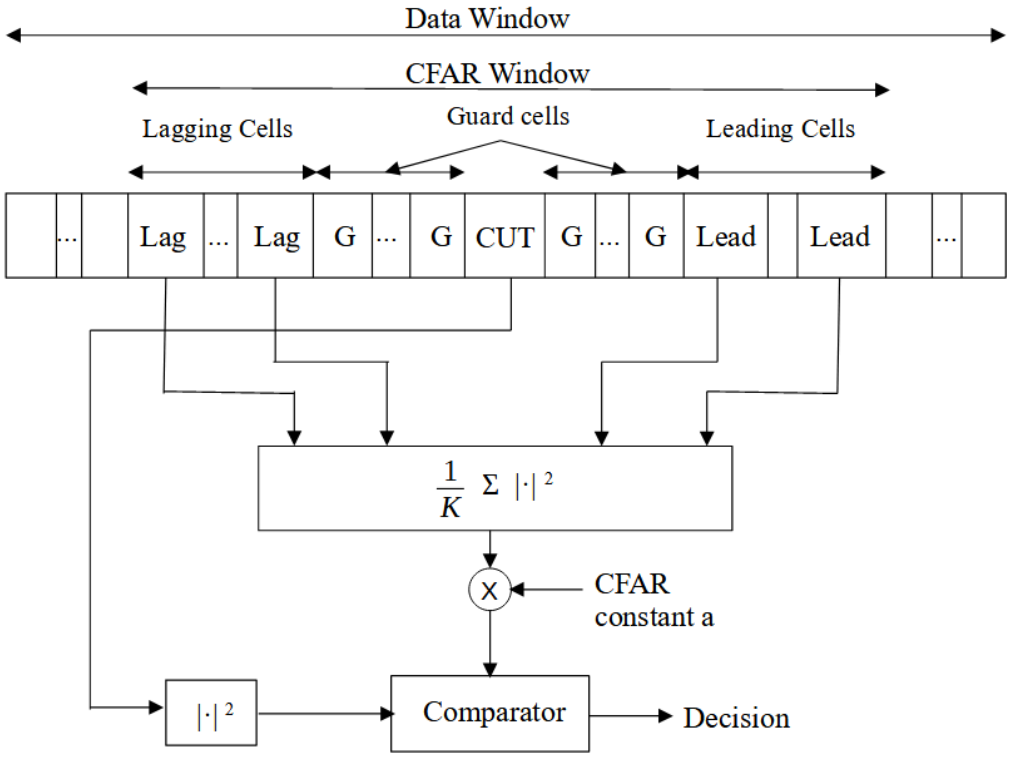

Figure 1.1: Architecture of CA-CFAR

In CA-CFAR (cell averaging-CFAR), NP is average power of the training cells as denoted in Figure 1.1 [Richards, 2014, Weiss, 1982]. Power of the cell under test (CUT) is compared with the average power of the leading and lagging cells as represented in Figure. 1.1 on either side of the CUT. On either side of the desired cell guard cells are left free to avoid target leakage. If, the CUT power is greater than the average power of the neighbouring cells, then their is presence of target in that cell else target is absent. This decision is represented by [Srinath et al., 2022]

$$\text{Decision} = \begin{cases} H_1, & |\tilde{r}_{\text{CUT}}|^2 > a\dfrac{1}{K}\displaystyle\sum_{i=1}^{K}|\tilde{r}_i|^2, \\ H_0, & |\tilde{r}_{\text{CUT}}|^2 \leq a\dfrac{1}{K}\displaystyle\sum_{i=1}^{K}|\tilde{r}_i|^2. \end{cases} \tag{1.6}$$

If there is presence of target, range is estimated from the range bin of the CUT.

In GOCA-CFAR (greatest of cell average-CFAR) and SOCA-CFAR (smallest of cell average-CFAR), the training cells are divided into two subsets namely, leading set and lagging set of size $\frac{K}{2}$. For each of the subset cells, cell averaging method is used to calculate the Th. Upon selecting the greatest value of the subset, Th of GOCA-CFAR is obtained [Lawrence, 1981, Gandhi and Kassam, 1988, Hansen and

Sawyers, 1980, Rohling, 1983]. Power in the lagging subset is given by [Lawrence, 1981]

$$Y_1 = \frac{a}{\frac{K}{2}} \sum_{i=1}^{K/2} |\tilde{r}_i|^2 \tag{1.7}$$

Power in the leading subset is given by

$$Y_2 = \frac{a}{\frac{K}{2}} \sum_{i=(K/2)+1}^{K} |\tilde{r}_i|^2 \tag{1.8}$$

Maximum of Y_1 and Y_2 is the Th for GOCA-CFAR scheme [Lawrence, 1981, Gandhi and Kassam, 1988].

$$Th_{GOCA} = max \begin{bmatrix} Y_1 & Y_2 \end{bmatrix} \tag{1.9}$$

Similarly, minimum of Y_1 and Y_2 is the Th for SOCA-CFAR scheme [Gandhi and Kassam, 1988].

$$Th_{SOCA} = min \begin{bmatrix} Y_1 & Y_2 \end{bmatrix} \tag{1.10}$$

OS-CFAR (order statistics-CFAR) sorts the amplitude values of training cells in ascending order (such arrangement is called order statistics) [Gandhi and Kassam, 1988, Han, 2000]. Out-off K cell values, one of the k^{th} cell value is selected for comparison with the value of CUT. P_{fa} for OS-CFAR is given by

$$P_{fa} = k \begin{pmatrix} K \\ k \end{pmatrix} \frac{(k-1)!\ (a+K-k)!}{(a+K)!} \tag{1.11}$$

1.2.2 Tracking

Tracking is the process of locating and following a moving object over time using sensor measurements. Process of target tracking involves detection and estimation. Detection is identifying the presence of a target in sensor's FoV. Estimation is predicting the future position and trajectory of target based on current and past positions. Finally, target is tracked over time by continuously updating the position and velocity estimates based on sensor's new measurement.

1.3 Interference

1.3.1 Unintentional Interference

Interference due to other mmWave sensors operating in same frequency band or due to other on-road users (automotive vehicles), by which detection process of a receiver is disrupted, is termed as unintentional interference.

1.3.2 Intentional Interference

A jammer is an electronic counter measure (ECM) or intentional interference present in the FoV of the radar, by which the normal operation of the radar is disrupted. Jamming attacks are of various types, namely sweep jamming (in this case, the power output of the jammer (jammer frequency) is swept back and forth over a very wide bandwidth.), barrage jamming (here, all the power output of the jammer is spread over a bandwidth much wider than that of the source radar signal. In other words, it involves the massive and simultaneous jamming of the whole of the frequency band.), and spot jamming. Spot jamming is a type of noise jamming (it is the form of ECM where jammer transmits an interference signal (white noise) in the direction towards source radar so that the target reflection is completely submerged by the interference.), in which, all the power output of the jammer is concentrated in a very narrow bandwidth, ideally identical to that of the source radar[Lv et al., 2019].

1.4 Literature Survey

1.4.1 Multiple target detection and tracking by mmWave sensor

By extracting information about the target from mmWave sensor and further, utilizing ML or DL techniques, detected targets are classified. [Gupta et al., 2021b] presented ML tools for range-angle heatmap to classify various types of targets by using mmWave radar sensor. A challenging problem is addressed using mmWave radar sensor/AWR1843 BOOST, that is capable of detecting objects of low radar cross section (RCS) and successfully detected unmanned aircraft system (UAS) of RCS value of -20dBsm [Morris and Hari, 2021]. In another communication [Rai et al., 2021], using micro-Doppler signatures, aerial objects are detected by obtaining measurements in

real-time using mmWave radar sensor and further classified targets by deploying ML methods. Using RCS signatures of drones and DL techniques, malicious drones are detected by the measurements extracted from mmWave sensors [Fu et al., 2021]. Further, contributions from [Tiwari and Gupta, 2021, Zhang and Cao, 2018, Ninos et al., 2021, Jung et al., 2021] used mmWave radar sensors to detect human gestures for a short distance of about 2 m, and applied ML techniques to classify the movements ([Tiwari and Gupta, 2021] and [Zhang and Cao, 2018] used IWR1642 and AWR1642 respectively, while [Jung et al., 2021] used FMCW sensor at 61 GHz carrier frequency made by Bitsensing Inc.,)

Few of the recent contributions are focused on angle-of-arrival (AoA) algorithms. A novel approach is presented in [Cenkeramaddi et al., 2021b] to estimate AoA and demonstrate that FoV of mmWave sensor can be increased by rotating the sensor module. Besides that, AoA is precisely estimated in [Lin and Lee, 2020], by exploiting subarray techniques to the mmWave sensor's (Texas Instrument's (TI) AWR1642BOOST-ODS) antenna elements. Thus, mmWave radar sensors capable of detecting targets with range and angle information, yields target tracks for the detected objects. Tracking people in the indoor or outdoor environments in real-time is demonstrated in [Ninos et al., 2022] by using the multi-user macro gesture technique. In addition, it is shown in the same contribution that tracking accuracy is increased with increased number of sensor nodes.

Tracking of targets is one of the most important requirements for estimating the target's time-varying movements in the surveillance area. A 24 GHz radar sensor has been applied to detect range, velocity and azimuth angle of multiple targets and tracked them by applying data association followed by the kalman filter in [Macaveiu and Câmpeanu, 2013]. Besides, the work carried out in [Huang et al., 2021] proposed recursive kalman filter tracking along with simplified GNN for multiple people monitoring. Further, track before detect (TBD) method is demonstrated using radar sensor/AC1000 for the real-time autonomous applications in [Chen et al., 2020].

An efficient approach is presented to detect vehicles on-road with the help of field programmable gate array (FPGA) by using a wireless rotatable camera for 360^0 coverage in [Chen et al., 2019]. Moreover, the usage of sensors for an autonomous vehicle in smart cities is applied for collision avoidance in [Chen et al., 2021]. In a recent

contribution [Li et al., 2021a], fused information from multiple sensors are deployed to detect a ground-moving target by using a smart vehicle. Furthermore, range and velocity are estimated for moving targets in real traffic environments by using the single input single output (SISO) configuration of mmWave radar sensor/AWR1642 [Wan et al., 2019]. [Asensio Lopez et al., 2018] demonstrated the use of 24 GHz side-looking mmWave sensor to analyze traffic flow by extracting phase information of the targets. In addition, a novel software-based radar system for single and multiple target tracking by considering radar hardware and algorithms of signal processing is proposed in [Chen et al., 2018]. Further, simulation results of [Chen et al., 2018] are compared with 24 GHz FMCW automotive radar sensor, by employing an OSCA-CFAR detection scheme and polar-based tracking algorithm to estimate the positions and velocities of the targets.

From the above literature review, limited contributions are focused on target tracking aspect of the mmWave sensors. Moreover, earlier contributions have not carried out multiple target tracking in the presence of ECM. Hence, there is a need to understand the radar sensor performance under these conditions. Therefore, motivated to carryout multiple target detection and tracking by extracting real-time data from mmWave sensor.

1.4.2 Multiple target detection by YOLO V5

Identifying and tracking targets is also essential even in military applications. Two different algorithms for airborne or land surveillance using data from radar and electronic support measure (ESM) are presented in [Challa and Pulford, 2001] to track targets, one of the algorithm has feedback from target identity to tracking (joint target tracking classification) while, the other is without any feedback (direct identity fusion). Further, using bayesian approach target state and class are defined to track and classify. Advancements in ML and DL models made target classification much easier (by training process) at the cost of big-data.

In [Chavez-Garcia and Aycard, 2016], multiple sensors (camera, radar and Lidar) data association and fusion was adopted to detect and track multiple moving objects (car, pedestrian, bike, and truck). [Wang, 2021] used multi-sensor data to recognize spatial targets and by extracting target features like motion and perception, low cross

section obstacles like pedestrian and bicycles are classified by applying supervised and unsupervised ML techniques. [Bhatia et al., 2021] classified car, drone and pedestrian by applying 1D-FFT (1 dimension-fast fourier transform) on the raw data collected by mmWave FMCW radar. Classification of objects was based on features of peak obtained by range FFT. The peak width, its height, area under the peak are some of the statistical features fed to light weight ML models like support vector machine (SVM), naive bayes, logistic regression and light gradient boost models to identify targets. Another SVM based multi-target classifier is introduced in [Rizik et al., 2021] to monitor security gate for data taken out by short range 24 GHz FMCW sensor. Here, collected echo signals in the clutter environment by the radar was transferred to computer by Raspberry Pi. Detected targets are clustered and further tracked by α-β filter and by extracting the features of range profile, targets are classified. Another contribution by using 24 GHz for short distance target classification is by [Tavanti et al., 2022], where they used density based clustering and tracked targets by α-β filter. Further, targets were classified by $k - NN$ classifier. [Kosuge et al., 2022] proposed mmWave-YOLO (you only look once) model to detect multiple objects for real data collected by mmWave imaging radar.

By micro-Doppler signatures for the data collected by SIRS 77 GHz radar human motion for short distance was classified in [Bjorklund et al., 2012] by applying SVM software. Target classification and its moving direction is estimated simultaneously in [Kim et al., 2021] for real data collected by a 64 GHz mmWave sensor. The detection results are converted to RGB images by lossy compression technique and further by YOLO algorithm, targets are classified and with the help of detection results direction of motion is estimated. A novel way of estimating angle of a target adopting ML model and by using only one transmitting and one receiving element of an FMCW mmWave sensor placed on a rotor is reported in [Cenkeramaddi et al., 2021a]. [Gupta et al., 2021a], used rotating mmWave sensor to detect range and angle of the targets in sensor's vicinity. Also classified objects using convolutional neural network (CNN) architecture (YOLO V3). Range-angle heatmaps are used to train the ML module. Once again employing YOLO V3 on range-angle heatmaps multiple targets are detected, classified and localized in [Wilson et al., 2023] for real experimental dataset taken out by two different mmWave sensors namely, AWR2243

and AWR1843. With the modifications or improvement in the YOLO algorithm [Jiang et al., 2022], the current version is V5 and here are some literature on classification of objects by YOLO V5. In [Padilla Carrasco et al., 2023], tiny objects are detected by YOLO V5 for PKLot dataset. Large parking area is monitored in a cenital plane by a camera placed at high distance. Using multi scale model, the cars parked appearing as tiny objects by a cenital camera are identified. Similarly, another contribution in the detection of tiny objects is reported in [Luo et al., 2022]. Here, aircrafts are detected in remote sensing images obtained from Google Earth by adopting YOLO V5. [Ting et al., 2021] detects ship by extracting features and using YOLO V5 and GhostbottleNet algorithms. Another ship detection is in [Kim et al., 2022]. Detects objects using YOLO V5 for singapore maritime dataset and also dataset is improved by removing noise.

The contributions of the researchers in target detection by ML module is based on range-angle heatmaps but very limited literature is found on detection of targets for dataset in presence of interference using range-Doppler (RD) maps.

1.4.3 Sensor-to-sensor Interference Mitigation Techniques

As the mmWave radars' on-road traffic density increases, it creates problems of unintentional interferences. The automotive industry is investigating various methodologies to mitigate sensor-to-sensor interference and recover interference-free or uninterrupted signals from corrupted signals [Hakobyan and Yang, 2019].

Signal processing techniques like pulse amplitude control, noise canceller, and staggered pulse repetition frequency (PRF) are used to reduce interference effects [Brooker, 2007, Jin and Cao, 2019]. Traditional methods like pulse compression are also applied to FMCW sensor data to mitigate interference [Rameez et al., 2022]. Moreover, the OFDM-MIMO (orthogonal frequency division multiplexing-multiple input multiple outputs) and cognitive radar techniques are used to perform a tunable Q-factor wavelet transform and suppress the interference [Xu and Yuan, 2021]. A pruned exact linear time known change number (PELT-KCN) algorithm was proposed in [Liu et al., 2020] by exploiting the changes in peaks and weighted envelope normalization (WEN) to suppress FMCW radar interference. In addition, the research community tried the short-time fourier transform (STFT) technique for interference mitigation in combina-

tion with interpolation of beat-frequencies [Neemat et al., 2019] and one-dimensional CFAR zeroing [Wang, 2022]. Meanwhile, the problem was also addressed with the OS-CFAR followed by global nearest neighbor-extended kalman filter (GNN-EKF) based target tracking [Kumuda et al., 2023]. Initially, this interference mitigation problem is limited to signal processing and target tracking and later extends to the emerging field of ML and DL techniques. A fully connected convolutional neural network and quantized convolutional neural network (CNN) are also potential candidates for radar interference mitigation [Ristea et al., 2020, Rock et al., 2019]. Zhang et al. [2020] provided VANET assisted solution to nullify interference in automotive vehicles. A case study was done in a dense traffic environment, in which vehicles coordinated by exploiting multiple access techniques for the usage of spectrum. Uysal and Sanka [2018] gave morphological component analysis to nullify interference without the requirement of any prior information. Interference mitigation in automotive radars is carried out in Wang et al. [2023] by employing TFDMA (time-frequency division multiple access) method, in which performance was analysed in terms of number of interference free radar, density of detection and the probability of interference.

From the literature [Brooker, 2007, Jin and Cao, 2019, Rameez et al., 2022], these traditional techniques are well developed for the pulsed radar, and applicability has been seen for the current mmWave LFM (linear frequency modulation) wave radars. It is to be noted that the staggered PRF and pulse amplitude control techniques require a re-design of the waveform synthesizer. The ML and DL techniques are well-suited for research. Meanwhile, the data collection and size of the data are crucial for developing ML and DL algorithms based on interference mitigation [Ristea et al., 2020, Rock et al., 2019]. The solution should be very light and feasible without changing the existing hardware or data collection. This motivated to propose two algorithms namely, weighted beat signal normalization and clipping followed by hampel filtering algorithms for mitigating mutual interference in the time domain.

1.5 Objectives

Based on the research gaps identified from the literature review, this research investigation focuses on target detection or tracking algorithms in presence of jammer. The

objectives of the research are as follows:

- To present machine learning based multiple target detection and tracking algorithms for mmWave radar sensor experimental data.

- To present deep learning based multiple target detection algorithm for mmWave radar sensor experimental data.

- To develop novel and efficient algorithms to mitigate mutual interference for mmWave radar sensor simulated data.

1.6 Proposed Method for Each Objective

1.6.1 Detection and Tracking

Real-time experiments were conducted using mmWave radars with an objective to know about the relative position and velocity of neighboring vehicles at current time to navigate safely or to avoid collisions with other road users. Literature, reveals that mmWave radar sensors are used only for detection purpose and hardly there are few contributions on tracking multiple targets on-road. To evaluate or analyse the performance of mmWave radar sensors in presence of interference, one more mmWave sensor (AWR1642) was used as an intentional interferer. Contribution of the research, demonstrated that even in presence of interference, raw data extracted by these sensors is processed and tracks are generated for multiple targets.

The extracted raw data is processed offline. Four CFAR techniques namely, CA-CFAR, GOCA-CFAR, SOCA-CFAR, and OS-CFAR are used to detect targets. Furthermore, two different clustering (unsupervised ML) algorithms, such as density-based spatial clustering of applications with noise (DBSCAN) and K-means algorithm are employed for multiple target scenarios. Thereafter, the clustered measurements are fed to extended kalman filter (EKF) with global nearest neighbor (GNN) data association technique. Tracks generated by tracker module are analyzed with four

different tracking metrics (1.Tracks reported (TR), 2.Track segments (TS), 3.False tracks (FT), and 4.Track loss (TL)).

1.6.2 Multiple target detection by YOLO V5

The raw data is acquired by 77 GHz mmWave radar sensor to detect targets in the presence of an attack radar sensor operating at same frequency. The detections (RD-maps) got by CA-CFAR and OS-CFAR detection schemes are labeled by labelImg software. YOLO V5 module was trained by using these RD images. Results drawn by YOLO for both with and without jamming scenarios are used to compare the performance of the module. The average absolute error calculated for clean environment is less compared to jamming case, which is because of less false reflections in the former case.

1.6.3 Mutual Interference Mitigation Schemes

From literature, there is strong requirement to nullify the interference effect among mmWave sensors. Because of mutual interference, the amplitude of IF changes abruptly leading to false or missed detections. Therefore, two different algorithms were developed to identify changes in the IF signal and further to minimize the amplitude fluctuations by comparing the IF signal envelope to a threshold. The two signal processing algorithms, weighted beat signal normalisation and clipping with hampel filtering, uses interfered IF signal and produces interference minimized signal for detection process. These two signal processing blocks are introduced between ADC and FFT blocks without making much changes in the traditional process flow. Thus, it is simple to implement as it does not disturb the present hardware. By tuning the filter window size, both the proposed algorithms detected true targets immersed in interference environment.

1.7 Contribution of the Thesis

In this thesis, frameworks to detect multiple moving target in non-interfering and interfering environment for the experimental work carried by AWR1642 and IWR1642 are addressed. The key contributions of the thesis are as follows:

1. A real-time experiment is carried out using 77 GHz mmWave radar sensors to evaluate the target detection and tracking performance in the presence of an attack radar with the same frequency.

2. Four different CFAR detection schemes are applied to compare the performance of USRR (ultra short-range radar) and SRR (short-range radar) ranges with and without jamming scenarios.

3. Two unsupervised clustering algorithms (DBSCAN and K-means) are deployed to generate tracks by EKF with GNN association and performance of these tracks are evaluated using four different tracking metrics.

4. Suggested detection of multiple moving targets immersed in interference by exploiting DL model on the RD maps obtained by CFAR detection schemes.

5. Proposed two different signal processing algorithms to detect targets immersed in interference by minimizing the effect of mutual interference of mmWave radar sensors.

1.8 Overview

The rest of the thesis is organised as follows. Chapter 2 presents multiple target detection by four different CFAR detection schemes for two different modes of operation of mmWave sensors. In chapter 3, two unsupervised ML techniques employed for multiple targets and tracks generated by GNN-EKF tracker module are described. The generated track plots are compared by four different tracking metrics. The chapter 4 deals with detection of targets by YOLO V5 ML model for the detections obtained by CA-CFAR RD-maps on mmWave sensors. Chapter 5 describes two methods to detect targets immersed in interference environment for the synthetic data by reducing the interference effect and also gives detection of targets immersed in clutter environment. Finally, the conclusion and future work are presented in chapter 6.

Chapter 2

Multi-target Detection in 77 GHz mmWave Radars

This chapter describes about the detection of multiple targets for the real-time data extracted by mmWave radars in presence of a spot-jammer. Here, performance of four detection schemes of CFAR family namely, CA-CFAR, OS-CFAR, GOCA-CFAR, and SOCA-CFAR are analysed.

2.1 Problem Formulation

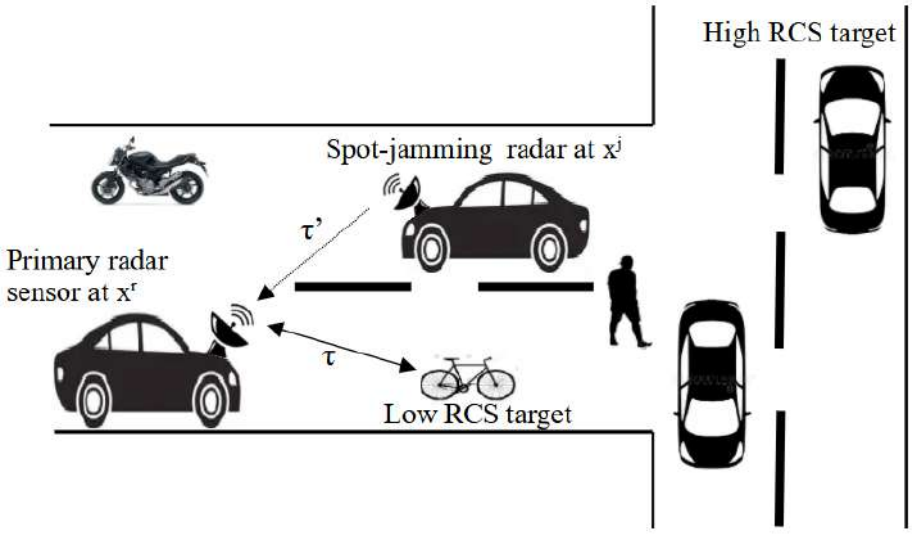

Figure 2.1: Scenario illustrating the geometry of primary radar sensor, jamming radar and targets

This section describes detection of target in clean and spot-jamming environment using traditional CFAR techniques.

2.1.1 Mathematical Model

A Target Detection in Clean environment

In a given surveillance, a FMCW radar sensor is located at $\mathbf{x}^r$ and detecting a target which is being located at $\mathbf{x}^t$ as shown in Figure. 2.1. FMCW radar sensor transmits a chirp signal $s_t(t)$ for duration of T_r (duration of a single sweep) having a positive slope of S and frequency sweeping between f_{min} to f_{max}, given by [Lv et al., 2019], [Alizadeh et al., 2019]

$$s_t(t) = A_t \exp(2\pi j f_{min} t + j\pi S t^2);\ 0 \leq t \leq T_r, \tag{2.1}$$

where, A_t is amplitude of the transmitted signal and slope S is given by

$$S = \frac{f_{max} - f_{min}}{T_r}. \tag{2.2}$$

and the second term of the exponential function in (2.1) consists of the frequency component that is transmitted, denoted by [Lin Jr et al., 2016],

$$f_T(t) = 2\pi \int_0^t S\ t\ dt \tag{2.3}$$

The FMCW radar sensor receives $r(t)$, which is delayed version of the transmitted signal reflected off from the target at $\mathbf{x}^t$ given by

$$r(t) = A_r \exp(2\pi j f_{min}(t-\tau) + j\pi S(t-\tau)^2) + n(t), \tag{2.4}$$

where, A_r is the amplitude of the received signal, delay τ is the round-trip time and $n(t)$ is the noise signal. Therefore, the delay is

$$\tau = \frac{2|\mathbf{x}^t - \mathbf{x}^r|}{c}. \tag{2.5}$$

where, $|\cdot|$ is an euclidean operator and c is speed of light in open-space environment.

The frequency component of received signal is represented by [Lin Jr et al., 2016]

$$f_r(t) = 2\pi \int_0^t (S\ (t-\tau) + f_d)\ dt \tag{2.6}$$

where,

$$\tau = \frac{2(R_0 + vt)}{c}$$
$$and \quad f_d = \frac{2v}{\lambda}$$

is the Doppler shift, R_0 is the initial range of target, v is the velocity of moving target and λ is the wavelength of the wave.

The received signal $r(t)$ is down-converted by mixer and further high frequency components are filtered out by IF filter as shown in Figure. 2.3. The in-phase (I) and quadrature phase (Q) components of IF filter outputs are given by [Zakerhaghighi et al., 2020]

$$\begin{aligned} S_{IFI}(t) &= \frac{1}{2}\, cos(2\pi f_{min}\tau + 2\pi t(S\tau - f_d)) \\ S_{IFQ}(t) &= \frac{1}{2}\, sin(2\pi f_{min}\tau + 2\pi t(S\tau - f_d)) \end{aligned} \tag{2.7}$$

In the IF output (2.7), the second term of I and Q components correspond to beat frequency having information about Doppler shift and range of the target.

The IF response for i^{th} target is given by

$$S_{IF,i}[n] = \exp(j2\pi\tilde{r}(\tau_i, f_{di})\mathbf{n}). \tag{2.8}$$

Assuming targets are moving at constant velocity, the range-Doppler (RD) matrix upon applying 2D-FFT is given by

$$RD = |\sum\, w[\mathbf{n}]x_{IF}[n]\exp(j2\pi\tilde{r}(\tau_i, f_{di})\mathbf{n})|. \tag{2.9}$$

where, w represents 2D window function, $\mathbf{n}$ is a vector obtained by combining slow time and fast time samples, and x_{IF} is IF sampled component. These RD maps are further processed by CFAR algorithm to obtain detections of targets in clean environment.

B Target Detection in Jamming Environment

In addition to the intended target, an ECM is present in the same environment (jamming signal). Consider a spot-jamming ECM, where a jammer located at $\mathbf{x}^j$ transmits signal, $s_j(t)$ at the same frequency as that of the actual radar sensor being located at $\mathbf{x}^r$ as in Figure. 2.1. Then the combined signal received by the radar located at $\mathbf{x}^r$ is given by

$$r(t) = A_r \exp(2\pi j f_{min}(t-\tau) + j\pi S(t-\tau)^2) + s_j(t) + n(t), \tag{2.10}$$

where,

$$s_j(t) = \exp(2\pi j f_{min}\tau' + j\pi S\tau'^2). \tag{2.11}$$

Received frequency components consists of both target and jammer, as given by

$$\begin{aligned} S_{IFIPJ}(t) = \frac{1}{2}\, cos(2\pi f_{min}\tau + 2\pi t(S\tau - f_d)) \\ + \frac{1}{2}\, cos(2\pi f_{min}(t+\tau') + \pi S(t^2 + \tau'^2)) \end{aligned} \tag{2.12}$$

$$\begin{aligned} S_{IFQPJ}(t) = \frac{1}{2}\, sin(2\pi f_{min}\tau + 2\pi t(S\tau - f_d)) \\ + \frac{1}{2}\, sin(2\pi f_{min}(t+\tau') + \pi S(t^2 + \tau'^2)) \end{aligned} \tag{2.13}$$

The IF response for i^{th} target in presence of jammer is given by

$$S_{IFPJ,i}[n] = \exp(j2\pi\tilde{r}(\tau_i, \tau', f_{di})\mathbf{n}). \tag{2.14}$$

The range-Doppler (RD) matrix upon applying 2D-FFT is given by

$$RD = |\sum\, w[\mathbf{n}]x_{IFPJ}[n]\exp(j2\pi\tilde{r}(\tau_i, \tau', f_{di})\mathbf{n})|. \tag{2.15}$$

Therefore, RD maps are distorted by the jamming signal, which are processed by same CFAR algorithm to obtain detections. The obtained detections are fed to tracker module, to generate tracks (described in chapter 3) for the moving targets.

Traditionally, CA-CFAR and OS-CFAR are popular to provide detections pertain to the target. Assume a target is moving in the vicinity of the mmWave sensor. CA-CFAR provides detection at range 8.5 m as shown in Figure. 2.2a in clean-environment. In the case of spot-jamming, detections are reported as shown in Figure. 2.2b and Figure. 2.2c for CA-CFAR and OS-CFAR respectively. In both CA-CFAR and OS-CFAR, jammer was placed at 5 m away from primary radar sensor. Target is detected at 13.6 m and multiple detections are reported at that point, which is because of huge target and low range resolution.

2.1.2 Observations

- CA-CFAR and OS-CFAR provides multiple detections even though a single target is present in the vicinity.

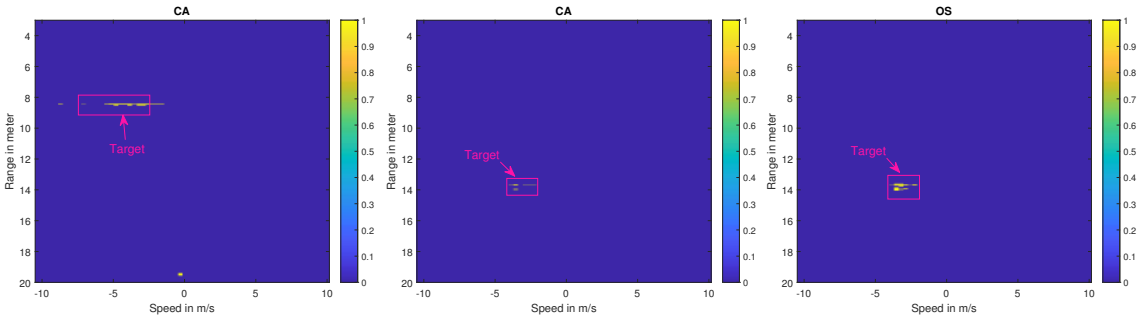

(a) In clean environment by CA-CFAR

(b) Target immersed in Jamming environment by CA-CFAR

(c) Target immersed in Jamming environment by OS-CFAR

Figure 2.2: Range- Doppler of Target using CFAR variants

- The CFAR algorithm may/ may not provide the correct detections in every scan. Hence, a target tracking module should be adopted with both false alarms and target detections to provide target state estimate.

- The tracking algorithm should work for the multiple targets such that, the multiple measurements should be assigned to the established tracks without any ambiguity.

2.1.3 Sensor Description and Design Parameters

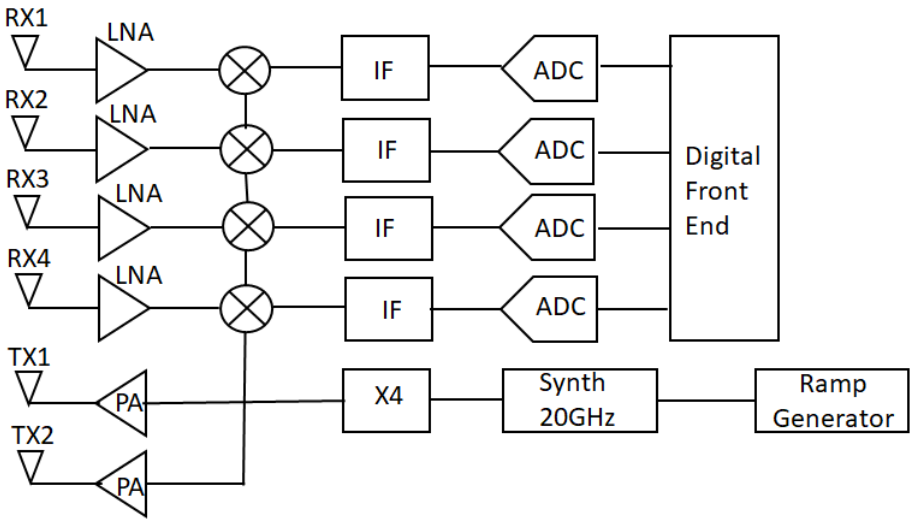

Figure 2.3: Analog Sub-system

Figure 2.3 gives the front end analog sub-system block diagram of AWR1642 and IWR1642 mmWave sensor Instruments [2018b]. TI's IWR1642 and AWR1642

mmWave radar sensors have co-located two transmitting (TX) antennas, separated by 2λ and four receiving (RX) antennas, separated by $\frac{\lambda}{2}$ spacing with in-built phase locked loop (PLL) and analog to digital converters (ADC). A ramp generator and a synthesizer (synth) are used to generate high frequency oscillations. Each receiving element has a low noise amplifier (LNA) followed by a down-converter (mixer and local oscillator (LO)) and ADC. Down-converted digital data from all four receiving elements are fed to the digital front end system, which stores the received in-phase and quadrature data from all four channels are further transmitted to signal processing and data processing modules.

The primary radar sensor IWR1642 transmits chirp signals, swept from frequencies 77 GHz (f_{start}) to 81 GHz. The spot-jammer AWR1642 also works with the same configurations as of primary radar sensor. IWR1642 sensor operated in two different modes, namely SRR and USRR. The parameters set for the real-time experiments conducted for both USRR and SRR modes are listed in Table 2.1, which are calculated by (2.16)-(2.18). Parameters were set referring to [Sakhnini] for the maximum range of 80 m and 20 m for SRR and USRR modes respectively.

The SRR provides 80 m maximum range ($R_{\max}$) with a range resolution (ΔR) of 36.6 cm. Similarly, the USRR mode provides $R_{\max}$ of 20 m and ΔR of 4.3 cm. The USRR is suitable for short-range applications like changing the lane, choosing a parking slot, detect stationary objects like poles, pedestrians walking, patient monitoring etc Alizadeh et al. [2019]. Whereas, the SRR gained its applications in long range applications like moving target detection [Wan et al., 2019]. The range resolution is calculated as Li et al. [2021b]

$$\Delta R = \frac{c * f_s}{2S * N_{adc}} \tag{2.16}$$

where, S is the frequency slope, f_s is ADC sampling frequency, N_{adc} represent the number of ADC samples and c is speed of light in open-space. The bandwidth B of the radar is calculated as

$$B = \frac{c}{2 * \Delta R} \tag{2.17}$$

The Doppler resolution ΔD is obtained by Li et al. [2021b]

$$\Delta D = \frac{c}{2 * f_{min}\ (t_i + t_e) *\ M} \tag{2.18}$$

(a) Radar with jammer (b) One target (c) Two targets

(d) Three targets (e) Four targets (f) Five targets

Figure 2.4: Measurement setup with various scenarios

where, f_{min} is the start frequency (77 GHz), t_i and t_e are idle time and ramp end time respectively and M is the number of pulses or chirps in one coherent processing interval (CPI). Angle resolution θ_{res} is given by [Li et al., 2021b]

$$\theta_{res} = \frac{\lambda}{N_{Rx} * d\ cos\theta} \tag{2.19}$$

where, N_{Rx} is number of receiving antenna elements, d is the separating distance between antenna elements, λ is wavelength of the wave and θ is the AoA.
From (2.19), as the number of receiving antenna elements N_{Rx} increases, angular resolution increases, meaning two targets moving at same velocity separated by this small angle can also be detectable. As the antenna elements in the array increases, directivity of antenna increases and beamwidth reduces, thereby allowing detection of two closely spaced targets in azimuth direction Balanis [2015]. Further, the sum of four receive channel data is utilized for CFAR detection algorithms. This summed data from all four channels provides improved detection performance compared to single receive channel data. The proposed tracking algorithm with two different clustering methods are general techniques and can be applied to any other radar sensor that can provide range and azimuth measurements.

Table 2.1: Parameters set for Experiment

Parameters	**SRR mode**	**USRR mode**	**Explanation**
Idle time (t_i) (μs)	3	7	Period during which the mmWave sensor is not actively transmitting or receiving signals.
Ramp end time (t_e) (μs)	56	87.3	Duration of time it takes for the frequency ramp (chirp) to complete.
Number of ADC samples (N_{adc})	256	512	Number of samples produced by ADC.
Frequency slope (S) (MHz/μs)	8	42	Rate at which the transmitted signal's frequency changes over time during each sweep of the sensor waveform.
Number of chirps (M)	128	64	Number of chirps transmitted in one frame interval.
Chirp duration (T_r) (μs)	59	94.3	Time it takes for the frequency to sweep from the starting frequency to the ending frequency within one chirp.
ADC sampling frequency (f_s) (ksps)	5000	6250	Rate at which the analog signal received is sampled and converted into digital samples.
Range resolution (ΔR) (cm)	36.6	4.3	Ability of the sensor to distinguish between two closely spaced targets.
Maximum range (R_{max}) (m)	80	20	Maximum detectable distance by mmWave radar sensor.
Velocity resolution (m/s)	0.25	0.32	Ability of the sensor to distinguish between two targets moving at different velocities.
Maximum velocity (kph)	90	36	Highest velocity that can be accurately measured by mmWave radar sensor.

2.1.4 Experimental Setup

Experiments were conducted by using FMCW mmWave radar sensors, IWR1642 [Instruments, 2018a], [https://www.ti.com/sensors/mmwave-radar/automotive/technical documents.html] to capture the raw data. This IWR1642 was interfaced to a DCA1000EVM, data capture board, to capture and store data in binary files. Initially, conducted experiments for target only case, to show the working of existing algorithms. Thereafter, experiments were conducted with target and jammer. In a given surveillance of primary radar sensor, another sensor AWR1642 was present which acts as spot-jammer to primary radar sensor. The targets like car (target 1), a motor-cycle (target 2), two motor-bikes of different RCS (targets 3 and 4), and a pedestrian (target 5) are investigated in this experimental study as shown in the Figure 2.4. Figure 2.4a shows primary radar sensor and a spot-jamming radar, placed opposite to it at 5 m. Figure 2.4b-Figure 2.4f shows targets of different cross sections moving in the vicinity of primary sensor.

2.2 Results and Discussion

This section deals with results of detection for four CFAR detection variants, in both clean and jamming environment. Real-time experiments were conducted for one (car), two (car, and a motor-cycle), three (car, cycle, and a motor-bike), four (car, cycle, and two motor-bikes) and five targets (car, cycle, two motor-bikes, and a pedastrian) (refer Figure. 2.4) in the presence and absence of jammer. Here, five target's case detection results are described.

2.2.1 Scenario generation

2.2.2 Detection of Targets in the Absence of Jammer (AJ)

A primary radar sensor was stationary, in its surveillance a spot-jammer was placed at 5 m away from the primary sensor (spot-jammer was present only for the jammer case, refer Figure. 2.4). The primary radar sensor operated in a multiple input multiple output (MIMO) configuration for both USRR and SRR modes in the presence of jamming radar, while in the absence of jammer for SRR mode primary radar sensor was configured to single input multiple output (SIMO) mode (to detect closely moving

targets, all the receiving elements were used). The targets were assumed to be moving at constant velocity in the vicinity of the primary radar sensor, target's starts at 1s and ends at 10 s. The sampling time of the mmWave sensor is 107.3 ms (frame time is 7.3 ms and frame periodicity is 100 ms). Hundred number of frames were collected and all the frames were processed using four CFAR techniques, to get range and azimuth measurements. Obtained measurements are clustered and fed to tracker module.
In-order to analyze the performance of mmWave sensors and the effect of jamming, spot-jamming is placed at three different positions (2 m, 3 m, and 5 m). Raw data was extracted by placing spot-jammer at different azimuth angles (-30^0, 0^0 and 30^0) with respect to primary radar. In addition to this, different number of targets are considered while the radar is operating in SRR mode.

Experimental results of five targets in the clean environment are reported in this section. A car, a motor-cycle, two motor-bikes and a pedestrian were the five targets considered. Figure. 2.5 and Figure. 2.6 show the results of four CFAR schemes for both USRR and SRR modes respectively. The results reported here are for the frame numbers 71 and 70 for USRR and SRR modes respectively. Targets are detected at 5.3 m, 6.9 m, 8.4 m, 10 m and 13.2 m in USRR and 2.9 m, 4.3 m, 8.4 m, 13.9 m and 24.5 m in SRR mode. Spread of the target is observed in USRR because of less range resolution (ΔR).

USRR mode of mmWave radar sensor is capable of detecting targets within 20 m range while SRR detects within a range of 80 m. The range resolution of USRR is less compared to that of SRR. The width of one range bin in USRR is 4.3 cm and 36.6 cm in SRR mode of mmWave radar sensor. Because of this targets fall into neighboring bins in USRR mode. Thus, their is more spread up in the detections of USRR mode as compared to that of SRR mode.

2.2.3 Detection of Targets in the Presence of Jammer (PJ)

Experimental results of five targets in the presence of spot-jammer is reported in this section. The scenario to collect raw data was same as that of previous case, targets moved in the vicinity of the primary radar sensor and a spot-jammer was placed at 5 m away from primary radar sensor (Figure. 2.4a). Once again, the primary radar sensor was operated both in USRR and SRR mode. Same targets were considered in the AJ

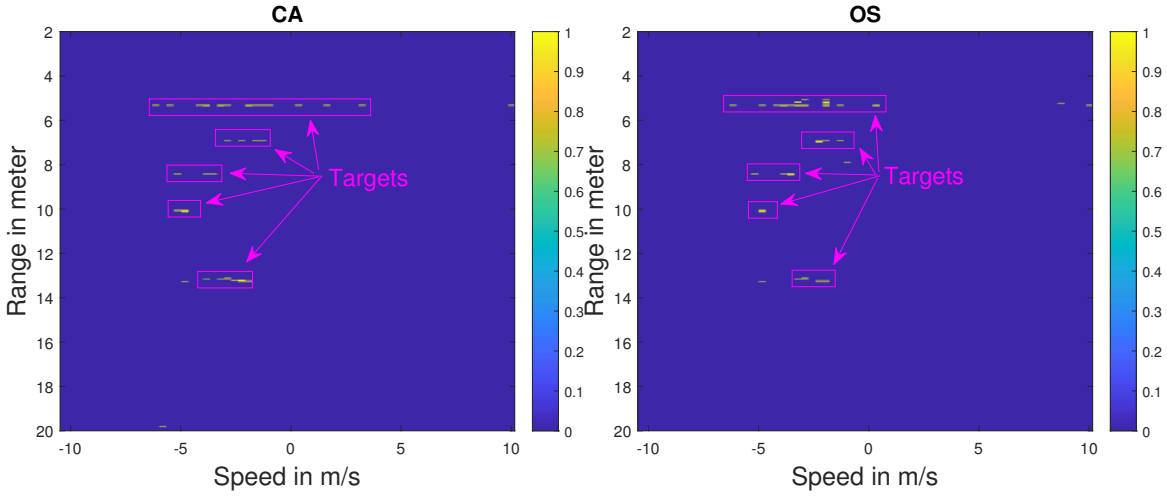

(a) CA-CFAR

(b) OS-CFAR

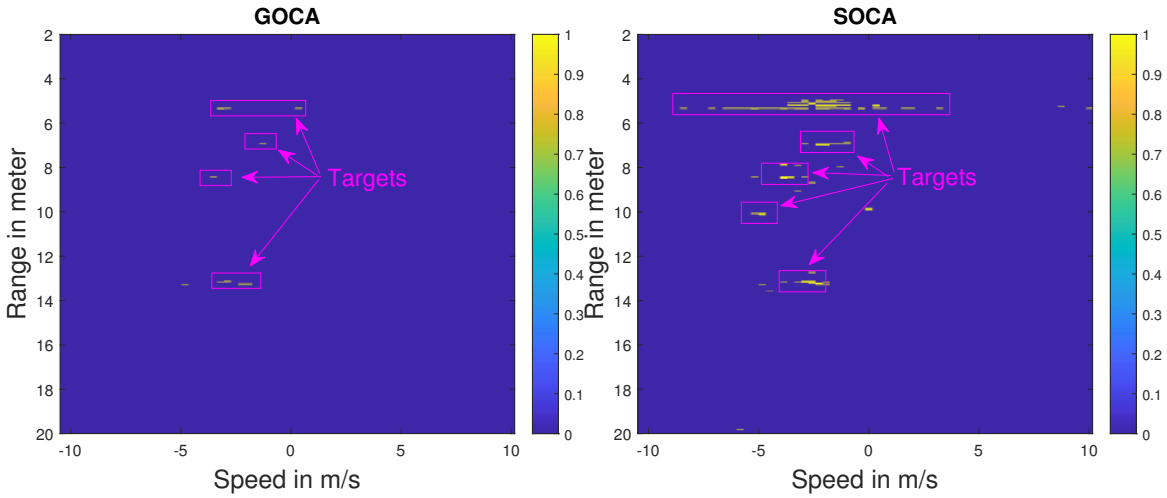

(c) GOCA-CFAR

(d) SOCA-CFAR

Figure 2.5: RD of five targets in USRR mode for frame number 71

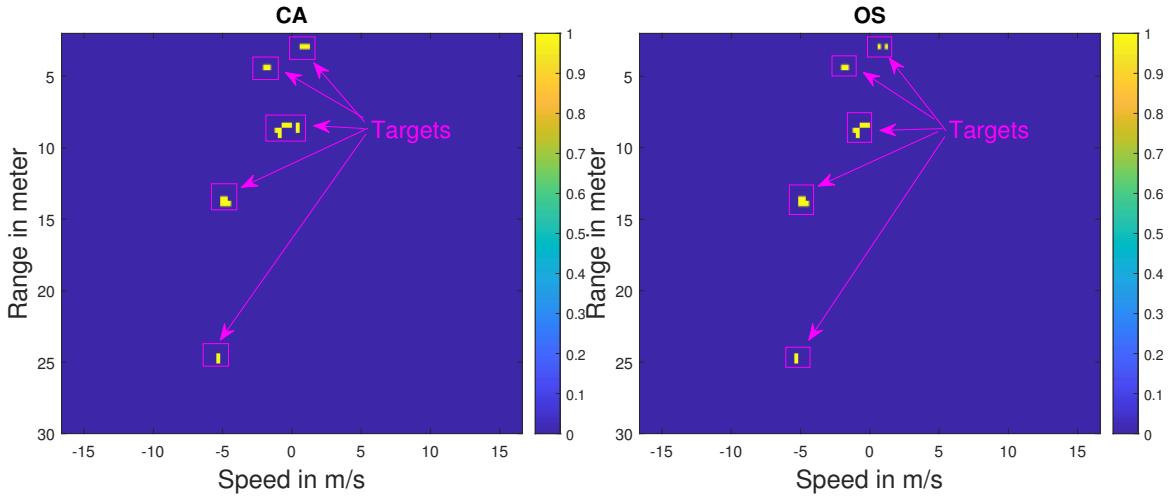

(a) CA-CFAR

(b) OS-CFAR

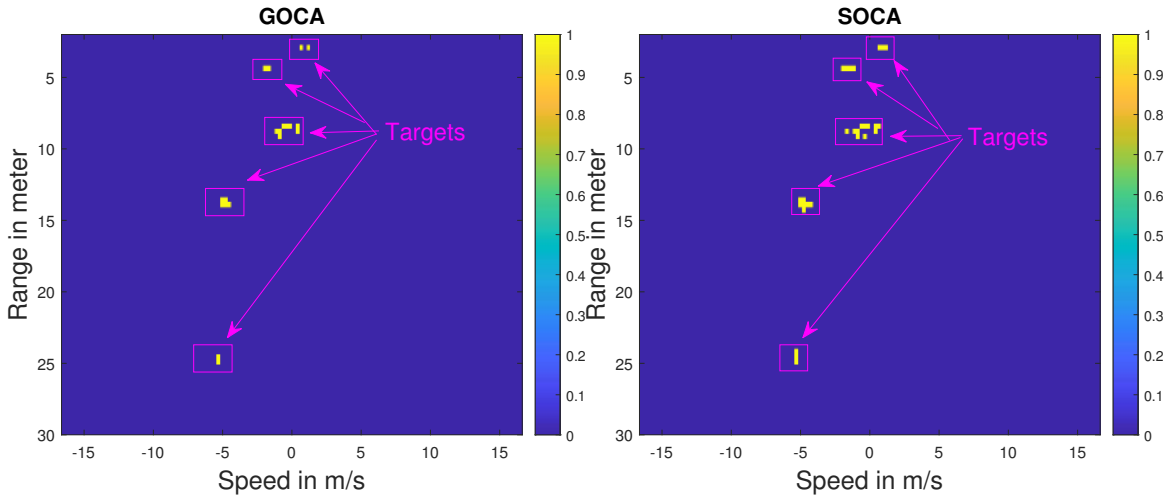

(c) GOCA-CFAR

(d) SOCA-CFAR

Figure 2.6: RD of five targets in SRR mode for frame number 70

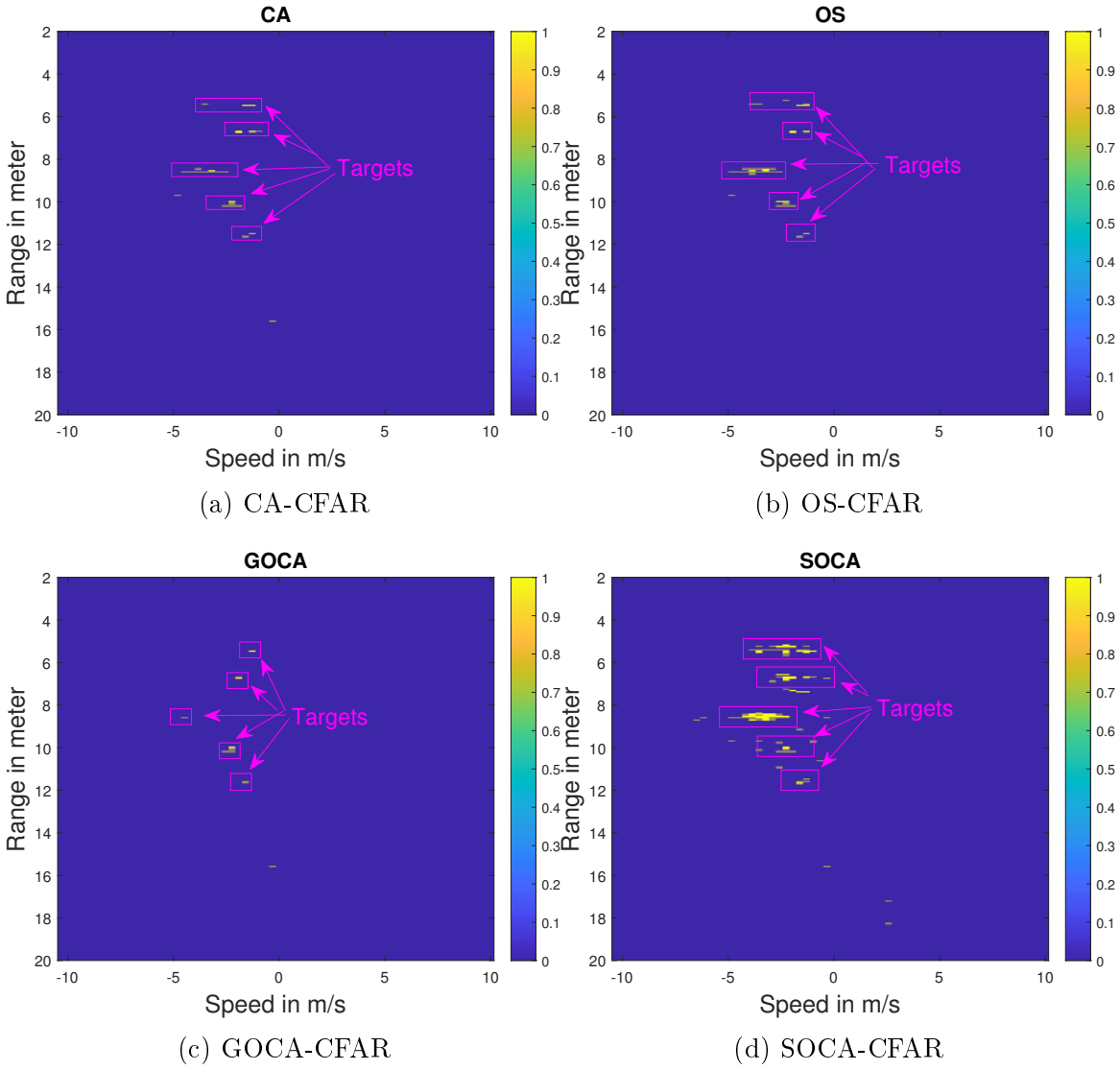

(a) CA-CFAR (b) OS-CFAR

(c) GOCA-CFAR (d) SOCA-CFAR

Figure 2.7: RD of five targets with jammer in USRR mode for 55th frame

case. Figure. 2.7 and Figure. 2.8 reports the detection results of four CFAR schemes for both USRR and SRR modes respectively. The results reported here are for the frame numbers 55 and 18 for USRR and SRR respectively. Targets are detected at 5.4 m, 6.6 m, 8.5 m, 10.1 m and 11.6 m in USRR and four targets are detected in SRR (for this frame number) at 4.39 m, 16.8 m, 31.8 m and 47.5 m in SRR mode.

2.2.4 Detection of Targets with Jammer at Different Angles

Figure. 2.9 reports the detections for SRR mode of mmWave radar sensor for all four CFAR detection schemes for frame number 33 and when the spot-jammer is at distance of 3m, and at angle of 30^0 from the primary radar sensor.

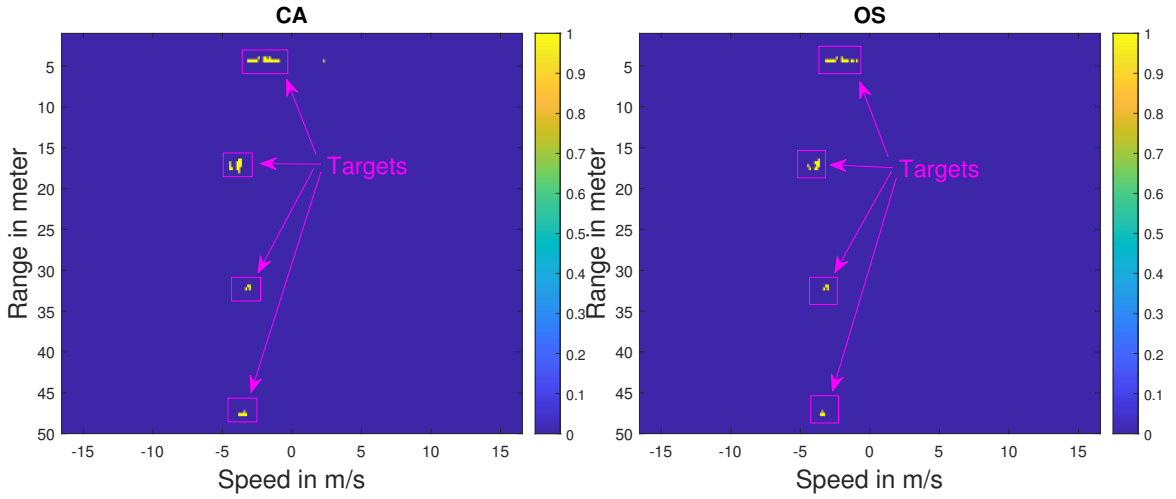

(a) CA-CFAR

(b) OS-CFAR

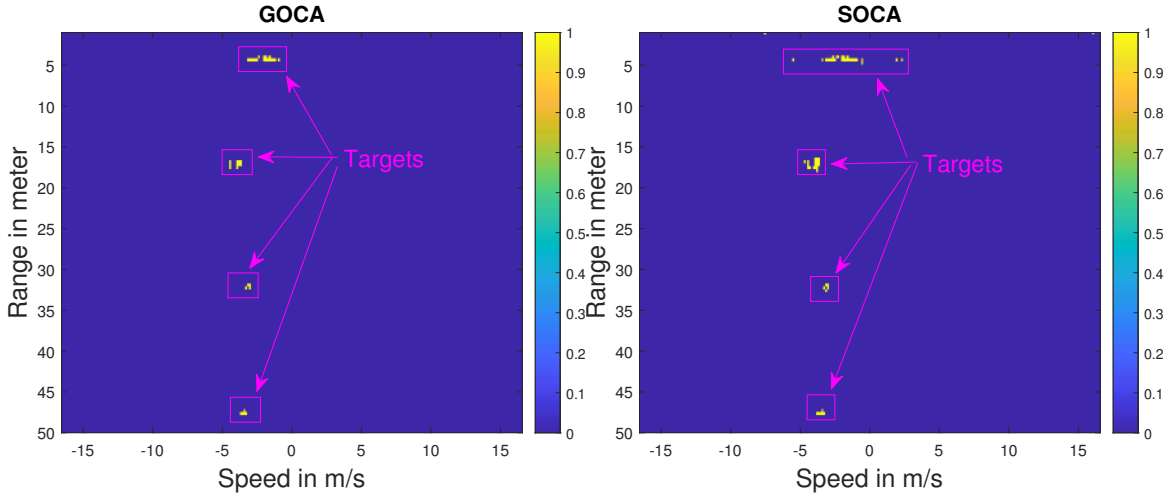

(c) GOCA-CFAR

(d) SOCA-CFAR

Figure 2.8: RD of five targets with jammer in SRR mode for 18th frame

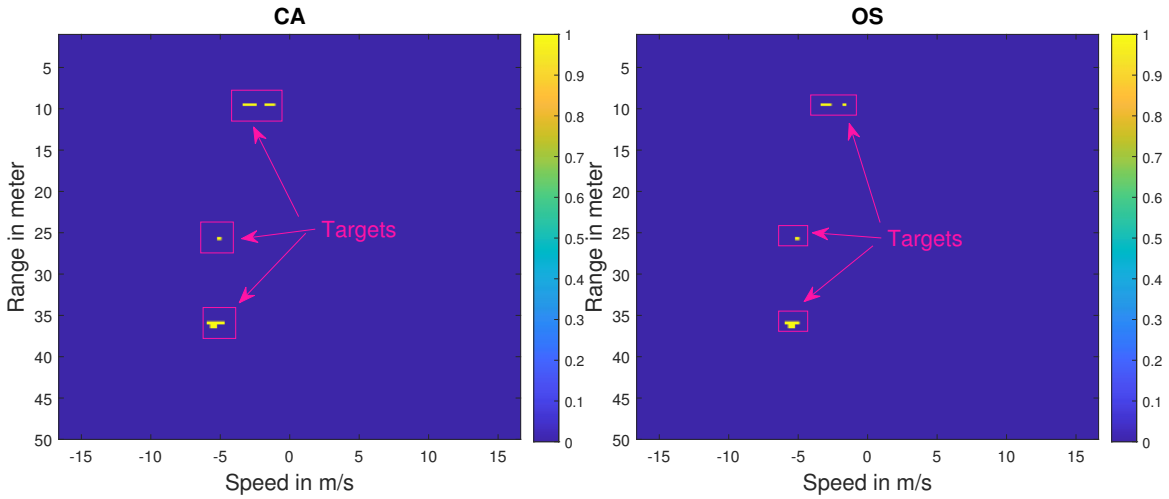

(a) CA-CFAR

(b) OS-CFAR

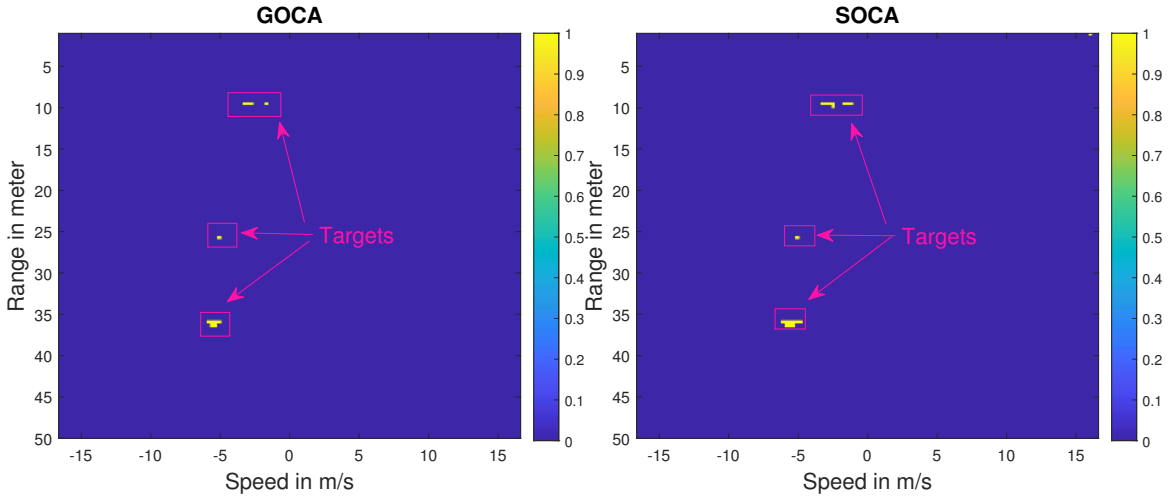

(c) GOCA-CFAR

(d) SOCA-CFAR

Figure 2.9: RD of three targets in SRR mode with jammer at 3m and 30^0 for frame number 33

Comparison of four CFAR schemes is described below:

CA-CFAR : Average power value of the neighboring cells is applied as threshold to detect targets. False detections are less compared to SOCA and even missed detections are less compared to GOCA.

OS-CFAR : Here, in OS-CFAR, the power of cells are arranged in ascending order and random cell value is picked as threshold. OS-CFAR performed similar to that of CA-CFAR in detecting targets.

GOCA-CFAR : In GOCA, greatest power value of the leading or the lagging subset is applied as the threshold for the detection process. Since there is rise in the threshold level compared to other CFAR schemes, true target detections are missed.

SOCA-CFAR : In this scheme, the threshold level is smallest power of the leading or the lagging subset of the CFAR algorithm. More spread in the detections or false detections were noticed.

2.3 Conclusion

Here, in this chapter, multiple targets of various RCS are detected for the real-time data extracted by mmWave radars in presence of a spot-jammer. The, performance of four detection schemes of CFAR family namely, CA-CFAR, OS-CFAR, GOCA-CFAR, and SOCA-CFAR are analysed and compared. Accordingly, CA-CFAR and OS-CFAR detections schemes are better compared to GOCA-CFAR and SOCA-CFAR.

Chapter 3

Multi-target Tracking by Mitigating Spot Jammer Attack in 77 GHz mmWave Radars

As discussed in chapter 2, obtained detections by all four CFAR algorithms are fed to tracker module to generate track plots. Generated track plots are analysed by four different tracking metrics. This chapter deals with tracker, and tracking metrics.

3.1 Tracking

3.1.1 Measurements- Range and Angle Estimation

IWR1642 radar sensor was used for real-time experiments and the collected data is processed in MATLAB for four variants of CFAR detection techniques. The target detected range bin gives the range and the angle is estimated by beam forming technique. Thus, the range and angle estimates are the measurements to tracker module. Here, the acquired measurements be $\mathbf{Z} = z_1(m), z_2(m), z_{n_m}(m)$. Here, z_{n_m} is defined to state scan-to-scan number of measurements are different.

3.1.2 Clustering

Since target falls into multiple bins (Figure. 2.2b), the measurements are clustered by clustering techniques before feeding the measurements to the tracker. Two different clustering algorithms are used, they are: DBSCAN (density based spatial clustering of applications with noise) and K-means. The results obtained after clustering, followed by tracker module are compared. Here, two different clustering algorithms are described.

A DBSCAN

DBSCAN aims cluster areas of data set with high-density points. In this algorithm, points that are close to each other, measured usually based on euclidean distance satisfying the required minimum number of points, given as input will be clustered and the points that lie outside are termed as noisy points [Xue et al., 2021]. This DBSCAN algorithm is based on two parameters namely, epsilon and minimum points. The former one refers to the distance between the two neighbouring points to form a cluster and the later one refers to the minimum number of points required to form cluster within the radius specified by epsilon. Noisy points outside the cluster are eliminated and the clusters obtained are indexed, and fed to tracker.

B K-means

It is one of the iterative and single-level clustering algorithm, which groups data into k number of groups. To proceed with clustering the data set, k value needs to be specified, which is the number of clusters required [Dairi et al., 2018, Wen and Aris, 2022]. From the data set k points are selected on random basis as cluster centres and by using distance metric, distance to each sample is calculated and assigned to the centre of the cluster. The data point is assigned to the cluster based on the minimum of distance. Further, by calculating each cluster's mean or centroid, a new cluster center is found, and reassigned the samples to the nearest cluster center is done. This keeps on iterating till their is no change in the cluster centre. The k-means clustering algorithm aims to minimize the function D given by

$$D = \sum_{q=1}^{k} \sum_{p=1}^{x} \|X_p - C_q\|^2 \tag{3.1}$$

where, $\|X_p - C_q\|^2$ is distance chosen for a measure or distance between data point X_p and centre of cluster C_q. Distance for all data points are calculated with respect to the cluster centre. Once the algorithm is converged, the clusters are indexed. These indexed data is fed to the tracker. However, disadvantage of this clustering scheme is that, it accepts k as input (number of required clusters), since the number of targets to be detected or tracked in the experiment are known, accordingly k value was given.

3.1.3 Tracker

A Filtering

Predictions, gain calculation, and updation are the three main steps of the filter [Sinha et al., 2012, Bar-Shalom et al., 2009] . The predicted state and covariance are given by

$$\hat{X}(m|m') = \mathbf{F}\hat{X}(m'|m') \quad \text{and} \tag{3.2}$$

$$\mathbf{P}(m|m') = \mathbf{F}\mathbf{P}(m'|m')\mathbf{F}^T + \mathbf{Q}(m') \tag{3.3}$$

respectively. Where, X is a state of a target and defined as $X = [\text{x, y, } \dot{x}, \dot{y}]$. Whereas $\mathbf{F}$ indicates the state transition matrix and assumed to be constant velocity ie.,

$$\mathbf{F} = \begin{bmatrix} I_2 & t_s\ I_2 \\ O_2 & I_2 \end{bmatrix} \tag{3.4}$$

where I_2 is identity and O_2 indicates zero matrix with order two. Moreover, the m and m' are current and previous time steps and t_s = m -m', $()^T$ is transposition operator and $\mathbf{Q}$ is process noise covariance. The measurement prediction is given by

$$\hat{z}(m) = \mathbf{H}\hat{X}(m|m'). \tag{3.5}$$

Here, $\mathbf{H}$ is a linearized form of measurement transition matrix and is given by

$$\mathbf{H} \approx \begin{bmatrix} \frac{\partial r}{\partial x} & \frac{\partial r}{\partial \dot{x}} & \frac{\partial r}{\partial y} & \frac{\partial r}{\partial \dot{y}} \\ \frac{\partial \theta}{\partial x} & \frac{\partial \theta}{\partial \dot{x}} & \frac{\partial \theta}{\partial y} & \frac{\partial \theta}{\partial \dot{y}} \end{bmatrix}. \tag{3.6}$$

The partial derivatives are given by $\frac{\partial r}{\partial x} = \frac{y}{\sqrt{x^2 + y^2}}$, $\frac{\partial r}{\partial y} = \frac{x}{\sqrt{x^2 + y^2}}$, $\frac{\partial \theta}{\partial x} = \frac{-y}{\sqrt{x^2 + y^2}}$, $\frac{\partial \theta}{\partial y} = \frac{x}{\sqrt{x^2 + y^2}}$ and rest of the partial derivatives are zero. Since clustering methods are applied, in some scans the detections are not obtained. Hence, gating technique is used. Whenever detections fall in gate, they are used to find innovation, else the no detection is reported to track management module. Innovation is given by

$$\gamma = z(m) - \hat{z}(m|m'), \tag{3.7}$$

where $\hat{z}(m|m')$ is determined by the data association module.

The Kalman gain G is computed as

$$\begin{aligned} \mathbf{G}(m) =& \mathbf{P}(m/m')\mathbf{H}(m)^T \\ & \left[\mathbf{H}(m)\mathbf{P}(m/m')\mathbf{H}(m)^T + \mathbf{R}\right]^{-1}, \end{aligned} \tag{3.8}$$

where, R is the measurement noise covariance matrix.

The updated state and covariance are given by

$$\hat{X}(m|m) = \hat{X}(m|m') + \mathbf{G}(m)\gamma(m) \tag{3.9}$$

and

$$\mathbf{P}(m|m) = \mathbf{P}(m|m') - \mathbf{G}(m)\mathbf{H}(m)\mathbf{G}'(m) \tag{3.10}$$

respectively.

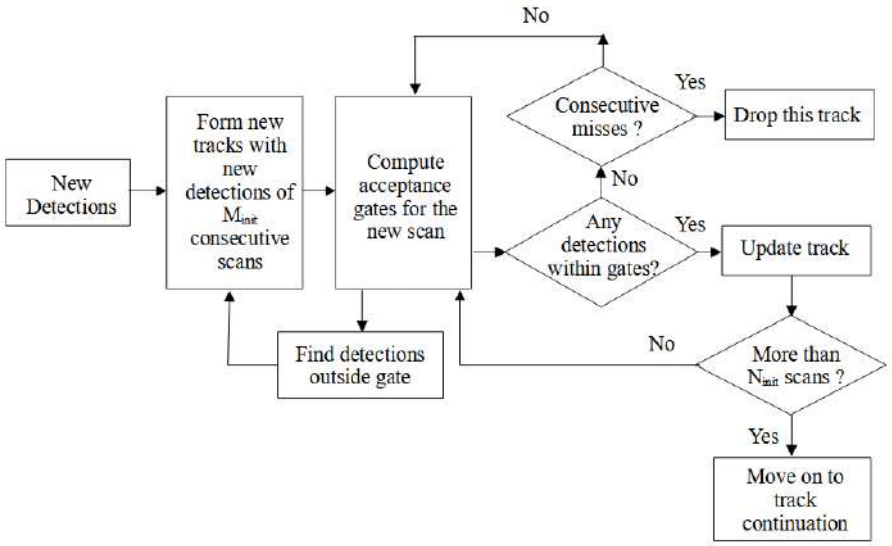

Figure 3.1: Track management

B GNN Data association

Decision is made by data association by associating the obtained measurements at m' to the established tracks at m'', and to update the track at m'. GNN is a 2D assignment that matches the measurement list at m to the predicted tracks list $T_{m'}$ by formulating the global optimization problem. The optimization minimizes the overall cost C of the measurement-to-track as

$$C = \sum_{j=0}^{q_m} \sum_{t=0}^{T_{m'}} a(j,t)c(j,t) \tag{3.11}$$

subjected to

$$\sum_{j=0}^{q_m} a(j,t)c(j,t) = 1, \quad t = 1, 2, \cdots T_{m'}$$
$$\sum_{t=0}^{T_{m'}} a(j,t)c(j,t) = 1, \quad j = 1, 2, \cdots q_m$$

Here q and T represent measurement list and track list respectively. $a(j,t)$ is a binary assignment variable such that

$$a(j,t) = \begin{cases} 1; & \text{measurement } j \text{ associated with target } t \\ 0; & \text{otherwise} \end{cases} \tag{3.12}$$

Here, measurements are indexed by j, and all the tracks are indexed by t to form a 2D matrix. Whereas, C is the cost associated with measurement-to-track; which is equal to the distance between predicted measurement $H\hat{X}(m/m')$ and measurement $z_j(m)$. The above optimization is solved using munkres algorithm Bourgeois and Lassalle [1971].

C Track management

Figure. 3.1, describes the flow of track management process. Tentative tracks and confirmed tracks are the two available tracks provided by the tracker. If there are fewer measurements associated than the required number of measurements over a specified time limit, that refers to tentative tracks. Confirmed tracks are the tentative tracks that receive more associated measurements and are promoted to be confirmed ones. If in case, any inadequate number of measurements are associated with the tentative track, within the specified time, then that will be deleted. For the maintenance of track, the logic-based rule is used, given in Sinha et al. [2012]. 1) For track initialization: if there are at least M_{init} measurements associated for last N_{init} measurement frames then a track is formed and marked as tentative otherwise nothing is done (refer Figure. 3.1). 2) For a tentative track: if there are at least M_{tent} measurements associated to the track out of the last N_{tent} measurement frames, then the track is promoted as confirmed, else delete the track. 3) For a confirmed track: out of the last N_{conf} measurement frames if at least M_{conf} measurements are associated to the track, then do nothing otherwise, delete it.

3.1.4 Tracking Metrics

Since the truths are not known, in real scenarios, its difficult to have performance metrics for the tracks obtained [Gorji et al., 2011], [Song et al., 2022]. Metrics that are used for the tracker output are number of TR, TS, TL and FT. TR, is the total number of tracks obtained after processing all the collected frames. After the frames were processed, due to lack of measurements the TR were broken into small segments with all CFAR detectors and with both the clustering schemes. TS is the count of number of broken (pieces) tracks. If B_l is the last time instant that the track is associated to the measurement and if B_l is lesser than the l^{th} measurement appeared time, then the number for the broken track is one, indicating a break in the estimated track. Due to lack of measurements, if a track is not generated for the target, then that is TL. If a track is not associated to target, then such tracks are termed as FT. The average number of the FT is given by Gorji et al. [2011]

$$Num_{false} = \frac{1}{Mc} \sum_{i=1}^{Mc} Num_{false} \tag{3.13}$$

where, Mc is the number of monte carlo runs and Num_{false} is the number of FT. Because of real data, Mc=1.

3.2 Track Plots

The obtained measurements from each of the CFAR processing schemes are fed to DBSCAN and K-means clustering algorithms. DBSCAN accepts two parameters, epsilon and the minimum number of points required to form clusters, while K-means asks for the number of clusters required, which was given based on the number of targets in the experiment. The mean of the clustered data was given to the EKF associated with GNN. Results generated from four CFAR processing techniques with both clustering schemes are compared.

The initial state and constant velocity of the target are

$$\begin{aligned} X(0) &= [x, y, \dot{x}, \dot{y}]' \\ &= [x(1), y(1), 0, 0]' \end{aligned} \tag{3.14}$$

Process noise is used to model the target protuberance in both position and velocity components. The tunable parameters like process noise covariance and the

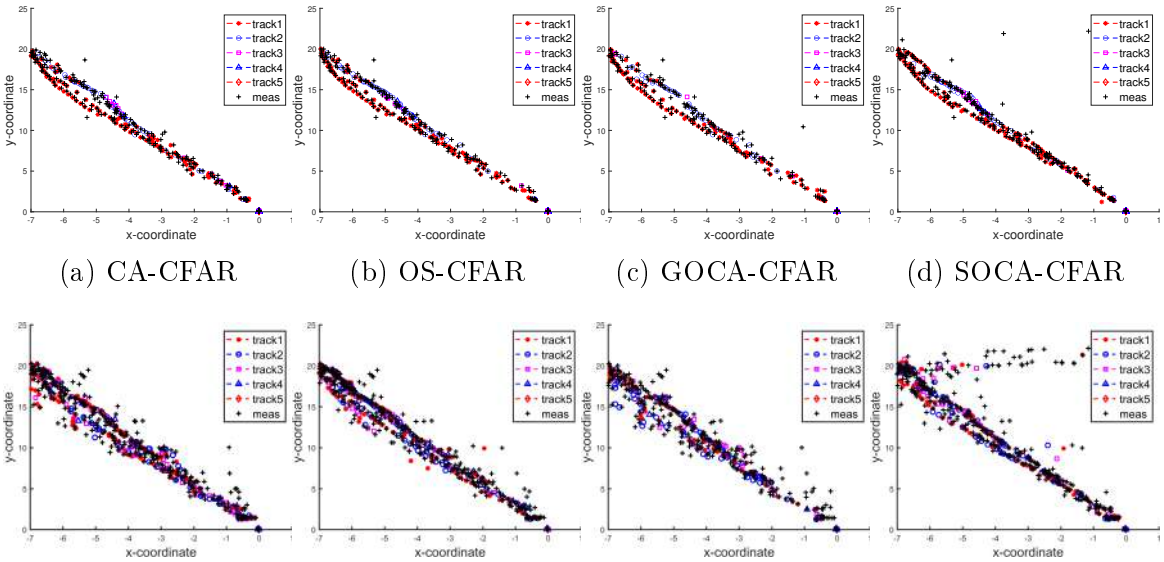

(a) CA-CFAR (b) OS-CFAR (c) GOCA-CFAR (d) SOCA-CFAR

(e) CA-CFAR (f) OS-CFAR (g) GOCA-CFAR (h) SOCA-CFAR

Figure 3.2: Five targets tracking without jammer (AJ) in USRR (a-d) clustered by DBSCAN (e-f) clustered by K-means

measurement noise covariance are tuned to

$$Q = \text{diag}([0.1^2\ 0.1^2\ 0.1^2\ 0.1^2]) \tag{3.15}$$

$$R = \text{diag}([0.1^2\ 0.1^2]) \tag{3.16}$$

3.2.1 Tracking in USRR mode in AJ

Mean of the clustered data was fed to the tracker and the track generated by four CFAR variants are reported.

Figure. 3.2 shows the tracks obtained for five targets.

From the tracking plots yielded and from the metrics in table 3.1, K-means clustering algorithm fails to identify the clusters from the data points.

From tracking results of single and two targets, compared to DBSCAN clustering algorithm, K-means reported measurements were unassociated to the tracks and further it fails to generate clusters for the entire set of measurements, which results in incomplete tracks. Furthermore, as the number of targets increases, the number of TR by K-means clustering algorithm is higher than DBSCAN clustering algorithm, which is result of wrong measurement association/inability to identify clusters correctly (K-means clustering algorithm has higher values of TS and FT). Thus, our observation is that, DBSCAN clustering algorithm provides improved performance compared to

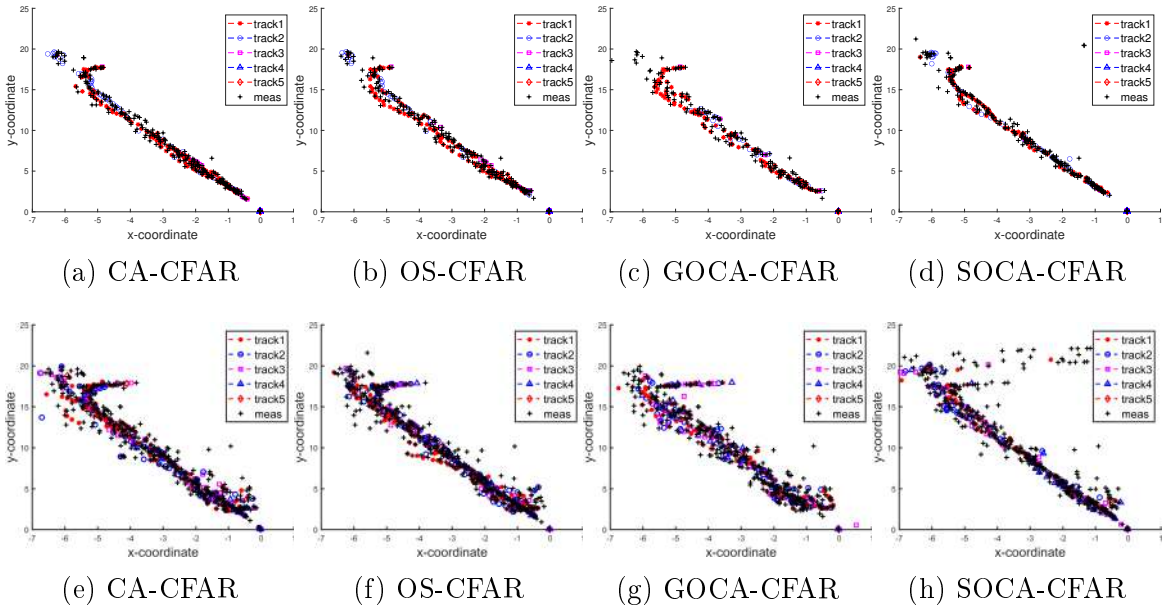

(a) CA-CFAR (b) OS-CFAR (c) GOCA-CFAR (d) SOCA-CFAR

(e) CA-CFAR (f) OS-CFAR (g) GOCA-CFAR (h) SOCA-CFAR

Figure 3.3: Five targets tracking with jammer (PJ) in USRR (a-d) clustered by DBSCAN (e-f) clustered by K-means

K-means clustering algorithm.

Since the threshold for SOCA-CFAR is minimum of either the leading or the lagging cells, it reports more number of false detections or spread in the detections compared to other three detecting techniques. In case of GOCA-CFAR, because of the maximum threshold it failed to detect desired number of targets.

There by, the available measurements are few compared to other three detecting techniques. These measurements are insufficient to be grouped by DBSCAN clustering algorithm as they are not within the specified region of epsilon (radius) leading to lack of measurements for the tracker to obtain track for the complete track length. Besides, CA-CFAR and OS-CFAR clustered by DBSCAN algorithm reports similar track plots, while GOCA-CFAR failed to assign track for complete track length. Therefore, inference based on the track plots and the metrics of tracks is DBSCAN clustered CA-CFAR and OS-CFAR are better compared to GOCA-CFAR and SOCA-CFAR.

3.2.2 Tracking in USRR mode in PJ

For the similar scenario and same configuration of primary radar sensor as that of the previous case, a jammer was placed at 5 m as shown in Figure. 2.4.

Figure. 3.3 reports the tracks generated for five targets in a jamming environment.

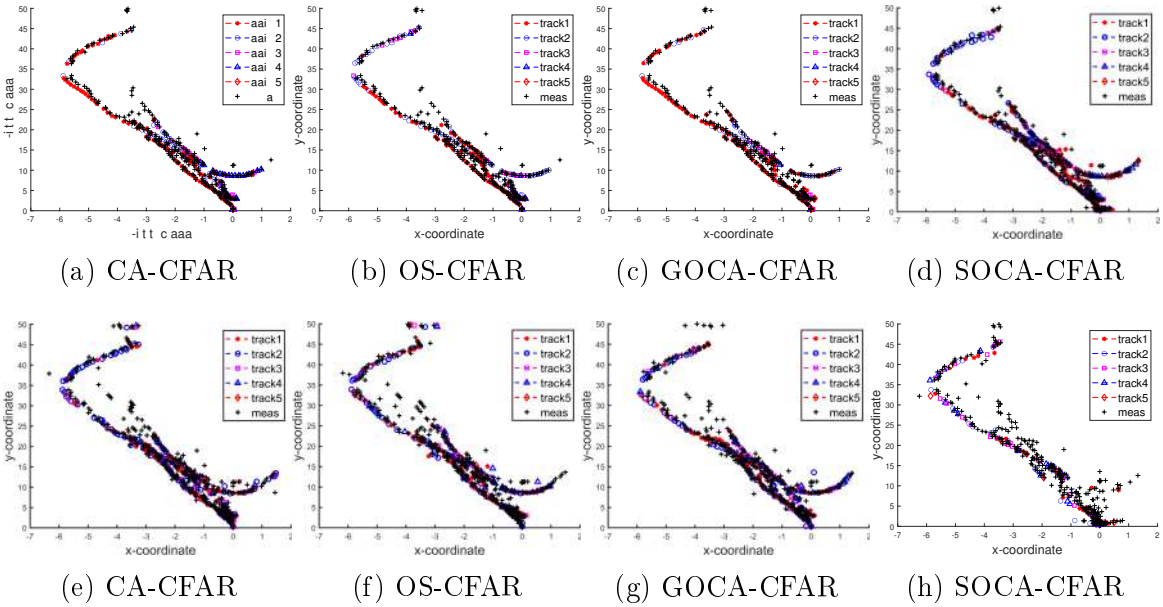

(a) CA-CFAR (b) OS-CFAR (c) GOCA-CFAR (d) SOCA-CFAR

(e) CA-CFAR (f) OS-CFAR (g) GOCA-CFAR (h) SOCA-CFAR

Figure 3.4: Five targets tracking without jammer (AJ) in SRR (a-d) clustered by DBSCAN (e-f) clustered by K-means

Once again, DBSCAN clustering algorithm outperforms the K-means clustering algorithm. Here also, once again DBSCAN clustered GOCA-CFAR (failed to detect desired number of targets) is unable to have track for full track length and reports more TS. Similar to AJ case, CA-CFAR and OS-CFAR clustered by the DBSCAN algorithm provide improved performance compared to the K-means clustering algorithm.

3.2.3 Tracking in SRR mode in AJ

For the same scenario (without jammer), primary radar sensor was operated in SRR mode, Figure. 3.4 shows the tracks obtained for five targets. Once again, same observations were made as those of USRR mode of operation. K-means clustering algorithm performance is inferior in identifying clusters compared to the DBSCAN clustering algorithm. However, in the case of DBSCAN clustering algorithm, GOCA-CFAR provides superior performance compared to SOCA-CFAR. Further, DBSCAN clustering algorithm performs better in SRR mode compared to USRR mode.

3.2.4 Tracking in SRR mode in PJ

For the same scenario (with jammer) primary radar sensor operated in SRR mode, Figure. 3.5 reports the tracks generated for five targets. Once again same observations

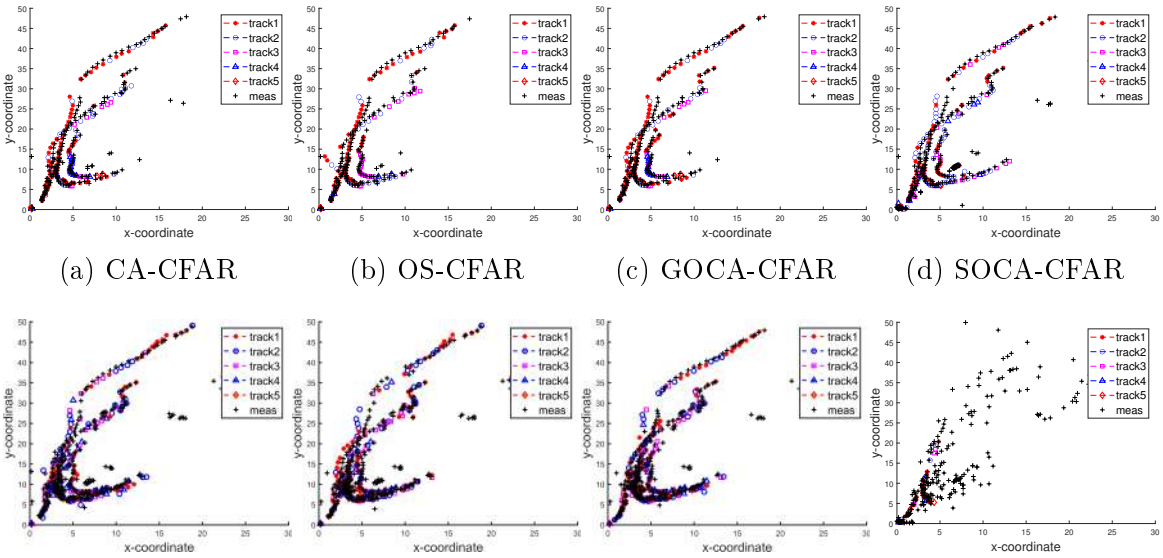

(a) CA-CFAR (b) OS-CFAR (c) GOCA-CFAR (d) SOCA-CFAR

(e) CA-CFAR (f) OS-CFAR (g) GOCA-CFAR (h) SOCA-CFAR

Figure 3.5: Five targets with jammer (PJ) (a-d) clustered by DBSCAN (e-f) clustered by K-means

were made as that of USRR mode. DBSCAN clustering algorithm provides improved performance compared to K-means clustering algorithm. Besides that, both SOCA-CFAR and GOCA-CFAR performed better in SRR mode compared to USRR mode and also has tracks generated similar to that of OS-CFAR and CA-CFAR.

Tracking metrics for both USRR and SRR modes in the absence and in the presence of spot-jammer cases are tabulated in the table 3.1. Each AJ and PJ column has two values, one outside the bracket is for USRR mode and the other inside the bracket is for SRR mode operation. From the tabulated values, it is apparent that DBSCAN clustering algorithm provides superior performance compared to K-means clustering algorithm.

3.2.5 Tracking of Targets in SRR mode with Jammer at Different Angles

Figure. 3.6 provides the generated track plots for the spot-jammer deployment at 3m and 30^0 angle from the primary radar sensor. In the same Figure. 3.6, for the ease of comparison of cluster algorithm, the Figure. 3.6(a–d) are drawn for DBSCAN and Figure. 3.6(e–h) plots corresponding to K-means clustering. All the CFAR algorithms (CA-CFAR, OS-CFAR, GOCA-CFAR, and SOCA-CFAR) are also verified for the above-mentioned case. It is clearly observed that CA-CFAR, OS-CFAR, and

Table 3.1: Tracking metrics for mutiple targets in the absence and in the presence of jammer for both USRR and SRR modes of mmWave sensor

		CA-CFAR				**OS-CFAR**				**GOCA-CFAR**				**SOCA-CFAR**			
Targets	Metrics	**DBSCAN**		**K-means**		**DBSCAN**		**K-means**		**DBSCAN**		**K-means**		**DBSCAN**		**K-means**	
		AJ	PJ	AJ	PJ	AJ	PJ	AJ	PJ	AJ	PJ	AJ	PJ	AJ	PJ	AJ	PJ
1	TR	2(1)	2(3)	4(1)	1(2)	2(1)	2(3)	2(1)	2(2)	4(1)	5(3)	2(1)	2(2)	2(1)	2(3)	1(-)	3(1)
	TS	12(3)	3(4)	8(1)	0(3)	8(3)	3(4)	6(2)	1(2)	7(3)	2(5)	6(0)	1(3)	8(3)	4(3)	8(0)	3(11)
	FT	0(1)	0(1)	0(0)	0(0)	0(1)	0(0)	0(0)	0(0)	0(1)	0(3)	0(0)	0(0)	0(1)	0(1)	2(0)	0(0)
	TL	0(0)	0(0)	0(0)	0(0)	0(0)	0(0)	0(0)	0(0)	0(0)	0(0)	0(0)	0(0)	0(0)	0(0)	0(0)	0(0)
2	TR	4(3)	5(4)	3(6)	5(5)	3(5)	4(4)	2(5)	4(5)	3(3)	5(3)	2(6)	4(5)	3(4)	5(3)	4(3)	4(1)
	TS	7(1)	2(6)	4(4)	3(13)	8(1)	2(12)	7(5)	2(8)	8(1)	5(5)	3(4)	3(8)	6(2)	2(3)	5(1)	4(3)
	FT	2(0)	0(1)	0(0)	2(8)	1(0)	0(8)	0(0)	0(4)	1(1)	0(3)	0(0)	0(5)	1(1)	0(3)	0(0)	0(3)
	TL	0(0)	0(0)	0(0)	0(0)	0(0)	0(0)	0(0)	0(0)	0(0)	0(1)	0(0)	0(0)	0(0)	0(0)	0(0)	0(0)
3	TR	5(6)	5(6)	7(7)	5(10)	5(3)	5(6)	8(6)	5(9)	7(4)	5(6)	8(7)	6(7)	5(4)	6(6)	5(4)	5(3)
	TS	5(7)	3(8)	8(6)	2(13)	5(4)	3(8)	7(5)	0(12)	7(5)	6(8)	6(8)	4(12)	5(2)	1(8)	6(6)	2(3)
	FT	0(0)	0(2)	2(1)	0(5)	0(0)	0(2)	1(2)	0(6)	2(2)	0(1)	1(2)	1(3)	0(0)	1(5)	3(6)	0(3)
	TL	0(0)	0(0)	0(0)	0(0)	0(0)	0(0)	0(0)	0(0)	0(0)	0(0)	0(0)	0(0)	0(0)	0(0)	0(0)	0(0)
4	TR	5(5)	7(6)	9(8)	11(10)	5(5)	7(7)	10(6)	11(8)	5(5)	7(6)	10(6)	10(9)	7(5)	7(7)	10(5)	8(6)
	TS	8(2)	3(6)	7(2)	2(11)	10(3)	3(6)	7(4)	2(9)	5(3)	5(7)	9(4)	6(8)	7(3)	4(7)	8(5)	4(6)
	FT	0(4)	0(2)	0(2)	0(5)	0(1)	0(1)	1(2)	0(5)	0(3)	1(2)	0(0)	0(4)	0(1)	0(3)	2(2)	1(2)
	TL	0(0)	0(0)	0(0)	0(0)	0(0)	0(0)	0(0)	0(0)	0(0)	0(0)	0(0)	0(0)	0(0)	0(0)	0(0)	0(0)
5	TR	5(6)	8(8)	9(10)	11(14)	6(7)	6(9)	9(7)	9(12)	5(8)	6(8)	8(9)	12(15)	5(8)	4(10)	8(9)	9(4)
	TS	5(1)	3(10)	0(1)	0(10)	5(1)	4(10)	4(1)	0(10)	5(1)	4(10)	7(1)	0(13)	3(1)	2(11)	3(4)	2(6)
	FT	0(0)	2(1)	0(1)	1(3)	1(0)	0(1)	1(0)	1(3)	1(0)	0(1)	1(1)	1(4)	0(0)	1(2)	0(1)	1(3)
	TL	0(0)	0(0)	0(0)	0(0)	0(0)	0(0)	0(0)	0(0)	0(0)	0(0)	0(0)	0(0)	0(0)	0(0)	0(0)	0(0)

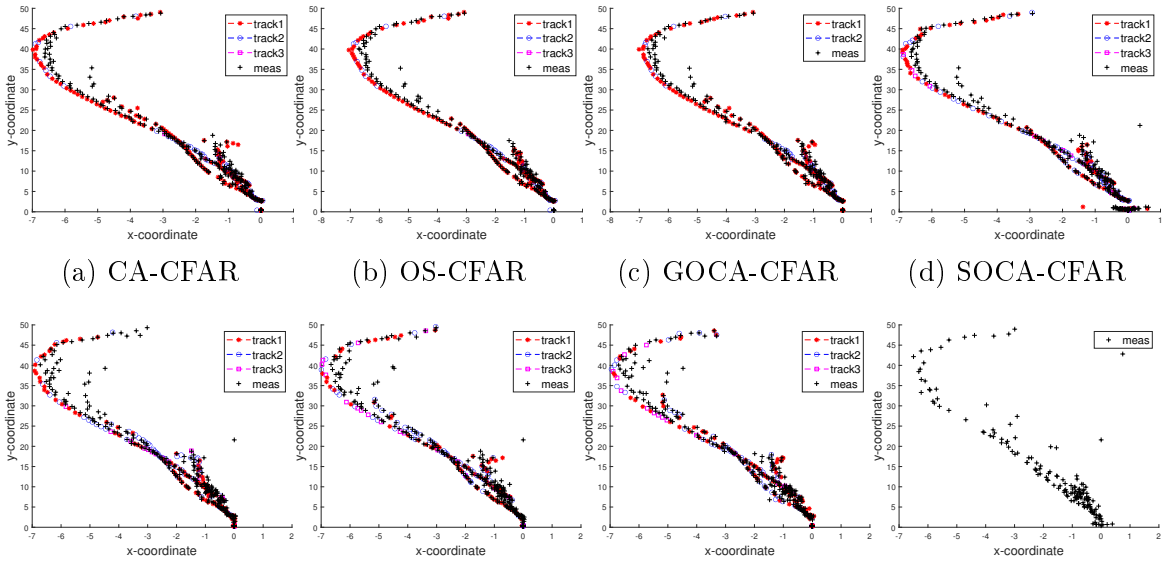

(a) CA-CFAR (b) OS-CFAR (c) GOCA-CFAR (d) SOCA-CFAR

(e) CA-CFAR (f) OS-CFAR (g) GOCA-CFAR (h) SOCA-CFAR

Figure 3.6: Three targets in SRR mode with jammer at 3m and 30^0 (a-d) clustered by DBSCAN (e-f) clustered by K-means

SOCA-CFAR provide three tracks pertaining to three different targets for DBSCAN clustering (refer Figure. 3.6(a), Figure. 3.6(b), and Figure. 3.6(d)). Whereas, CA-CFAR, OS-CFAR, and GOCA-CFAR schemes working perfectly with the K-Means clustering (refer Figure. 3.6(e), Figure. 3.6(f), and Figure. 3.6(g)). It is important to note that, the SOCA-CFAR is not able to provide the tracks with K-means clustering, this is due to tuning parameters within the clustering algorithm. It is also worth to note that, the DBSCAN tries to provide the tracks, this is due to the tuning parameter, epsilon. As the tuning parameter within DBSCAN increases, the cluster points disperse and unable to provide unique clusters.

Table 3.2 gives the tracking metrics for one, two and three targets. The value written outside the bracket is for jammer at 2 m, and the value inside the bracket is for jammer at 3 m. Meanwhile, Table 3.3 reports tracking metrics for one, two and three targets for jammer located at 5 m distance. From the tracking metrics, the K-means clustered based SOCA-CFAR method has inadequate measurements to generate tracks and reports track loss. The experimental results further reveal, that DBSCAN performs better compared to K-means.

CA-CFAR : Average value of the neighboring cells is applied as threshold to detect targets. False detections are less compared to SOCA and even missed detections are

Table 3.2: Tracking metrics for mutiple targets with jammer at 2m and 3m and at different angles for SRR mode of mmWave sensor

		CA-CFAR						OS-CFAR						GOCA-CFAR						SOCA-CFAR					
Targets	Metrics	DBSCAN			K-means			DBSCAN			K-means			DBSCAN			K-means			DBSCAN			K-means		
		-30^0	LOS	30^0	-30^0	LOS	30^0	-30^0	LOS	30^0	-30^0	LOS	30^0	-30^0	LOS	30^0	-30^0	LOS	30^0	-30^0	LOS	30^0	-30^0	LOS	30^0
1	TR	1(1)	1(2)	1(1)	1(1)	2(1)	1(2)	1(1)	2(1)	1(1)	2(1)	2(1)	2(1)	1(1)	1(2)	2(1)	1(0)	1(1)	1(2)	2(1)	7(2)	2(1)	0(0)	0(0)	0(0)
	TS	0(0)	0(0)	0(0)	0(2)	0(3)	3(0)	2(0)	3(1)	0(0)	0(2)	2(3)	3(0)	2(1)	3(1)	2(2)	0(0)	0(0)	4(0)	2(5)	6(5)	4(3)	0(0)	0(0)	0(0)
	FT	0(0)	0(0)	0(0)	0(0)	0(0)	0(0)	0(0)	0(0)	0(0)	0(0)	0(0)	1(0)	0(0)	0(0)	0(0)	0(0)	0(0)	0(0)	0(0)	0(0)	0(0)	0(0)	0(0)	0(0)
	TL	0(0)	0(0)	0(0)	0(0)	0(0)	0(0)	0(0)	0(0)	0(0)	0(0)	0(0)	0(0)	0(0)	0(0)	0(0)	0(0)	0(0)	0(0)	0(0)	0(0)	0(0)	1(0)	1(0)	1(0)
2	TR	4(4)	4(4)	3(3)	4(5)	3(3)	3(4)	3(4)	3(3)	3(3)	3(3)	3(3)	4(4)	4(4)	4(4)	4(3)	5(4)	5(3)	4(4)	5(4)	4(4)	5(2)	1(1)	0(2)	2(0)
	TS	0(0)	3(0)	4(2)	3(3)	2(3)	2(3)	0(2)	3(2)	2(2)	3(3)	3(3)	3(3)	0(0)	0(0)	3(2)	3(3)	4(2)	3(3)	2(3)	3(2)	5(2)	0(0)	0(2)	2(0)
	FT	0(0)	0(0)	0(0)	0(0)	0(0)	0(0)	0(0)	0(0)	0(0)	0(0)	0(0)	0(0)	0(0)	0(0)	0(0)	0(0)	0(0)	0(0)	0(0)	0(0)	0(0)	0(0)	0(0)	0(0)
	TL	0(0)	0(0)	0(0)	0(0)	0(0)	0(0)	0(0)	0(0)	0(0)	0(0)	0(0)	0(0)	0(0)	0(0)	0(0)	0(0)	0(0)	0(0)	0(0)	0(0)	0(0)	0(0)	2(0)	0(0)
3	TR	6(6)	4(4)	5(4)	8(6)	7(5)	7(6)	6(6)	4(4)	5(3)	7(6)	6(7)	5(6)	5(6)	4(5)	5(4)	8(6)	6(6)	6(6)	4(6)	5(4)	5(4)	1(0)	0(2)	2(2)
	TS	0(3)	2(2)	0(1)	4(5)	0(1)	0(1)	0(3)	2(2)	0(1)	5(5)	0(2)	2(1)	0(4)	2(2)	0(2)	4(4)	0(2)	2(0)	0(5)	2(3)	2(0)	0(0)	0(0)	0(0)
	FT	0(0)	0(0)	0(0)	0(0)	0(0)	0(0)	0(0)	0(0)	0(0)	0(0)	0(0)	0(0)	0(0)	0(0)	0(0)	0(0)	0(0)	0(0)	0(0)	0(0)	0(0)	0(0)	0(0)	0(0)
	TL	0(0)	0(0)	0(0)	0(0)	0(0)	0(0)	0(0)	0(0)	0(0)	0(0)	0(0)	0(0)	0(0)	0(0)	1(0)	0(0)	0(0)	0(0)	0(0)	0(0)	0(0)	0(0)	0(0)	3(0)

Table 3.3: Tracking metrics for mutiple targets with jammer at 5m and at different angles for SRR mode of mmWave sensor

		CA-CFAR				OS-CFAR				GOCA-CFAR				SOCA-CFAR			
Targets	Metrics	DBSCAN		K-means		DBSCAN		K-means		DBSCAN		K-means		DBSCAN		K-means	
		-30^0	30^0	-30^0	30^0	-30^0	30^0	-30^0	30^0	-30^0	30^0	-30^0	30^0	-30^0	30^0	-30^0	30^0
1	TR	1	1	2	1	1	1	0	1	1	1	2	1	1	2	0	0
	TS	0	0	0	0	0	0	0	0	0	2	0	0	2	2	0	0
	FT	0	0	0	0	0	0	0	0	0	0	0	0	0	0	0	0
	TL	0	0	0	0	0	0	1	0	0	0	0	0	0	0	1	1
2	TR	2	3	4	5	2	3	6	4	2	3	4	7	4	2	1	1
	TS	2	2	2	3	2	2	3	4	2	3	3	3	3	2	0	0
	FT	0	0	0	0	0	0	0	0	0	0	0	0	0	0	0	0
	TL	0	0	0	0	0	0	0	0	0	0	0	0	0	0	0	0
3	TR	4	5	6	5	4	6	3	4	4	4	7	5	4	6	2	1
	TS	3	3	5	4	3	1	4	3	3	3	6	3	4	4	2	0
	FT	0	0	0	0	0	0	0	0	0	0	0	0	0	0	0	0
	TL	0	1	0	0	0	1	0	0	0	0	0	0	0	0	1	0

less compared to GOCA. This resulted in full length tracks from the tracking module, which gave appreciable tracking metrics compared to SOCA-CFAR and GOCA-CFAR.

OS-CFAR : Here, in OS-CFAR, the cell values are arranged in ascending order and random cell value is picked as threshold. OS-CFAR performed similar to that of CA-CFAR in detecting targets. The four tracking metrics obtained from the track plots also showed similar performance as that of CA-CFAR.

GOCA-CFAR : In GOCA, greatest of the leading or the lagging subset is applied as the threshold for the detection process. Since there is rise in the threshold level compared to other CFAR schemes, true target detections were missed, leading to more false tracks (FT) compared to CA-CFAR and OS-CFAR. tracks reported (TR) and track segments (TS) are similar to CA-CFAR and OS-CFAR.

SOCA-CFAR : In this scheme, the threshold level is smallest of the leading or the lagging subset of the CFAR algorithm. More spread in the detections or false detections were noticed, which resulted in improper clustering both by DBSCAN and K-means algorithms. So, full length tracks were not produced by the tracking module and reported more false tracks (FT) and track segments (TS). More number of detections also resulted in more number of tracks compared to other CFAR detection techniques. mmWave radars are sensitive, they are capable of detecting targets within the visible region of the radar. So, tack loss (TL) is not reported in any of the four detection schemes.

Therefore, CA-CFAR and OS-CFAR performance is better compared to GOCA and SOCA-CFAR.

In terms of DBSCAN and K-means clustering algorithms, DBSCAN performed better compared to K-means. FT and TS reported by K-means by all the CFAR detection techniques are more compared to DBSCAN.

3.3 Conclusion

Multiple moving targets detected by RD-maps of four CFAR schemes are fed into two unsupervised ML (clustering) algortithms followed by GNN EKF tracking module. The track reports obtained are presented in this chapter. Track plots are analysed

by four different tracking metrics namely, TR, FT, TL, and TS. Accordingly, plots reported for CA-CFAR, and OS-CFAR for DBSCAN ML algorithm performance is better compared to K-means algorithm.

Chapter 4

Deep Learning based (YOLO) Target Detection using Range-Doppler maps obtained from CFAR techniques

This chapter describes about the detection of multiple targets for the real-time data extracted by mmWave radars in presence of interference by employing deep learning YOLO (you only look once) algorithm.

4.1 System Representation

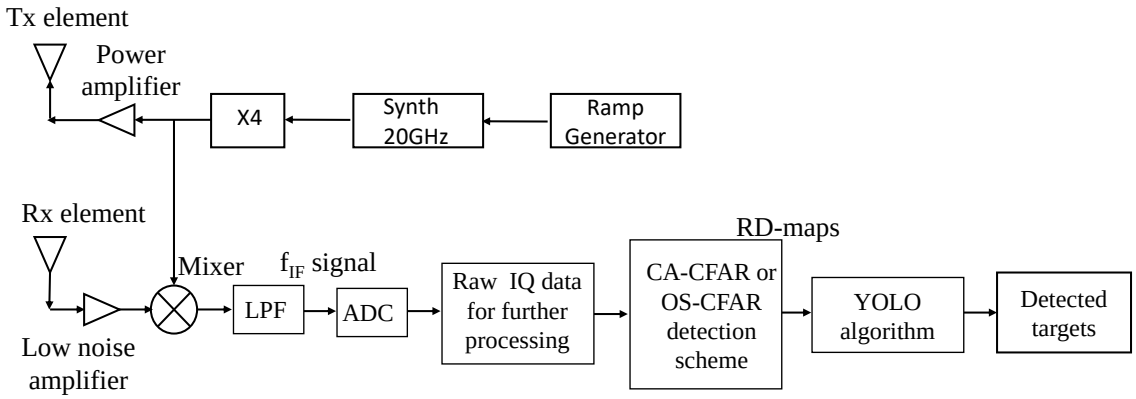

Figure 4.1: Schematic representation

The schematic representation of the system is presented in Figure. 4.1. Chirp signals of carrier frequency 77 GHz generated by a local oscillator (LO) with a slope of 8 MHz/μs are transmitted by a mmWave sensor at the rate of 59 μs. Transmitter consists two transmitting antenna elements separated by 2λ distance. Transmitted signal $s_t(t)$ is given by

$$s_t(t) = A_t \exp(2\pi j f_{min} t + j\pi \frac{BW}{T} t^2);\ 0 \leq t \leq T_r, \tag{4.1}$$

where, A_t is amplitude and S is slope of the transmitted signal and is given by

$$S = \frac{BW}{T}. \tag{4.2}$$

Here, BW is bandwidth and T is one sweep time interval.

Reflected echo signals from the targets present in the FoV of mmWave sensor are received by the receiving antenna consisting four elements separated by $\lambda/2$ distance and is represented by

$$r(t) = \sum_{i=1}^{N_t} s_t(t - \tau_i), \tag{4.3}$$

where, N_t is the total number of targets present in the surveillance region of mmWave sensor and τ_i is the round-trip time delay of target i. Therefore, the delay is

$$\tau = \frac{2|\mathbf{r}^t - \mathbf{r}^r|}{c}. \tag{4.4}$$

where, $(\mathbf{r}^t - \mathbf{r}^r)$ is the distance R between the target and mmWave radar sensor, c is speed of light in free space and $|\cdot|$ is an euclidean operator.

Upon down converting the received signal $(r(t))$, the i^{th} target IF response is given by

$$S_{IF,i}[n] = \exp(j2\pi\tilde{r}(\tau_i, f_{di})\mathbf{n}). \tag{4.5}$$

On adopting 2D-FFT on RD data gives

$$RD = |\sum_{i=1}^{N_t} w[\mathbf{n}] x_{IF}[n] \exp(j2\pi\tilde{r}(\tau_i, f_{di})\mathbf{n})|. \tag{4.6}$$

where, w represents window function of 2-dimension, x_{IF} is IF sampled component and $\mathbf{n}$ is a vector combination of fast and slow time samples. By, applying CA-CFAR (cell averaging-constant false alarm rate) algorithm on these RD maps, detections are obtained for clean environment.

Eq. (4.3) represents received signal in the absence of jammer. In the presence of jammer, the received signal by mmWave radar sensor is sum of two components. First is the sum of echo return from the targets in surveillance region of source and second is the sum of the signals from jammers in source vicinity. Therefore, the received signal $R^I_{rx}(t)$ is

$$R^I_{rx}(t) = \sum_{i=1}^{N_t} s\ (t - \tau_i)\ +\ \sum_{j=1}^{J} s^I(\tau'_j), \tag{4.7}$$

where $s^I(t)$ is the jamming signal, given by

$$s^I(t) = \sum_{j=1}^{J} A^I_j \exp(2\pi j f_{min}\tau'_j + j\pi \frac{BW}{T}\tau'^2_j) \tag{4.8}$$

where, A^I_j is amplitude and τ'_j is the time of j^{th} jammer.

The i^{th} target, IF response in presence of jammer is given by

$$S^I_{IF,i}[n] = \exp(j2\pi\tilde{r}(\tau_i, \tau', f_{di})\mathbf{n}). \tag{4.9}$$

2D-FFT on RD data gives

$$RD = |\sum_{i=1}^{N_t}\ w[\mathbf{n}]x_{IFPJ}[n]\exp(j2\pi\tilde{r}(\tau_i, \tau', f_{di})\mathbf{n})|. \tag{4.10}$$

For the experiments conducted, one jammer ($J = 1$) and five targets ($N_t = 5$) are considered in source's FoV.

Thus, digitized raw IF data post-processed in MATLAB to obtain detections by CA-CFAR detection scheme. Obtained RD maps are used to train the DL module to detect targets.

4.2 Architecture of YOLO V5

YOLO is one of the widely used algorithm for object detection. It was introduced by Joseph Redmon in Darknet [Redmon et al., 2016]. Further, developments and improvements brought with respect to speed and accuracy resulted in the current version V5. It is released with five different model sizes having same internal structure but differs in depth and width multiple and in turn the number of convolutional cores. Namely, n-(extra small), s-(small), m-(medium), l-(large), and x-(extra large)

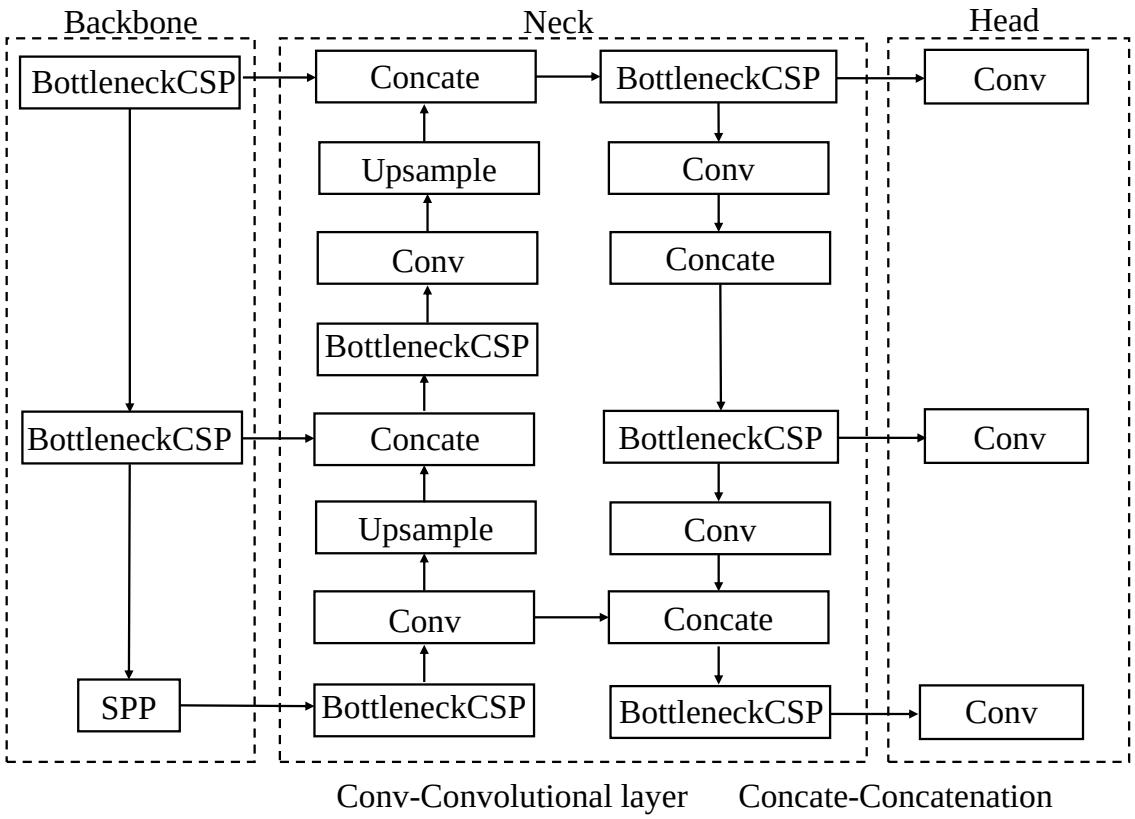

Figure 4.2: YOLO V5 Architecture

[Ting et al., 2021]. YOLO V5 algorithm is trained by using deep convolutional neural network (CNN) to identify objects in the image by dividing it into grids and predicting bounding boxes, class probabilities, and confidence scores for each grid cell [Xu et al., 2021]. YOLO V5 is widely adopted for computer vision applications such as autonomous driving, object tracking, and surveillance systems.

YOLO V5 architecture has many layers that connect to each other. The operations performed can divide into three different components. First is the backbone of the network, second is the neck and the third or the last layer is the head. Backbone - a CNN which aggregates and extracts image features at different levels, by CSP (cross stage partial) Darknet53. Convolution, concatenation, and max-pooling are some of the common operations performed in this layer. It also forwards the features extracted from the image to the next layer. CSP Darknet assists YOLO to get to know the complex features from images fed as input. The speed and accuracy is improved by reducing the parameters to train and reducing the floating-point operations performed per second.

In a second layer, neck combines features of images evaluated by the backbone

layer and prepares to pass them to the next level, by SPP (spatial pyramid pooling) and PANet (path aggregation network) [Liu et al., 2018]. Improvised version of PANet is deployed in YOLO V5. This enables bidirectional pyramid network, by which the feature information flow is fast and easy. By the usage of SPP net [He et al., 2015], repeated computations of convolutional features are avoided. The feature maps are computed only once and further pool the features to create fixed length representations to train the detectors.

The last layer head, gets features from the neck and further, moves on to process of class prediction, same as in YOLO V4. Three (18×18, 36×36, 72×72) different size feature maps are generated, providing advantage to deal with small, medium and big objects. In YOLO V5 uniform scaling of depth, width, and resolution is performed for all the networks at the same instant, which leads to increase in accuracy.

4.2.1 Performance Metrics

Metrics used to analyse the performance of ML model are discussed in this section [Ghori et al., 2020, Wilson et al., 2023]. Metrics mainly depend on the identification of the class of the object. An object class can be predicted as true (positive) or false (negative) by ML model. If suppose class is predicted as true with the actual class as positive, then observation is true positive (TP) and if class is correctly predicted as negative, then observation is true negative (TN). When class is predicted as true but actually it is negative, then that implies false positive (FP) and when class predicted as false and actual class is positive, then that is false negative (FN).

Accuracy is a fraction of predictions that model got right. It defines how TP and TN are predicted by model and is computed by following expression

$$Acc = \frac{Number\ of\ correct\ predictions}{Total\ number\ of\ predictions}. \tag{4.11}$$

$$Acc = \frac{TP\ +\ TN}{TP\ +\ TN\ +\ FP\ +\ FN}. \tag{4.12}$$

4.2.2 Dataset

Real data was taken out by the experiments conducted with the help of TIs mmWave radar sensors. Two sensors having same characteristics were used to draw two different

(a) Source with Spot-jamming radar

(b) Four targets with source radar

(c) Five targets with Spot-jamming radar

Figure 4.3: Experimental setup for various cases

datasets. In the first case, data was collected having IWR1642 Instruments [2018a] as the source and in its surveillance region five different targets moved at constant velocity. Initially, one target (car) of large radar cross section (RCS) moved in the vicinity of IWR1642. Next, combination of two targets (car and a motor-cycle), three targets (car, a motor-cycle, and a motor-bike), four targets (car, a motor-cycle, and two motor-bikes of varying RCS), and five targets (car, a motor-cycle, two motor-bikes and a pedestrian) were considered for the experimental purpose. Figure. 4.3 shows experimental set-up for two different cases. Figure. 4.3a shows the presence of jamming radar in the vicinity of source radar. Figure. 4.3c shows five targets with a jamming radar sensor while four targets in the absence of spot-jammer are seen in Figure. 4.3b. For each case of experiment conducted, that is for each addition of new target hundred number of frames were collected and data was extracted for 10 s. The source sensor operated in short range radar mode (SRR), for which maximum observable range is 80 m with range resolution of 36.6 cm.

In the second dataset, in addition to five different targets in source vicinity, an intentional stationary jammer operating at the same frequency band (spot-jammer) as that of the source that is, AWR1642 [TI, 2018] was used in experiments. Once again real-time experiments were conducted by spatially changing the distance and angle of the jammer (interferer). For one, two and three target cases, data was taken out by placing jammer at 30^0, line of sight (LOS) and at -30^0 at distances of 2 m, 3 m, and 5 m with respect to source IWR1642. While, for four and five target cases, jammer was placed at a distance of 5 m in LOS to IWR1642. Hundred number of frames were collected for each target case and for each spatial change of jammer (AWR1642).

Table 4.1: Experimental Parameters

Parameters	**SRR mode values**
Idle time (t_i) (μs)	3
Ramp end time (t_e) (μs)	56
Number of ADC samples (N_{adc})	256
Frequency slope (S) (MHz/μs)	8
Number of chirps (M)	128
Chirp duration (T) (μs)	593
ADC sampling frequency (f_s) (ksps)	5000
Range resolution (ΔR) (cm)	36.63
Maximum range (R_{max}) (m)	80

Table 4.1 lists the parameter values set for experiment. The extracted data was in .bin (binary) format. It's processed in MATLAB to convert .bin data to IF data. The obtained IF data matrix is of size $M \times N_{adc}$ (number of chirps in one coherent processing interval×number of ADC samples). Two dimensional fast fourier transform (FFT) was applied on IF data to obtain RD-maps. Further, RD-maps were fed to CA-CFAR, threshold detection scheme to get detections. Furthermore, target detected images were labeled by LabelImg software to train the DL module.

4.2.3 Training Dataset

YOLO algorithm requires marking of the objects in images that has to be fed into it. Purpose of marking is to create ground truth. Here, RD-maps are the images used to train the YOLO model, so LabelImg software is used to mark the detections. A rectangular box is drawn to each of the detection as shown in Figure. 4.4 for a combination of three target case. For each labeled image a text file is generated based on the coordinates of the boxes. The presence of each object in the text file is indicated by the following information: class, x coordinate, y coordinate, width and height of the object enclosed in the rectangular box.

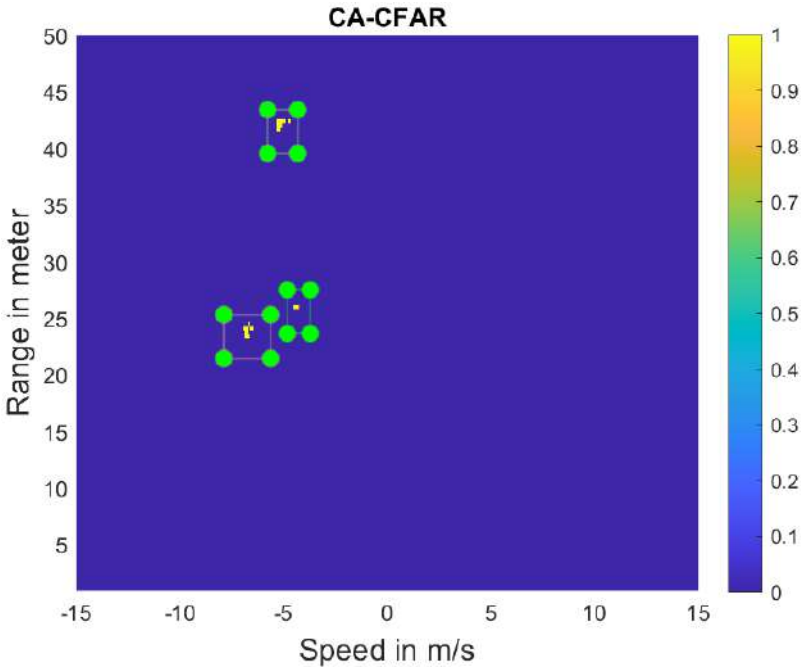

Figure 4.4: Bounding box for three targets RD-map

4.3 Results

As described in the dataset section, 100 frames for each case of the experiment were collected. Hence, total of 500 samples for the scenario in which the jamming radar is absent are obtained. In the scenario where the jamming radar is present, a total of 2900 samples are collected. The labeled dataset is divided in (80, 10, 10) for train, test, and validation. The labeled RD maps from the training set are then used to train the YOLO V5 model as reported in Figure. 4.4. Note that the detections resulted from CA-CFAR technique are also labeled as target class.

Figure. 4.5b and Figure. 4.6b shows the results obtained from the trained YOLO V5 model when applied to some of the images in the test set. Figure. 4.5b refers to the 43rd frame in a one target scenario in which the jamming radar is absent. Figure. 4.5a reports CA-CFAR detection obtained for the same scenario. The probability value for the detection to be classified as the 'target' class is also displayed. On the other hand, Figure. 4.6b refers to the 3rd frame of a one target scenario in which the spot-jamming radar is at 2 m and -30^0 from source. It can be observed that the CA-CFAR detects targets as shown in Figure. 4.5a. YOLO V5 also detects the corresponding target.

Figure. 4.7b and Figure. 4.8b shows the results obtained from the trained YOLO V5 model when applied to some of the images in the test set. Figure. 4.7b refers to

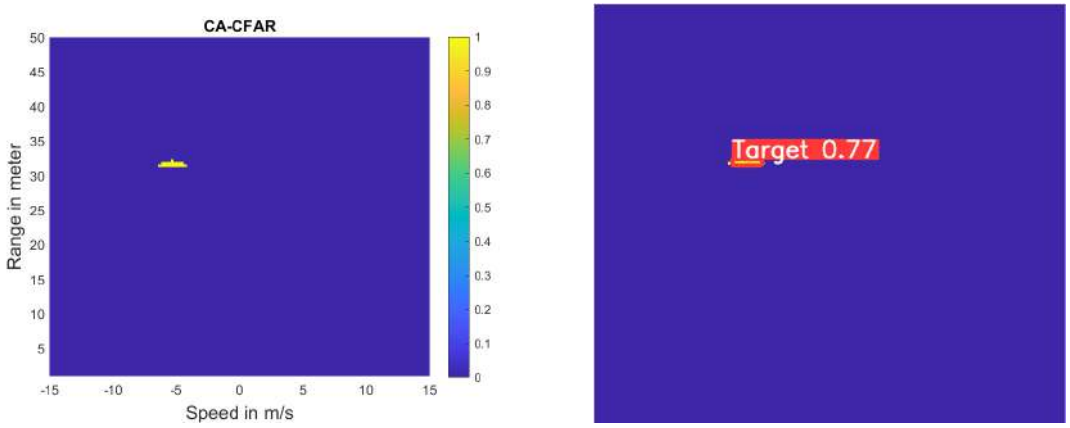

(a) Detections by CA-CFAR (b) Detections by YOLO

Figure 4.5: Detections in absence of spot-jammer

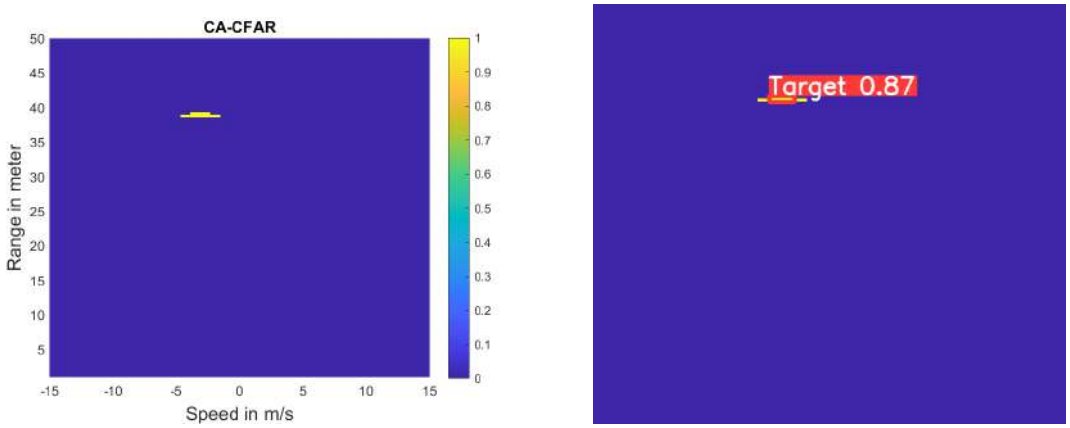

(a) Detections by CA-CFAR (b) Detections by YOLO

Figure 4.6: Detections in presence of spot-jammer

the 54th frame in a 4 target scenario in which the jamming radar is absent. A total of 4 detections were obtained by the CA-CFAR algorithm (refer Figure. 4.7a). It can be observed in Figure. 4.7b that the YOLO V5 also detects the 4 targets. The probability values for all 4 detections to be classified as the 'target' class is also displayed. On the other hand, Figure. 4.8b refers to the 46th frame of a 4 target scenario in which the spot-jamming radar is present. It can be observed that the CA-CFAR detects 2 targets as shown in Figure. 4.8a. YOLO V5 also detects the corresponding 2 targets.

Each detection of the 'target' class by the YOLO V5 algorithm is characterized by drawing a bounding box around the detection. By extracting the centroid of these bounding boxes and mapping the centroid pixel value to the range and velocity span, accurate range and velocity of the target at each frame are obtained. These calculated

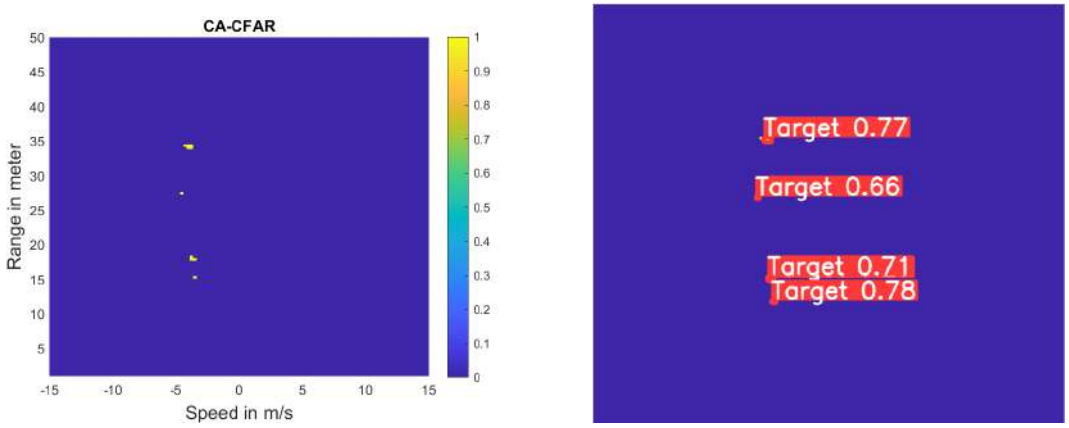

(a) Detections by CA-CFAR (b) Detections by YOLO

Figure 4.7: Detections in absence of spot-jammer

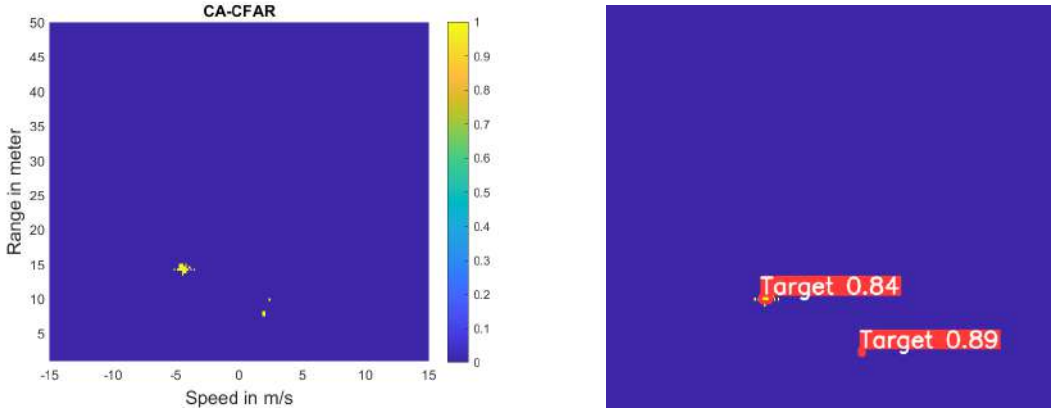

(a) Detections by CA-CFAR (b) Detections by YOLO

Figure 4.8: Detections in presence of spot-jammer

range and velocity values are then compared with the ground truth range and velocity values that can be obtained from the labeled RD-maps. Table 4.2 provides the mean absolute error values for the range and velocity for both with and without jamming scenarios. It can be observed that the mean absolute error for the range value is slightly higher in interfering case as compared to the non-interfering case. This is due to the fact that there are more false reflections in the interfering case.

Figure. 4.9a and Figure. 4.9b reports false detections of targets by YOLO model. Figure. 4.9a is without jammer, two target case for frame 87. Here, CA-CFAR identifies three detections but YOLO model reports the false reflection, which is denoted by low probability value. Similarly, Figure. 4.9b also has a target detected by low probability, which is once again a false detection for, with jammer one target case

Table 4.2: Error values

Environment	**Range in m**	**Velocity in m/s**
Non-interfering	0.1998	0.133
Interfering	0.2255	0.0293

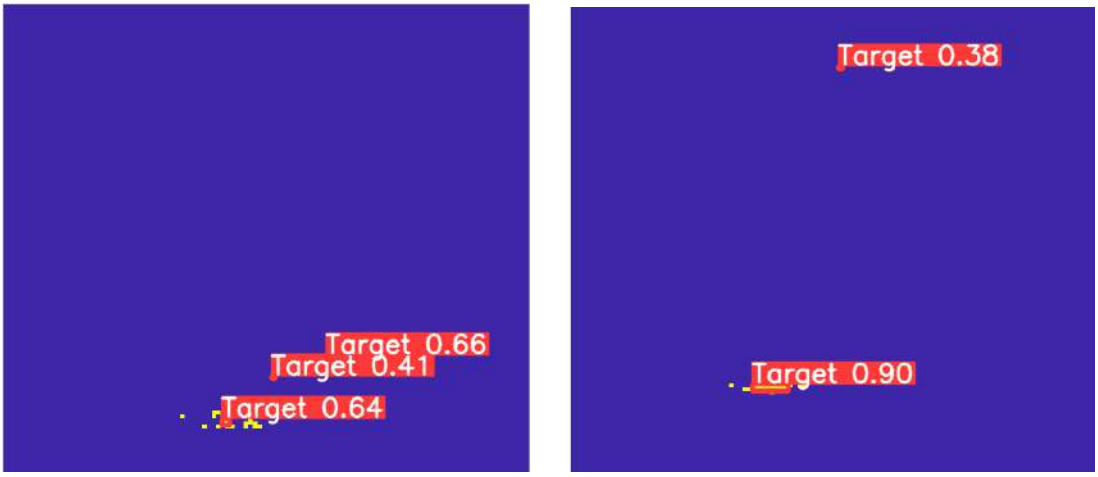

(a) Interference free environment (b) Interference environment

Figure 4.9: Miss-detection of targets

with interfering radar located at 2 m distance and at 30^0 angle with respect to source radar for frame 57. It was observed, with jammer case has more number of false reflections as compared to without jammer cases.

4.4 Conclusion

For the real-time experiments conducted using mmWave radar sensor in the prsence of interfering radar, multiple moving targets are detected by DL YOLO V5 model. DL model was trained by the detcetions obtained by RD-maps of CA-CFAR algorithm.

Chapter 5

Algorithms to Mitigate Mutual Interference in FMCW Radars

In this chapter two different algorithms namely, weighted beat signal normalization and clipping with hampel filtering to mitigate mutual or senor-to-sensor interference in FMCW radars are described. Simulation results for the same are reported.

5.1 Problem Formulation

In this section, the mathematical model of mutual interference is derived.

5.1.1 Mathematical model

Consider a dense on-road traffic model as shown in Figure. 5.1a, where the primary radar is on the ego vehicle, and other secondary radars are on the traffic participants. Here traffic participants refer to other on-road vehicles. A FMCW radar is considered an automotive radar. The primary radar faces mutual interference from the secondary radars within the field of view (FoV) and vice-versa. The primary duty of the mmWave radar is to get the detections of the targets within the FoV to perform the functionalities like automatic cruise control, emergency brake assists, path following, etc.

A Interference free environment

The primary radar transmits the FMCW signal with a chirp of duration T_r and slope of S with minimum carrier frequency f_{min}. The mathematical representation of the

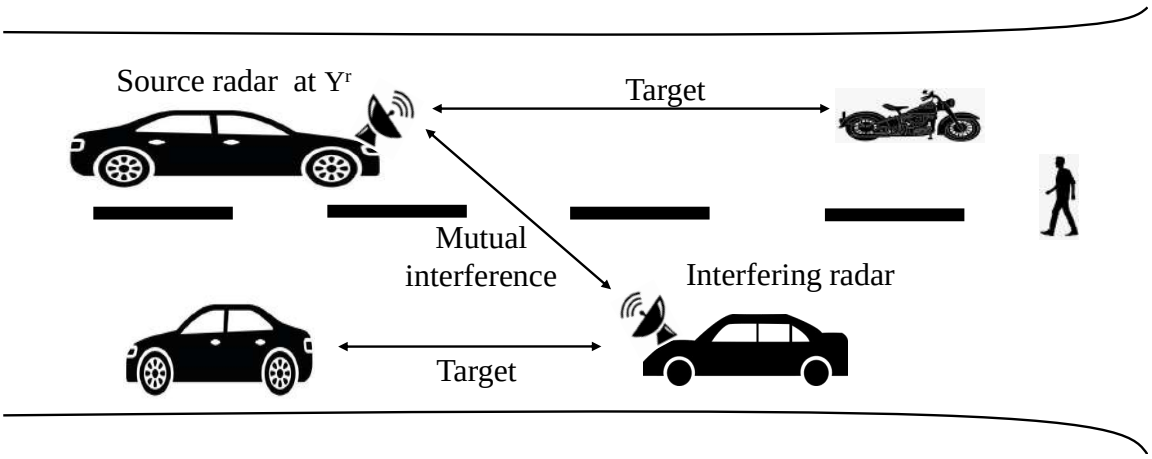

(a) Mutual interference to primary radar

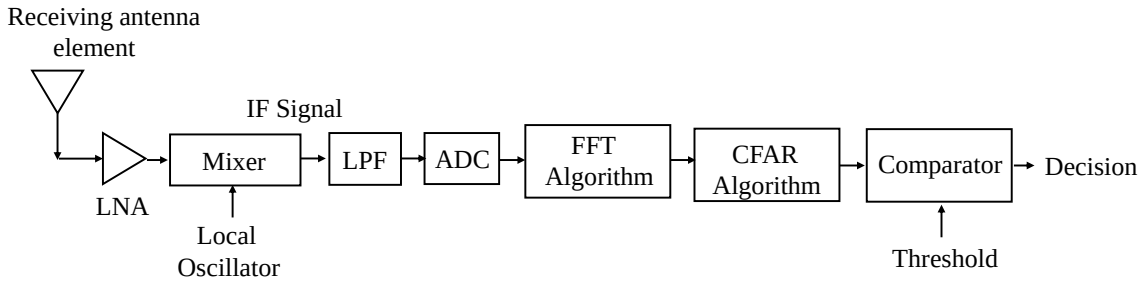

(b) Process flow

Figure 5.1: Illustration of scenario and traditional detection algorithm steps

transmitted signal $s_t(t)$ is

$$s_t(t) = A_t \exp(2\pi j f_{min} t + j\pi S t^2);\ 0 \leq t \leq T_r. \tag{5.1}$$

Here, A_t is amplitude of the transmitted signal. The slope S is given by

$$S = \frac{f_{max} - f_{min}}{T_r}. \tag{5.2}$$

From the Eqn. 5.1, the first part of the exponential signal contains carrier frequency. Whereas, the second part of the exponential signal in Eqn. 5.1 provides frequency of the transmitted signal, and is given by

$$f_T(t) = 2\pi \int_0^t S\ t\ dt. \tag{5.3}$$

The signal $s_t(t)$ impinge on targets and reflected back as $r(t)$. The received signal from N targets with in FoV is modelled as

$$r(t) = \sum_{i=1}^{N_t} A_{ri} \exp(2\pi j f_{min}(t - \tau_i) + j\pi S(t - \tau_i)^2);\ 0 \leq t \leq T_c. \tag{5.4}$$

Here, A_{ri} is the received amplitude and τ_i is the round-trip time delay from target i. The received signal frequency component corresponds to target i is represented by

$$f_{rxi}(t) = 2\pi \int_0^t (S\ (t - \tau_i) + f_{dri})\ dt. \tag{5.5}$$

Meanwhile, the round trip corresponds to target i is

$$\tau_i = \frac{2(R_{0i} + v_i t)}{c} \tag{5.6}$$

with R_{0i} as the starting range of target i, c is velocity in free space, and v_i is the i^{th} moving target velocity. Similarly, the f_{dri} is Doppler shift of target i and given by

$$f_{dri} = \frac{2v_i}{\lambda}, \tag{5.7}$$

where λ represents the wavelength of the wave.

The received signal $r(t)$ is fed to the mixer as shown in Figure. 5.1b, and thereafter low pass filtering (LPF) takes place. The higher frequencies are removed and down-converted signal is given by

$$r_s(t) = \sum_{i=1}^{Nt} A_i \exp(2\pi j f_{min} \tau_i + j2\pi t(S\tau_i - f_{dri})). \tag{5.8}$$

This signal, $r_s(t)$ is converted to digital by analog to digital converter (ADC) and then fast Fourier transform (FFT) followed by a constant false alarm rate (CFAR) detection scheme is applied to get the target detections. For simplicity, and for better understanding, let us consider targets are within FoV without any mutual interference and follows the process flow given in Figure. 5.1b. Therefore, the beat frequency can be visualized as shown in Figure. 5.2a; corresponding target detections are visualized as given in Figure. 5.2b.

B Interference environment

In this case, the total received signal of the primary radar is due to two reasons. The first signal is due to primary radar transmitted-reflected back from Nt targets as given in Eqn. 5.8. The second signal is due to MI secondary radars transmitting and primary radar receiving them, as shown in Figure. 5.1a. In this model, it is assumed that all the mmWave radars are of the same type: same frequency, bandwidth, and chirp duration. The received signal is modelled as

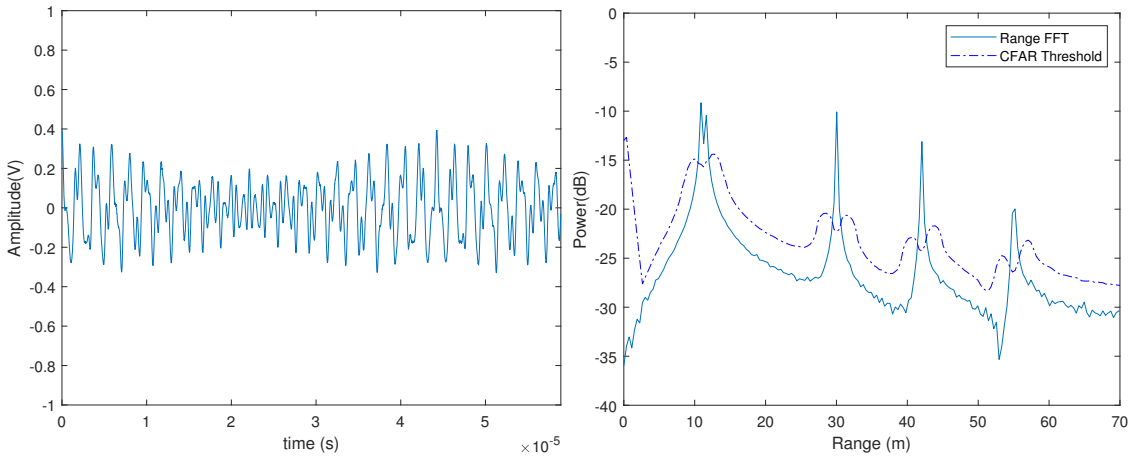

(a) IF signal (b) Detections

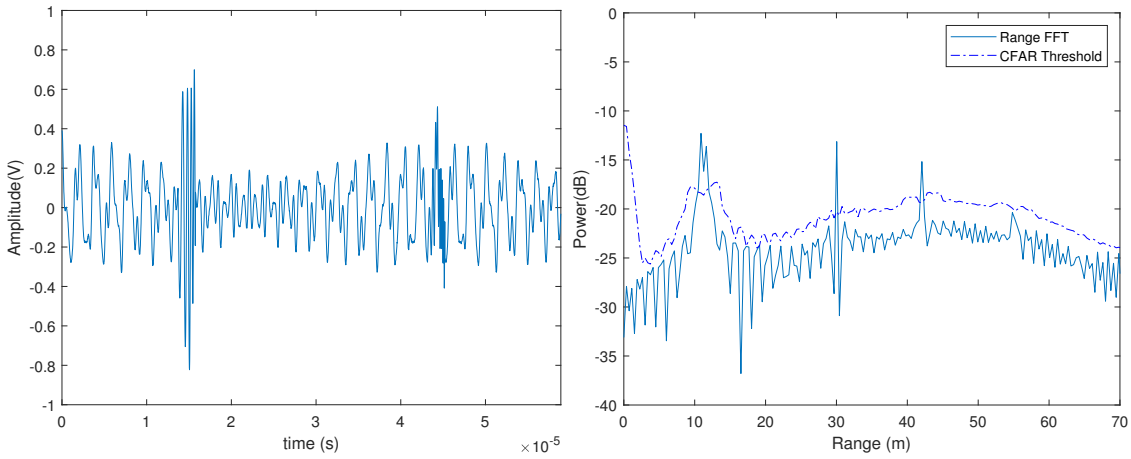

(c) IF signal (d) Detections

Figure 5.2: (a) Beat signal without interference (b) Detections in interference free environment (c) Beat signal with interference and (d) Detections in interference environment

$$r^I(t) = \sum_{i=1}^{Nt} A_i \exp(2\pi j f_{min}(t-\tau_i) + j\pi S(t-\tau_i)^2) + \sum_{j=1}^{MI} A_j \exp(2\pi j f_{min}\tau_j' + j\pi S\tau_j'^2);\ 0 \le t \le T_r, \tag{5.9}$$

The whole received signal is passed through the mixer and LPF to attain IF signal as

Table 5.1: Range of targets inserted

	Range of targets inserted in m				
Environment	**Target 1**	**Target 2**	**Target 3**	**Target 4**	**Target 5**
Interference free	10.8	11.6	30	42	55
Interference	10.8	11.64	30.4	42	54.8 (not detected)

$$r_s^I(t) = \sum_{i=1}^{Nt} A_i \exp(2\pi j f_{min}\tau_i + j2\pi t(S\tau_i - f_{dri})) + \sum_{j=1}^{MI} \exp(2\pi j(f_{min} + f_{drj})(t + \tau_j') + j\pi S(t^2 + \tau_j'^2)). \quad (5.10)$$

Similar to the non-interference case, the IF signal is passed through ADC, FFT, and CFAR blocks to get the target detections. To simplify the problem, consider five targets ($Nt = 5$) and two interference source ($MI = 2$). The same traditional process is repeated for interference case; the IF signal comes as shown in Figure. 5.2c, and corresponding detections appear in Figure. 5.2d. It is to be observed that there is missed target detection due to mutual interference.

Table 5.1, gives the comparison of target range in interference free and interfering environment. Five targets were inserted at 11 m, 11.5 m, 30 m, 42 m, and 55 m. All five targets are detected in non-interfering environment at the ranges as given in Table 5.1. But the power level of the echo signal received is less in interfering environment compared to non-interfering scenario as seen in Figure 5.2b and Figure 5.2d. This resulted in missed detection of a target at 55 m (refer Figure 5.2d).

5.2 Proposed Algorithms

Two algorithms, proposed process flow and respective results are briefly explained in this section.

5.2.1 Weighted beat signal normalization

This algorithm identifies changes in the IF signal and further minimizes the amplitude by comparing the IF signal envelope with the threshold. The threshold is calculated by using the forward and backward samples. Further, the IF envelope of the beat signal is

normalized by the threshold. Thus, the signal-to-interference ratio (SINR) is increased by nullifying the interference signal. The algorithm's pseudo-code to mitigate the interference by considering the IF signal as input is described in Algorithm 1.

Algorithm 1: Pseudo-code of Weighted beat signal normalization

Input: IF Signal $\{x_t\}_{t=1}^{l}$
Output: Weighted and normalized beat signal
Step 1: Forward Sliding
$\mathbf{x_t^{maxF}} = max(abs(x_{t\ mod\ l}))$
Estimate the maximum envelope by forward sliding window of length l.
Step 2: Backward Sliding
$\mathbf{x_t^{maxB}} = max(abs(x_{t\ mod\ l}))$
Estimate the maximum envelope by backward sliding window of length l.
Step 3: Estimate minimum
$\mathbf{r_t} = min_t(x_t^{maxF},\ x_t^{maxB}))$
Minimum of either forward or backward envelope is chosen.
Step 4: Estimate weights
$w_t = \frac{1}{r_t}$
IF signal is normalized by the weights w_t in each sliding window.

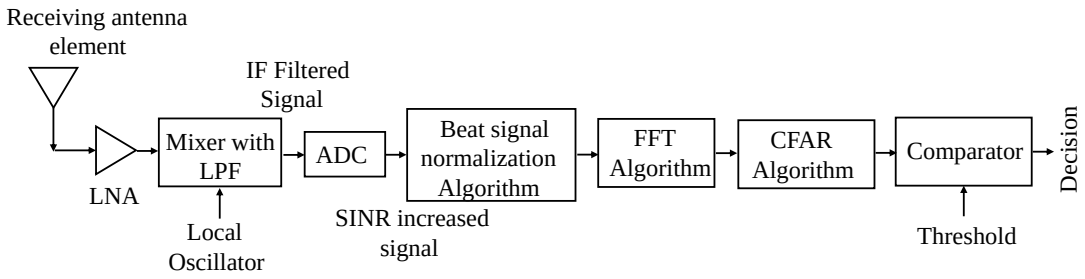

Figure 5.3: Process flow for interference environment

A Proposed Process flow

This algorithm can either nullify the interference effect or decrease the number of false detections. The algorithm block is easy to implement as an additional processing block rather than modifying the existing hardware. The proposed approach of nullifying the effect is in the time domain IF signal; hence, it can be the next processing block. The sharp peaks within IF are nullified by using a to-and-fro windowing technique. Therefore, the process occurs for every chirp signal and does not require any previous history. Figure. 5.3 gives the modified process flow to detect targets in the presence of interference.

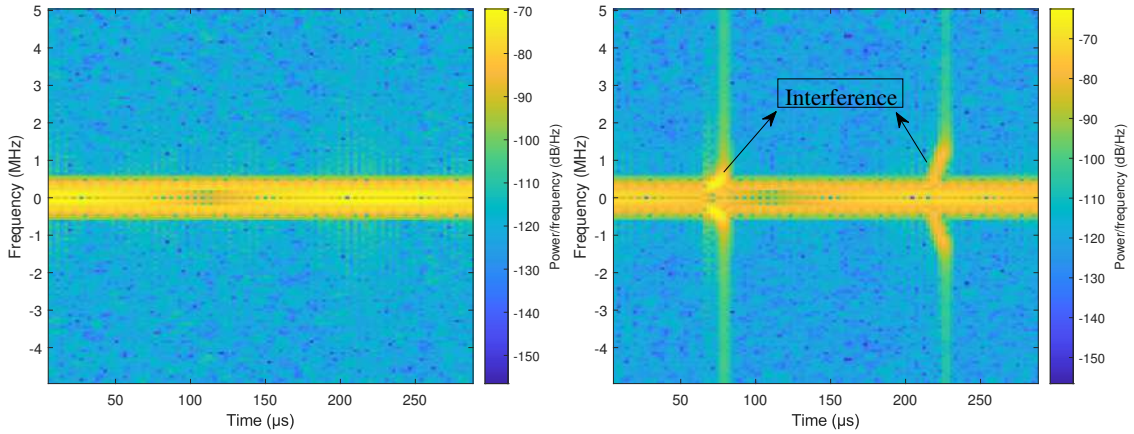

(a) without interference (b) with interference

Figure 5.4: STFT of IF signal (a) without interference (b) with interference.

B Simulation Scenario

To illustrate the scenario, consider the mmWave radar which is operating in 77 GHz with a chirp duration of 59 μs, bandwidth of 400 MHz, and sampling frequency is set to 50 MHz. Five targets are injected at 11 m, 11.5 m, 30 m, 42 m, and 55 m respectively. Inorder to analyse detections of closely spaced targets, two targets were positioned at 11 m and 11.5 m, having separation distance of 0.5 m, which is slightly greater than range resolution (0.375 m). If two target separation distance is kept below 0.375 m, then those two targets are not resolved as two instead, those two targets are identified as one. The maximum range of the radar considered is 70 m. The interference is introduced in the mmWave radar with the same frequency. Due to the interference, the disrupted IF appeared as shown in Figure. 5.2c. Meanwhile, the time-frequency plot by applying STFT on the IF can be visualized in Figure. 5.4. Figure. 5.4a shows STFT on non-interfered IF signal while Figure. 5.4b shows STFT on interfered IF signal. It is clearly seen an abrupt bends in time-frequency plot (refer Figure. 5.4b).

C Target Detection

The weighted beat signal normalization algorithm block is to process the IF signal as shown in Figure. 5.3. In this proposed algorithm, the window size is tunable paramater, which moves both forward and backward in sliding fashion. On the processed IF signal, one-dimensional FFT is applied followed by CA-CFAR (cell averaging -

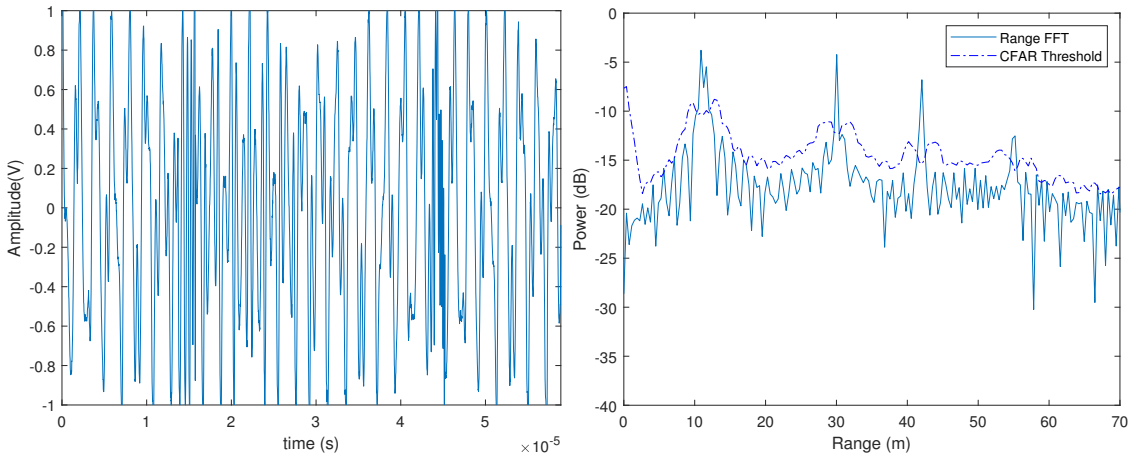

(a) Weighted IF signal (b) Detections

Figure 5.5: (a) Weighted IF signal and (b) Detections by proposed algorithm for window length 80

CFAR) detection technique, with one guard cell and six neighbouring cells.

In no-interference case, five targets are detected at 10.8 m, 11.6 m, 30.04 m, 42 m, and 54.8 m as shown in Figure. 5.2b. Whereas in the case of interference, the traditional detection algorithm (refer Figure. 5.1b) leads to missed detections (refer Figure. 5.2d). In-order to detect targets immersed in interference, the proposed process flow (refer Figure. 5.3) is used. The Figure. 5.5a depicts the weighted and normalized beat signal with window size of 80. Similarly, it is observed that sucessful detections are reported in Figure. 5.5b, by adopting the proposed process flow.

D Impact of Window Size

The only tunable parameter in this process is window size. Hence, the effect of window length on target detection is provided in Table 5.2. It also provides explanation, regarding detection of targets with varying window size. False detections for lower window size (20 and 50) are noticed. Further, increase in the window size (beyond 1500) reports missed detection. Figure. 5.6a and Figure 5.6c gives the weighted and normalized IF signal for the window length 20 and 3000 respectively. Here, because of the selection of too less or more number of samples within a window length, the IF signal is not uniformly normalized, causing missed or false detections. Figure. 5.6b shows target detections with window length of 20, it is noticed that in addition to the detections of five targets, there are few more detections reporting false alarms. The

Table 5.2: Impact of Window length

Window length	False detections	Missed detections	Inference
20	Yes	No	In addition to true targets, 5 more detections were observed
50	Yes	No	In addition to true targets, 3 more detections were observed
90	Yes	No	In addition to true targets, one false detection was noticed
1000	Yes	No	In addition to true targets, 2 more detections were observed
1500	No	Yes	Only four targets detected, one of it is missed
2000	No	Yes	Only four targets detected, one of it is missed
2500	No	Yes	Only four targets detected, one of it is missed
3000	No	Yes	Only four targets detected, one of it is missed

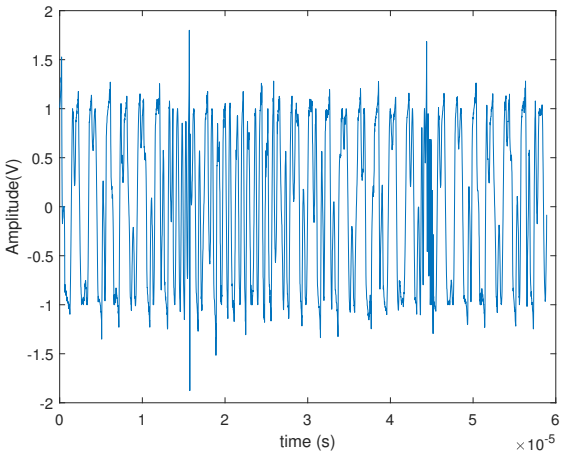

(a) Weighted IF signal

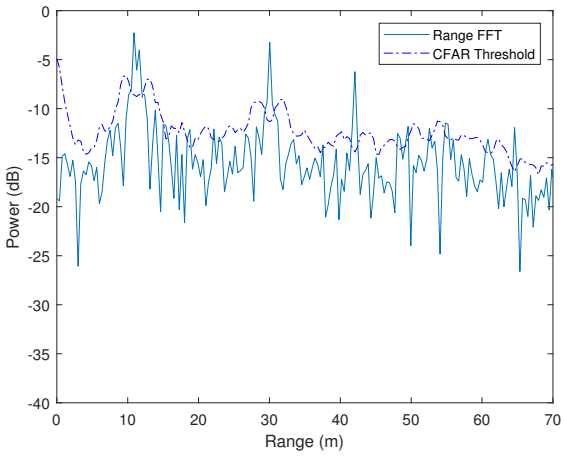

(b) Detections for window length 20

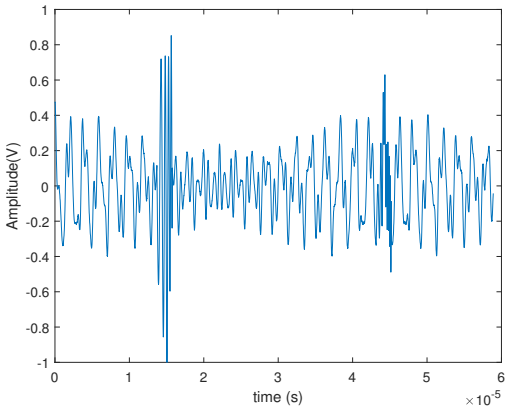

(c) Weighted IF signal

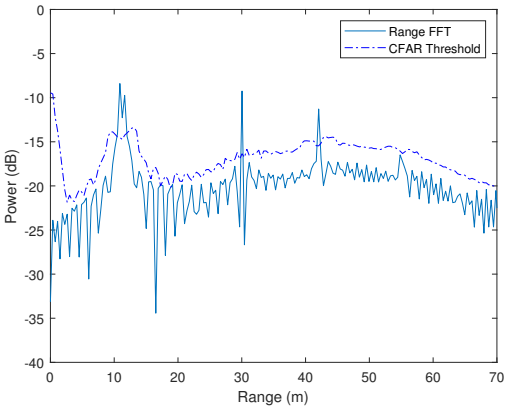

(d) Detections for window length 3000

Figure 5.6: (a and c) Weighted IF signal and (b and d) Detections by proposed method showing false and missed detection.

reason behind this false alarm is due to small window size and inturn increased noise power compared to CFAR threshold. Further, Figure. 5.6d gives target detections at 10.8 m, 11.6 m, 30.04 m, and 42 m. Target at 55 m is missed. This missed detection arises since more number of samples fall within the same window length. Upon normalizing by the weights, the power is reduced and resulted in missed detection by CFAR algorithm. Hence, one has to choose the window size in such a way that, only true target information's are obtained.

5.2.2 Clipping and Hampel Filtering

The algorithm is proposed by exploiting clipping followed by Hampel filtering the interfered beat signal. As observed from Figure. 5.7c, the IF signal has drastic changes in amplitude at certain time instants compared to the non-interfered IF signal (refer

Figure. 5.7a). Therefore, firstly these variations in amplitudes are clipped off by the use of a clipper. Clipping is done on both the positive and negative sides of the signal. Threshold for the positive clipper is set to a level equivalent to the standard deviation (std) of the interfered IF signal, while for the negative clipper threshold is -std. Further, the clipped signal passes through the Hampel filter, which is a type of median filter. The Hampel filter accepts window size as input. For each sample, the filter calculates the median value of a window consisting of the sample and its neighboring samples specified by the window size on either side of the sample. The filter also estimates the standard deviation for each of the samples about its local median. If a sample differs from the median by more than the standard deviation specified, it is replaced with the median. Thus, it detects and eliminates the outliers and smoothens the signal. The pseudo-code of the proposed algorithm is described in Algorithm 2 which suppresses the interference by examining the IF signal.

Algorithm 2: Pseudo-code of proposed method

Input: Interfered beat signal $\{b_t\}_{t=1}^{l}$
Output: Clipped and median filtered signal
Step 1: Clipping
1. If ($\{b_t\}_{t=1}^{l} > std$) then
($\{b_t\}_{t=1}^{l} = std$) Positive clipping of beat signal.
2. If ($\{b_t\}_{t=1}^{l} < -std$) then
($\{b_t\}_{t=1}^{l} = -std$) Negative clipping of beat signal.
Step 2: Filtering by hampel filter
1. Choose the sliding window size.
2. Determine the median value for each window.
3. Compare each sample of the window to a local median.
4. Replace the sample with local median if it exceeds threshold.
If ($\{x_t\}_{t=1}^{l} > med$) then
($\{x_t\}_{t=1}^{l} = med$)

A Process Flow

Figure. 5.8 gives the signal processing blocks involved in the proposed method to detect targets in an interference environment. The proposed technique minimizes the interference effect. Clipper and Hampel filter are the two new blocks employed in this approach compared to the traditional way of detection (refer Figure 5.1b). The IF signal has to pass through these two blocks. Thus, it is simple to implement as it does

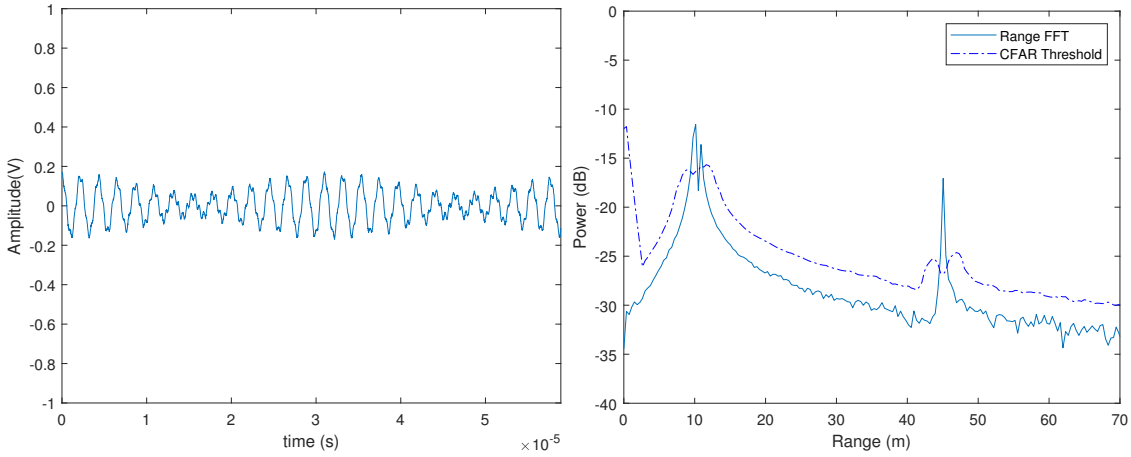

(a) Beat signal without interference

(b) Detections without interference

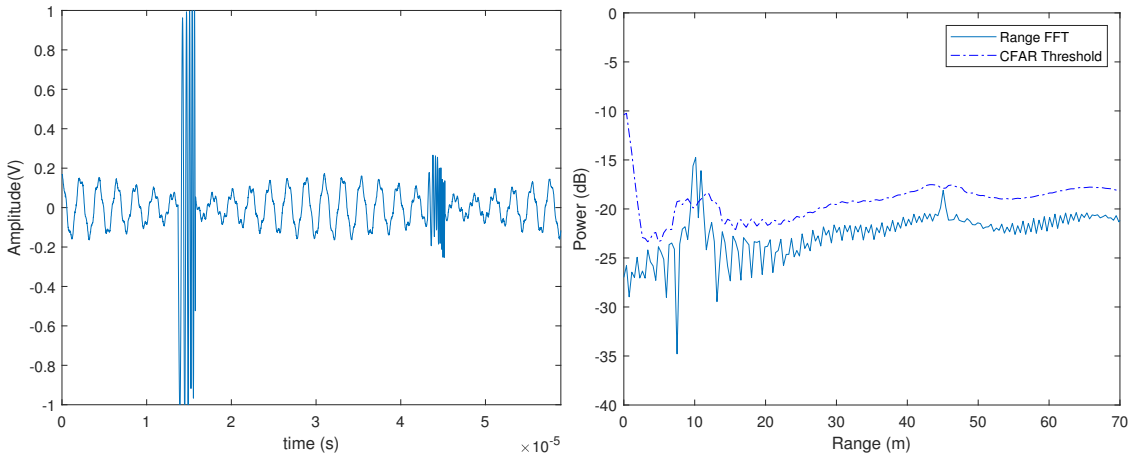

(c) Beat signal with interference

(d) Detections in interference environment

Figure 5.7: (a and c) Beat signal without and with interference (b and d) Detections without and with interference.

not disturb the present hardware. In either of the two blocks, the input signal samples are compared to a threshold and if the sample value is greater than the threshold it is replaced with the threshold determined by the respective block.

B Simulation Scenario

To examine the scenario, consider the FMCW radar operating at 77 GHz with 59 μs as chirp duration, and the sampling frequency is set to 50 MHz. Three targets are injected at 10 m, 10.7 m, and 45 m, respectively. A similar FMCW radar is used to introduce interference of the same frequency and the corrupted IF signal is given in Figure. 5.7c.

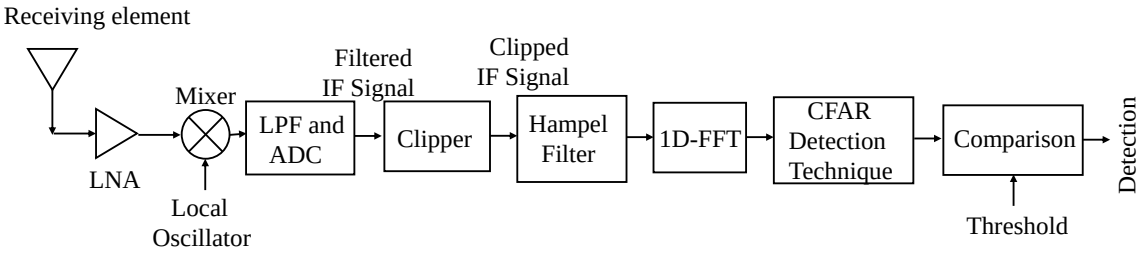

Figure 5.8: Proposed Process flow for interference environment

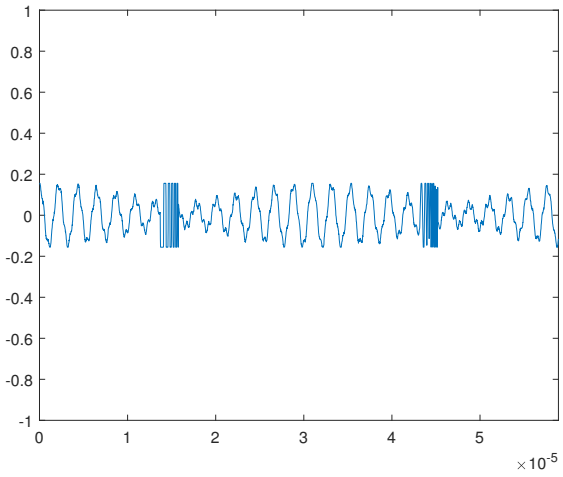

(a) Clipped IF signal

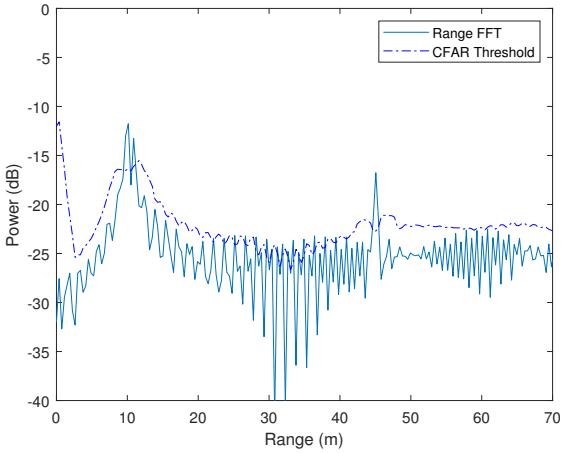

(b) Detections by clipped signal

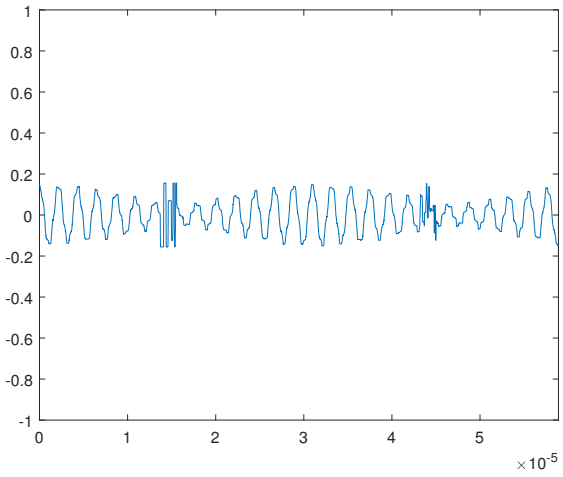

(c) Hampel filtered IF signal

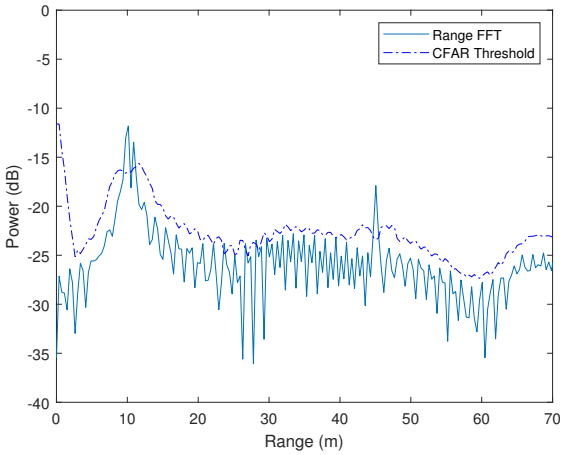

(d) Detections by hampel filter

Figure 5.9: (a) Clipped beat signal (b) Detections by clipped signal (c) Clipped and hampel filtered signal and (d) Detections by proposed algorithm for window size 9.

C Target Detection

The interfered IF signal is processed by the flow described in Figure. 5.8. The threshold for the clipper block is set to the standard deviation of the IF and the window

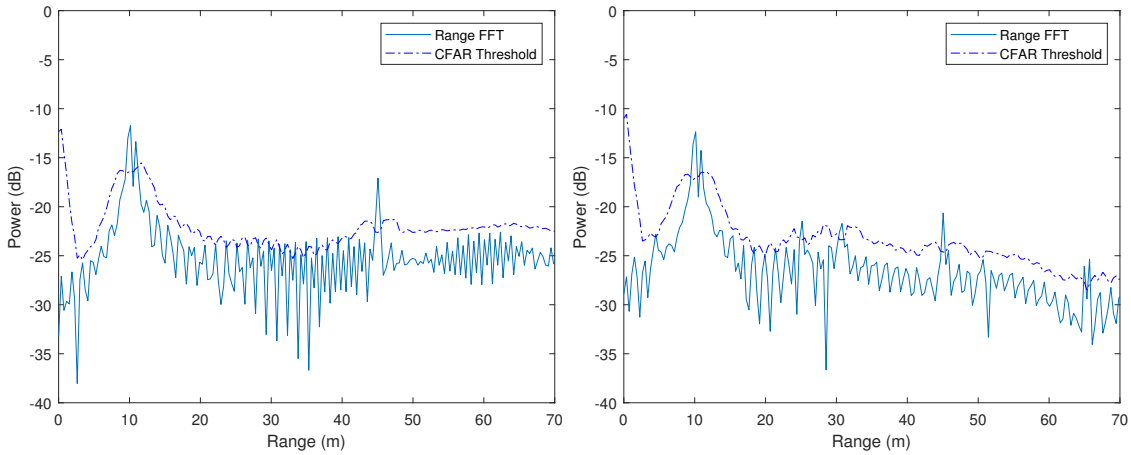

(a) Detections for hampel window length 5 (b) Detections for hampel window length 25

Figure 5.10: The proposed method shows false and missed detections for variable window length.

length of the Hampel filter is 9. Further, it passes through FFT to obtain a range-profile and then to the CFAR algorithm for detection. In CFAR threshold is computed by considering six adjacent cells and one guard cell.

Without interference case, the injected targets are detected at 10.1 m, 10.8 m, and 45.06 m respectively as reported in Figure. 5.7a. While by employing the traditional approach (refer Figure. 5.1b) to detect in presence of interference, two targets are detected at 10.1 m and 10.8 m and target at 45 m is missed (refer Figure. 5.7d). Thus, the proposed process flow for the detection of targets immersed in interference is used. Initially, it was tried to get detections by adopting a clipping block alone. For the same, the clipped IF signal is reported in Figure. 5.9a, and corresponding detections are, as in Figure. 5.9b. From Figure. 5.9b, false alarms are noticed. Thus, to detect true targets, this clipped-off signal (Figure. 5.9a) is passed through the hampel filter, to remove outliers. Figure. 5.9c shows the Hampel filter output and Figure. 5.9d gives the target detections at 10.1 m, 10.8 m, and 45.06 m for the hampel window size of 9.

D Impact of hampel filter

Here, window length is the variable parameter, which affects the detections. Figure. 5.10a and Figure. 5.10b represent the detections obtained for the window size 5 and 25 respectively. Figure. 5.10a shows targets detected at 10.1 m, 10.8 m, and

45.06 m, in addition false alarms are observed. Whereas Figure. 5.10b shows detections at 10.1 m, 10.8 m, 25.1 m, 30.7 m, 45.06 m, 64.9 m, and 65.7 m. Once again reporting false detections. Thus, varying the window length affects the performance. Therefore, one has to go with adaptive window length, to improve the performance of the proposed method.

5.3 Target detection in presence of clutter

Beyond the usage of mmWave radar sensors to detect targets, a work was carried to detect targets in clutter environment. Here, in this section a filter used to detect such targets is presented. Simulation results reports detection of multiple moving targets immersed in ground clutter.

Space-Time Adaptive Processing (STAP) is a radar signal processing technique used for suppression of clutter and jammer to detect moving targets in the presence of strong interference. Detection of targets has to be done in presence of severe clutter environment and also in the presence of jammers. Airborne radars will search for moving targets within its visible range. Because of the platform motion, the clutter seen by an airborne radar is spread across zero Doppler region. Ground targets moving at low velocity possess less Doppler and as a result may be buried in the clutter region. That is, Doppler spectrum may mask the potential targets. Clutter returns also depend on the direction of movement. Thus, echo returns depend on angle of arrival (AoA) and Doppler. So clutter suppression has to be done in two dimensional space (space and time) [Klemm and Mertens, 2008].

In 1973 Brennan and Reed published the first paper on STAP. In 1994 a report on STAP for airborne radar was given J.Ward. Further Klemm gave the degrees of freedom (DoF) for an airborne radar [Ward, 1998]. From the literature STAP filter works on radar data cube (3 dimensional data - Space, Time and Range) generated by antenna elements, pulses in one Coherent Processing Interval (CPI) and the range bins. Spatial dimension is got by using array of antenna elements (N). Temporal dimension comes from coherent train of pulses (M). The received signals are sampled at a series of L ranges referred to as range gates. STAP processing is applied to M×N matrix of samples collected at each such range. The received data for each range bin

may be organized into N×M matrix. This matrix is called a snapshot. The ensemble of snapshots at all successive ranges is referred to as a data cube and contains all the information available for target detection within a CPI [Lapierre et al., 2006]. The STAP filter has NM taps (spatio-temporal degrees of freedom, DoFs) and has to estimate these weight in such a way to maximize the return from desired target range cell at the same time minimizing returns from clutter. Interference will not be known a priori, which changes with time and in space. This interference characteristics have to be estimated in real time, which will be done based on the snapshots.

Fully adaptive STAP algorithm requires large number of training data (secondary data - data from adjacent range cells) to estimate the clutter covariance matrix. If a covariance matrix needs to be estimated accurately, then about 2NM to 3NM independent, identically distributed (i.i.d.) secondary data samples are required [Adve et al., 2000]. It is impractical to have such a large number of i.i.d. samples even if there are such large number of samples, that will lead to computationally expensive. Therefore, reduced dimension (RD) and reduced-rank (RR) STAP was proposed [William et al., 2004] with the intent to reduce computational burden and the number of secondary data for adaptivity. In both RR and RD STAP, methods data is applied for transformations to reduce the DoF. Further, RR STAP methods have the benefit of reduction in training data support but the processor must compute eigen values and eigen vectors of the interference covariance matrix, in real time, which has practical constraint.

Thus, in order to reduce the computational load while simultaneously maintaing the detection performance, limited channel based STAP techniques have been proposed. One sum channel (Σ), two difference channels (Δ) (difference azimuth (Δ_a) and difference elevation (Δ_e) and few guard channel could be used. $\Sigma\Delta$-STAP (sigma-delta-STAP) is one such algorithm which uses one sum channel and one difference azimuth. It requires less training samples compared to fully adaptive STAP. Authors in [Brown et al., 2000] Used only two channels, they proved that this method has a better clutter compression as compared to STAP that uses large number of channels. Further, authors in [Moo, 2001] performed simulation was done using the software RL-STAP for both homogeneous clutter environment as well as heterogeneous clutter environment. They proved that partially adaptive STAP techniques like post-Doppler

STAP and adjacent bin STAP shows a better performance when compared to fully adaptive STAP amidst computational complexity. In another communication authors in [Zhang and Wang, 1997] eliminates the drawback of the DPCA method by using two channels such as Sum and Difference. This has better clutter suppression as compared to the traditional STAP method that uses large number of channels. Most of the literature above focuses about clutter suppression but not about detection of multiple moving targets. Multiple target scenario has not been investigated in these contributions. Therefore, there is a need to carry out research in the multiple target detection using $\Sigma\Delta$ (Sigma-Delta)-STAP. This motivated us to conduct current research investigation of multiple target detection using $\Sigma\Delta$ -STAP.

This work is organised as follows: In section II $\Sigma\Delta$-STAP along with the generation of clutter is described. Section III provides problem formulation, while simulated results are discussed for detection of single and multiple moving targets at different velocities in section IV.

5.4 Sum and Difference ($\Sigma\Delta$)-STAP and Airborne clutter generation

5.4.1 $\Sigma\Delta$-STAP

In fully adaptive STAP the optimum weights that maximizes signal to interference plus noise ratio satisfies Weiner-Hoff [Guerci, 2014] equation is given by

$$w = R^{-1}s \tag{5.11}$$

where s is the desired target signal of interest and R is the clutter-plus-jamming-plus-noise covariance matrix. Since interference is not known a priori, the covariance matrix R is estimated by using secondary data as given by

$$\hat{R} = \frac{1}{L}\sum_{k=1}^{L} x_i x_i^{'} \tag{5.12}$$

where x_i denotes the target free snapshot, L is the number of training snapshots. The conventional STAP algorithm requires large number of training data (secondary data - data from adjacent range cells) to estimate the clutter covariance matrix as

shown in Figure. 5.11. Making use of large number of training data leads to computational load, so number of receiving channels have to be reduced. Figure. 5.12 shows block diagram of two channel STAP ($\Sigma\Delta$-STAP).

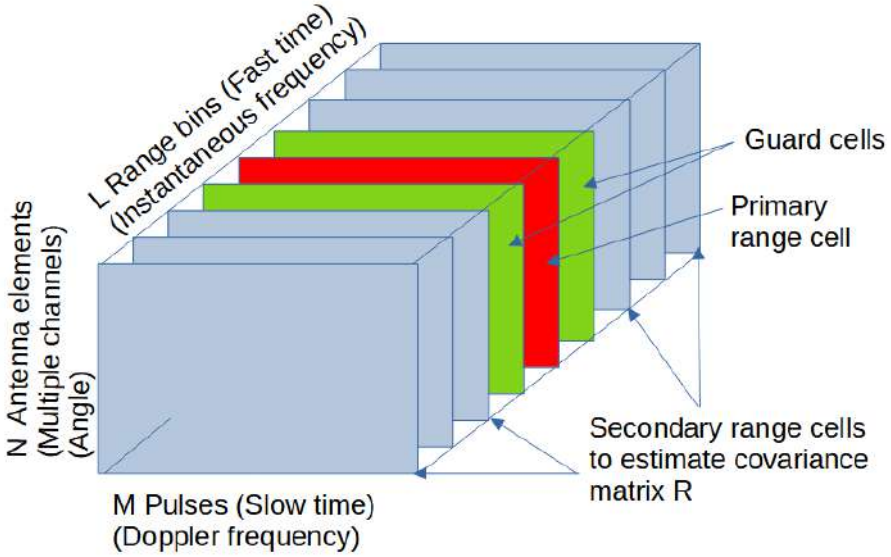

Figure 5.11: Structure of Radar Data cube

The adaptive processing is applied to digitized sum and difference channels. STAP for clutter suppression with sum and difference beams was proposed by [Brown et al., 1996, 2000]. $\mathbf{X}_\Sigma$ is sum and $\mathbf{X}_\Delta$ is difference channel data of a range cell before temporal DoF reduction. The data after reduction is given by

$$\tilde{\mathbf{X}}_{\mathbf{\Sigma}} = \mathbf{Q}^{\mathbf{H}}\mathbf{X}_{\mathbf{\Sigma}} \tag{5.13}$$

$$\tilde{\mathbf{X}}_{\mathbf{\Delta}} = [\mathbf{I}(\mathbf{N}_{\mathbf{ps}}) \otimes \mathbf{Q}^{\mathbf{H}}]\mathbf{X}_{\mathbf{\Delta}} \tag{5.14}$$

Where Q is the temporal DoF reduction matrix, N_{ps} is the number of difference channel. Let s_t be the temporal steering vector of a chosen Doppler bin and denote

$$\tilde{\mathbf{s}}_{\mathbf{t}} = \mathbf{Q}^{\mathbf{H}}\mathbf{s}_{\mathbf{t}} \tag{5.15}$$

$$\tilde{\mathbf{x}} = \begin{bmatrix} \tilde{\mathbf{x}}_{\mathbf{\Sigma}} \\ \tilde{\mathbf{x}}_{\mathbf{\Delta}} \end{bmatrix} \tag{5.16}$$

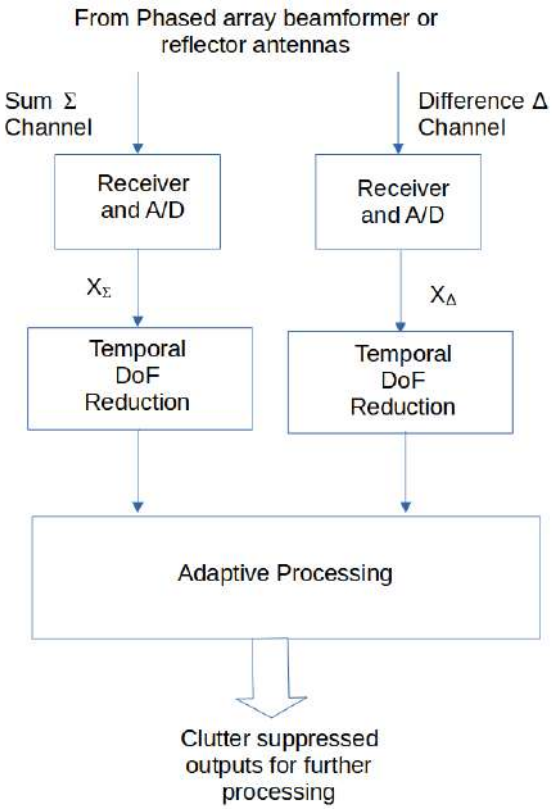

Figure 5.12: Block diagram of ΣΔ-STAP [Brown et al., 1996, 2000]

The maximum likelihood estimate of the covariance matrix is given by

$$\hat{\mathbf{R}} = \begin{bmatrix} \hat{\mathbf{R}}_{\Sigma\Sigma} & \hat{\mathbf{R}}_{\Sigma\Delta} \\ \hat{\mathbf{R}}_{\Sigma\Delta} & \hat{\mathbf{R}}_{\Delta\Delta} \end{bmatrix} \tag{5.17}$$

where,

$$\hat{\mathbf{R}}_{\Sigma\Sigma} = \frac{1}{L}\sum_{k=1}^{L} \tilde{\mathbf{x}}_{\mathbf{\Sigma l}} \tilde{\mathbf{x}}_{\mathbf{\Sigma l}}^{H} \tag{5.18}$$

$$\hat{\mathbf{R}}_{\Sigma\Delta} = \frac{1}{L}\sum_{k=1}^{L} \tilde{\mathbf{x}}_{\mathbf{\Sigma l}} \tilde{\mathbf{x}}_{\mathbf{\Delta l}}^{H} \tag{5.19}$$

$$\hat{\mathbf{R}}_{\Delta\Sigma} = \frac{1}{L}\sum_{k=1}^{L} \tilde{\mathbf{x}}_{\mathbf{\Delta l}} \tilde{\mathbf{x}}_{\mathbf{\Sigma l}}^{H} \tag{5.20}$$

$$\hat{\mathbf{R}}_{\Delta\Delta} = \frac{1}{L}\sum_{k=1}^{L} \tilde{\mathbf{x}}_{\mathbf{\Delta l}} \tilde{\mathbf{x}}_{\mathbf{\Delta l}}^{H} \tag{5.21}$$

$\tilde{\mathbf{x}}_{\mathbf{\Sigma l}}$, $\tilde{\mathbf{x}}_{\mathbf{\Delta l}}$ are Σ and Δ training cell data. Inverse of eq (5.17) is taken to estimate covariance matrix, which could be used to evaluate the signal power. This signal power, if greater than the pre-determined threshold (based on probability of detection and probability of false alarm) indicates the presence of target. In current research study, temporal DoF has not been applied and simulation is carried out to incorporate the same.

5.4.2 Clutter Generation

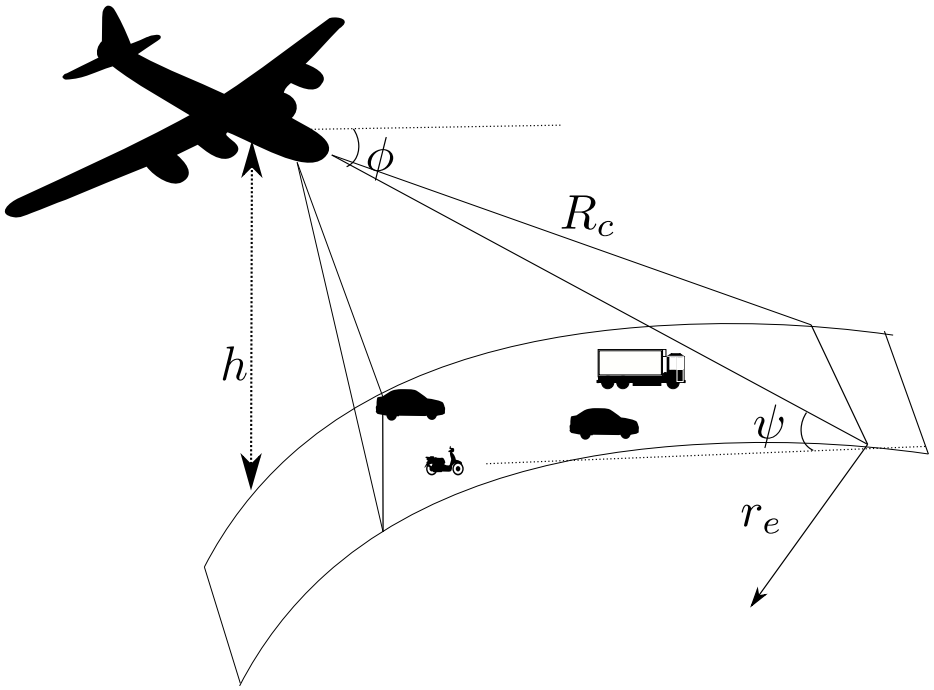

Figure 5.13: Clutter patch absorbed by an airborne radar

Earth's surface is the main source of clutter for an airborne. Clutter is generated based on the equations given below

$$\phi = -sin^{-1}\Big(\frac{R_c^2 + h(h+2r_e)}{2R_c(r_e+h)}\Big) \tag{5.22}$$

$$\Psi = -sin^{-1}\Big(\frac{R_c^2 - h(h+2r_e)}{2R_c r_e}\Big) \tag{5.23}$$

where ϕ, Ψ are the elevation and grazing angle to the clutter ring respectively, R_c is range to the clutter patch, h is the platform height, r_e is the earth's radius (refer to Figure. 5.13).

The clutter return for all the M pulses is computed by the equations below

$$C(R_c, n) = \sum_{i=1}^{N_f} \sum_{k=1}^{N_c} a(i,k) exp(j2\pi f_D(i,k) nT), for \;\; n = 0 : M-1 \tag{5.24}$$

$$\sigma(i,k) = \sigma_0(\phi_i, \theta_k) R_i \delta\theta \delta R sec(\Psi_i) \tag{5.25}$$

where $a(i,k)$ is the amplitude of clutter return from ith range and kth azimuth grid, f_D is the Doppler frequency, T is inverse of prf, $\sigma_0(\phi_i, \theta_k)$ is the normalized terrain reflectivity at ik^{th} clutter patch, δR is range resolution, R_i is range to iso-clutter ring.

The power received by the sum channel for ik^{th} clutter patch is given by

$$P_\Sigma(\phi_i, \theta_k) \;\; = \;\; \frac{P_t G_t(\phi_i, \theta_k) G_r(\phi_i, \theta_k) \lambda^2 \sigma(i,k) B\tau}{4\pi^3 R_i^4 L} \tag{5.26}$$

where P_t is power of transmitted pulse, $G_t(\phi_i, \theta_k)$, $G_r(\phi_i, \theta_k)$ are transmit and receive antenna gain in elevation and azimuth, λ wavelength, B bandwidth of radar. tau pulse width of transmitted pulse and L losses respectively. Upon substitution of $\sigma(i,k)$ in $P_\Sigma(\phi_i, \theta_k)$ got

$$P_\Sigma(\phi_i, \theta_k) \;\; = \;\; \frac{P_t G_t(\phi_i, \theta_k) G_r(\phi_i, \theta_k) \lambda^2 \sigma_0(\delta R)(\delta R\theta) sec(\psi_i) B\tau}{4\pi^3 R_i^3 L} \tag{5.27}$$

Similarly, equation for delta channel is

$$P_\Delta(\phi_i, \theta_k) \;\; = \;\; \frac{P_t G_t(\phi_i, \theta_k) G_r(\phi_i, \theta_k) \lambda^2 \sigma_0(\delta R)(\delta R\theta) sec(\psi_i) B\tau}{4\pi^3 R_i^3 L} \tag{5.28}$$

Below equation is the clutter power for guard channel for ikth clutter patch

$$P_g(\phi_i, \theta_k) \;\; = \;\; \frac{P_t G_t(\phi_i, \theta_k) G_g(\phi_i, \theta_k) \lambda^2 \sigma_0(\delta R)(\delta\theta) sec(\psi_i) B\tau}{4\pi^3 R_i^3 L} \tag{5.29}$$

5.5 Problem Formulation

Extraction of target information from a cluttered environment is a significant problem in radar and sonar applications. Consider a situation in which radar is located on an aircraft and observing targets on the earth's surface, as shown in Figure. 5.13. For simplicity, the flat-earth model is considered. More clutter returns are observed in this situation compared to the target observation using GMTI radar. Hence, a clutter mitigation algorithm in this airborne scenario is essential. The $\Sigma\Delta$ STAP is attaining

Parameters	Values
Carrier Frequency	10 GHz
Platform velocity	120 m/s
Platform Height	8 km
Pulse compression gain	1e6
prf	5 kHz
Duty cycle	0.1
Range	300 km
Antenna elements	16x12

popularity due to the low computational load compared to traditional, fully adaptive and reduced rank frameworks. In $\Sigma\Delta$ STAP, to estimate the noise covariance, one can use a lesser number of pulses information in the name of the DoF. In the literature, two frameworks are presented, namely two-channel and three-channel $\Sigma\Delta$ STAPs. The simulation results are investigated for 2-channel $\Sigma\Delta$ STAP considering moving targets of different radar cross sections (RCS). The table below lists the parameters considered for simulation.

5.6 Results and Discussions

5.6.1 Simulation scenario

Simulated an airborne scenario, in which an active radar is installed on an airplane and observed the ground target. The active radar (phased array with 184 elements in a rectangle fashion with rows 16 and columns 12) which was installed on the airborne platform emits the EM pulses with 10 GHz frequency and collects the returns, process them to extract the information about ground targets. The pulse repetition frequency of the radar is 5000 Hz and a duty cycle of 0.1. Due to very less returns, a pulse compression gain of 1e6 is given in the signal processing. The active radar is located on an air platform which is moving at a speed of 120 m/s at a height of 8000 m from the earths sea level. The curved earth model is considered in this simulation.

The elevation and azimuth swept are $[1^o - 70^o]$ and $[-90^o - 90^o]$ respectively. Both are having an incremental step of 0.1 rad. The sigma and delta beam patterns of a

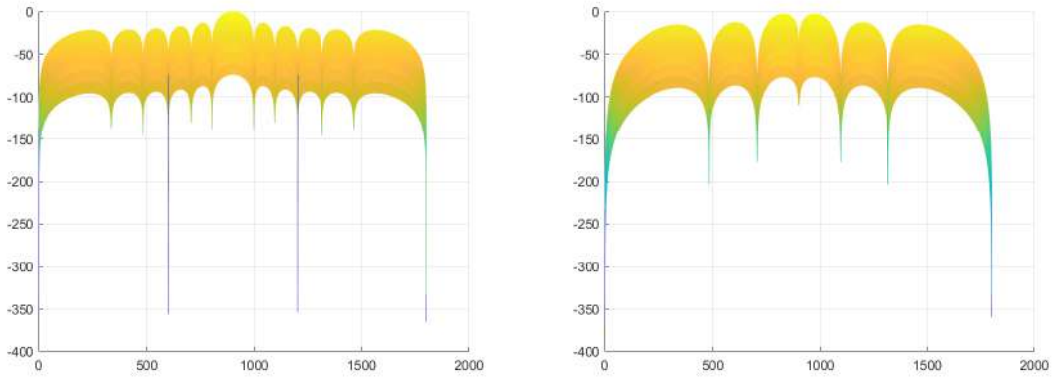

(a) Sigma beam pattern

(b) Delta beam pattern

Figure 5.14: Sum and Difference beam patterns(null without shifting the axis).

rectangular array is shown in the Figure. 4 and Figure. 5, where it can be observed that a peak in sigma pattern (ref Figure. 4) and a null in delta pattern (ref Figure. 5). The ground clutter associated with this sigma beam return and delta beam return are incorporated in the power calculation (Eqn. 19) and obtained the sigma and delta channel power returns. Using this sigma and delta channel data, the targets are detected.

Firstly, to investigate this, consider a target which is falling in the range bin of 150 with 0.1 normalized Doppler frequency. For this test bid, the sigma-delta stap is applied and the RD map acquired. The range bin view and Doppler view are presented in 5.15a and 5.15b. It can be observed that, even with a lesser Doppler, the algorithm is able to detect the target correctly in the given bin and given Doppler. From Figure. 5.15a, it is observed that a raise in peak value at a 140th bin which signifies the target presence. Similarly, in the Figure. 5.15b, the peak is obseved at the 0.1 normalized frequency.

Further, five targets are inserted from range bins 140 to 160 with a gap of 5 bins, each with normalized doppler frequency of 0.1 to 0.3 with a step of 0.5. For this test bid, the sigma-delta STAP is applied and the RD map aquired. The range bin view and Doppler view are presented in Figure. 5.16a and Figure. 5.16b. It is observed that, the algorithm is able to detect the target correctly in the given bin and given Doppler. From Figure. 5.16a, raise in peaks are noticed at 140th, 145th, 150th, 155th and 160th bins which signifies the target presence. Similarly, in Figure. 5.16b, the

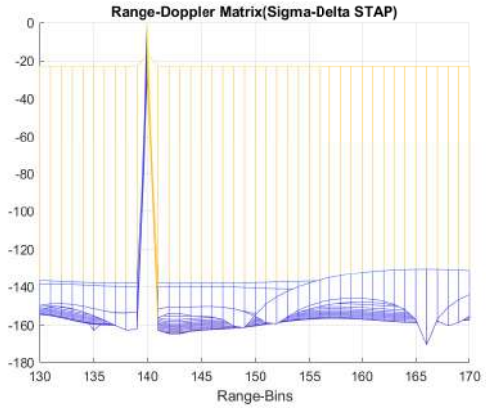

(a) Range of a single target

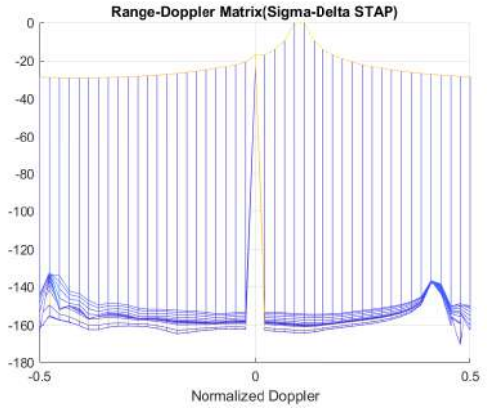

(b) Doppler of single target

Figure 5.15: Single target

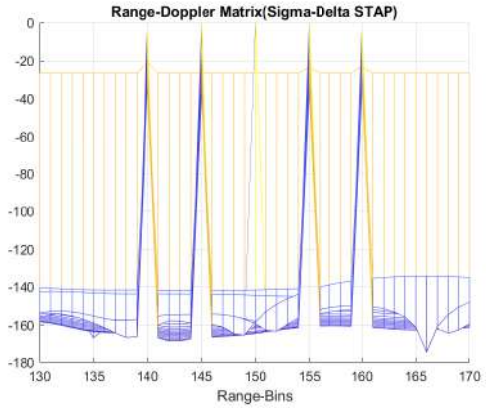

(a) Range of a multiple targets

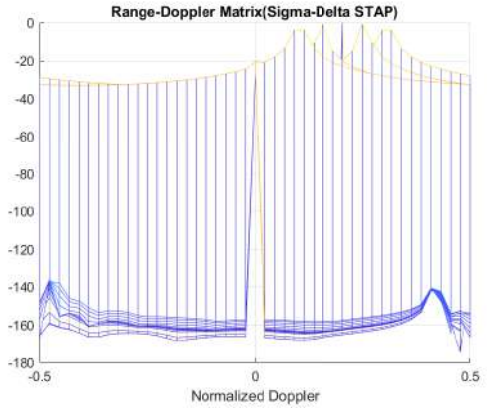

(b) Doppler of multiple targets

Figure 5.16: Five targets

peaks are observed at the 0.1, 0.15, 0.2, 0.25 and 0.3 normalized frequencies.

5.7 Conclusion

This chapter described two different algorithms to detect multiple targets immersed in interfering environment by mmWave radar. By proper selection of the filter window size, only desired targets are detected. Also, targets immersed in clutter environment are detected by Σ Δ-STAP filtering technique by an airborne radar.

Chapter 6

Conclusions and Future Directions

6.1 Conclusion

This thesis delt with detection and tracking frameworks for the experimental data extracted by TI's mmWave radar sensors. The results obtained in this research work demonstrated the usage of mmWave sensors in automotive industries. Further, it added significant domain knowledge in the application of FMCW radars with the following major contributions.

The primary focus of this research is in target detection and tracking modules. The performance of multiple target detection and tracking in the presence of spot-jammer has been experimentally evaluated using 77 GHz mmWave radar sensors. The DBSCAN and K-means clustering algorithms, along with GNN and EKF tracker, have been deployed to generate tracks for five different targets. Four different metrics, such as tracks reported, track segments, false tracks, and track loss, have been assessed to evaluate the performance. The experimental results revealed that DBSCAN algorithm has provided superior performance compared to K-means clustering method. The metrics of USRR with jammer case show that K-means outperforms DBSCAN, but K-means fails to identify the cluster, so the tracker fails to generate the full-length track, resulting in fewer track segments than without the jammer case. The DBSCAN clustering algorithm outperforms the K-means algorithm in both USRR and SRR modes of operations for both clean and jamming environments. CA-CFAR and OS-CFAR are better than GOCA-CFAR and SOCA-CFAR detection schemes.

Multiple moving targets are detected by YOLO V5 model. The model is trained by the RD maps of CA-CFAR detection method, obtained for the real-data captured

by 77 GHz mmWave radar sensor. The mean absolute error for range and velocity is evaluated by taking ground truth values obtained by the labeled images and the results obtained from YOLO model.

The proposed processing modules namely, weighted beat signal normalization and clipping with hampel filter are used to process the IF signal to minimize the effect of mutual interference among mmWave radar sensors. By these algorithms, the abrupt fluctuations of the IF signal are normalized by sliding window fashion. Implementation of these methods are easy since they does not disturb any existing receiver architecture processing modules. With an appropriate selection of window size, the true targets immersed in the interference are detected. Also, in the presence of clutter, multiple targets are detected by limited channel $\Sigma\Delta$ STAP filter.

6.2 Future Work

The mmWave radar sensors based real experiments has greater significance in designing autonomous vehicle as the radar is all weather candidate to trust with. One can carry out multiple research problems based on the current experimental evaluation carried out in this thesis. Some of the future directions are listed below

1. A true real on-road experiment may be carried out with radars mounted on the moving vehicle to collect the data in the presence of spot-jamming.

2. In the current investigation a single radar sensor is only considered, one may include multiple radar sensors to detect and track the multiple targets. This problem results in multiple sensor multiple target (MSMT) detection and tracking frameworks.

3. One can investigate novel fusion algorithms for MSMT scenario.

4. The current research work focuses only on one spot-jammer, to be more realistic future researchers may incorporate multiple spot-jammers at various directions to evaluate the detection and tracking performance of radar sensor.

5. The present thesis focused only on radar sensor in the presence of spot-jamming, the future research direction could be adding Lidar and camera to evaluate the comprehensive target detection and tracking performance.

6. The future researchers may look into alternative and efficient unsupervised clustering algorithms to carry out the spot-jamming based research investigation.

7. In this thesis, the DL method is YOLO V5, to carry out the future research one may look into alternative and efficient DL methods.

8. The mmWave frequency band used in this thesis is 77 GHz and one may use other frequency bands such as 60 GHz, 120 GHz to carry out the future research.

9. Further research may be carried out with multiple heterogeneous sensors mounted on a vehicle and taking the real data.

10. Largest RCS considered is only of the car. In future, various other large and small RCS targets may be considered to carry out the research work.

Bibliography

Raviraj S Adve, Todd B Hale, and Michael C Wicks. Practical joint domain localised adaptive processing in homogeneous and nonhomogeneous environments. part 1: Homogeneous environments. *IEE Proceedings-Radar, Sonar and Navigation*, 147 (2):57–65, 2000.

Mostafa Alizadeh, George Shaker, João Carlos Martins De Almeida, Plinio Pelegrini Morita, and Safeddin Safavi-Naeini. Remote monitoring of human vital signs using mmWave FMCW radar. *IEEE Access*, 7:54958–54968, 2019.

Alberto Asensio Lopez, Alvaro Duque de Quevedo, Franciso Salmeron Yuste, Jesus Munoz Dekamp, Víctor Aparicio Mequiades, Virgilio Medel Cortes, Daniel García Cobena, Diego Madueno Pulido, Fernando Ibanez Urzaiz, and Javier Gismero Menoyo. Coherent signal processing for traffic flow measuring radar sensor. *IEEE Sensors Journal*, 18(12):4803–4813, 2018. doi: 10.1109/JSEN.2017.2757699.

Constantine A Balanis. *Antenna theory: analysis and design*. John wiley & sons, 2015.

Yaakov Bar-Shalom, Fred Daum, and Jim Huang. The probabilistic data association filter. *IEEE Control Systems Magazine*, 29(6):82–100, 2009.

Jyoti Bhatia, Aveen Dayal, Ajit Jha, Santosh Kumar Vishvakarma, Soumya Joshi, M. B. Srinivas, Phaneendra K. Yalavarthy, Abhinav Kumar, V. Lalitha, Sagar Koorapati, and Linga Reddy Cenkeramaddi. Classification of targets using statistical features from range FFT of mmWave FMCW radars. *Electronics*, 10 (16), 2021. ISSN 2079-9292. doi: 10.3390/electronics10161965. URL `https://www.mdpi.com/2079-9292/10/16/1965`.

Svante Bjorklund, Tommy Johansson, and Henrik Petersson. Evaluation of a micro-Doppler classification method on mmWave data. In *2012 IEEE Radar Conference*, pages 0934–0939, 2012. doi: 10.1109/RADAR.2012.6212271.

Francois Bourgeois and Jean-Claude Lassalle. An extension of the munkres algorithm for the assignment problem to rectangular matrices. *Communications of the ACM*, 14(12):802–804, 1971.

Graham M. Brooker. Mutual interference of millimeter-wave radar systems. *IEEE Transactions on Electromagnetic Compatibility*, 49(1):170–181, 2007. doi: 10.1109/TEMC.2006.890223.

RD Brown, MC Wicks, Y Zhang, Q Zhang, and H Wang. A space-time adaptive processing approach for improved performance and affordability. In *Proceedings of the 1996 IEEE National Radar Conference*, pages 321–326. IEEE, 1996.

Russell D Brown, Richard A Schneible, Michael C Wicks, Hong Wang, and Yuhong Zhang. STAP for clutter suppression with sum and difference beams. *IEEE Transactions on Aerospace and Electronic Systems*, 36(2):634–646, 2000.

Linga Reddy Cenkeramaddi, Prabhat Kumar Rai, Aveen Dayal, Jyoti Bhatia, Aarav Pandya, J. Soumya, Abhinav Kumar, and Ajit Jha. A novel angle estimation for mmwave fmcw radars using machine learning. *IEEE Sensors Journal*, 21(8):9833–9843, 2021a. doi: 10.1109/JSEN.2021.3058268.

Linga Reddy Cenkeramaddi, Prabhat Kumar Rai, Aveen Dayal, Jyoti Bhatia, Aarav Pandya, J Soumya, Abhinav Kumar, and Ajit Jha. A novel angle estimation for mmWave FMCW radars using machine learning. *IEEE Sensors Journal*, 21(8): 9833–9843, 2021b.

S. Challa and G.W. Pulford. Joint target tracking and classification using radar and ESM sensors. *IEEE Transactions on Aerospace and Electronic Systems*, 37(3): 1039–1055, 2001. doi: 10.1109/7.953266.

Ricardo Omar Chavez-Garcia and Olivier Aycard. Multiple sensor fusion and classification for moving object detection and tracking. *IEEE Transactions on Intelligent Transportation Systems*, 17(2):525–534, 2016. doi: 10.1109/TITS.2015.2479925.

Chen Chen, Yuru Zhang, Mohammad R. Khosravi, Qingqi Pei, and Shaohua Wan. An intelligent platooning algorithm for sustainable transportation systems in smart cities. *IEEE Sensors Journal*, 21(14):15437–15447, 2021. doi: 10.1109/JSEN.2020.3019443.

Huanlei Chen, Meisong Tong, and Libo Huang. Target detection and tracking algorithm simulation for automotive millimeterwave radar based on systematic softeware-based radar system. In *2018 IEEE International Symposium on Antennas and Propagation & USNC/URSI National Radio Science Meeting*, pages 153–154. IEEE, 2018.

Long Chen, Qin Zou, Ziyu Pan, Danyu Lai, Liwei Zhu, Zhoufan Hou, Jun Wang, and Dongpu Cao. Surrounding vehicle detection using an FPGA panoramic camera and deep CNNs. *IEEE Transactions on Intelligent Transportation Systems*, 21(12): 5110–5122, 2019.

Yuhao Chen, Ying Wang, Feng Qu, and Wenhui Li. A graph-based track-before-detect algorithm for automotive radar target detection. *IEEE Sensors Journal*, 21 (5):6587–6599, 2020.

Abdelkader Dairi, Fouzi Harrou, Ying Sun, and Mohamed Senouci. Obstacle detection for intelligent transportation systems using deep stacked autoencoder and k -nearest neighbor scheme. *IEEE Sensors Journal*, 18(12):5122–5132, 2018. doi: 10.1109/JSEN.2018.2831082.

B N Dayananda, G S Vandana, Pathipati Srihari, and Bethi Pardhasaradhi. Real time vital sign monitoring system using AWR1642 radar module with remote access. In *2022 IEEE International Symposium on Smart Electronic Systems iSES*, pages 191–195. IEEE, 2022.

Rui Fu, Mohammed Abdulhakim Al-Absi, Ki-Hwan Kim, Young-Sil Lee, Ahmed Abdulhakim Al-Absi, and Hoon-Jae Lee. Deep learning-based drone classification using radar cross section signatures at mmWave frequencies. *IEEE Access*, 9:161431–161444, 2021. doi: 10.1109/ACCESS.2021.3115805.

Prashant P Gandhi and Saleem A Kassam. Analysis of CFAR processors in nonhomogeneous background. *IEEE Transactions on Aerospace and Electronic systems*, 24(4):427–445, 1988.

Xiangyu Gao, Guanbin Xing, Sumit Roy, and Hui Liu. Experiments with mmwave automotive radar test-bed. In *2019 53rd Asilomar Conference on Signals, Systems, and Computers*, pages 1–6. IEEE, 2019.

Khawaja Moyeezullah Ghori, Rabeeh Ayaz Abbasi, Muhammad Awais, Muhammad Imran, Ata Ullah, and Laszlo Szathmary. Performance analysis of different types of machine learning classifiers for non-technical loss detection. *IEEE Access*, 8: 16033–16048, 2020. doi: 10.1109/ACCESS.2019.2962510.

Aliakbar A Gorji, Ratnasingham Tharmarasa, and Thia Kirubarajan. Performance measures for multiple target tracking problems. In *14th International Conference on Information Fusion*, pages 1–8. IEEE, 2011.

Joseph R Guerci. *Space-time adaptive processing for radar*. Artech House, 2014.

Siddharth Gupta, Prabhat Kumar Rai, Abhinav Kumar, Phaneendra K. Yalavarthy, and Linga Reddy Cenkeramaddi. Target classification by mmWave FMCW radars using machine learning on range-angle images. *IEEE Sensors Journal*, 21(18): 19993–20001, 2021a. doi: 10.1109/JSEN.2021.3092583.

Siddharth Gupta, Prabhat Kumar Rai, Abhinav Kumar, Phaneendra K Yalavarthy, and Linga Reddy Cenkeramaddi. Target classification by mmWave FMCW radars using machine learning on range-angle images. *IEEE Sensors Journal*, 21(18): 19993–20001, 2021b.

Gor Hakobyan and Bin Yang. High-performance automotive radar: A review of signal processing algorithms and modulation schemes. *IEEE Signal Processing Magazine*, 36(5):32–44, 2019. doi: 10.1109/MSP.2019.2911722.

Dong-Seog Han. Detection performance of CFAR detectors based on order statistics for partially correlated chi-square targets. *IEEE Transactions on Aerospace and Electronic Systems*, 36(4):1423–1429, 2000.

V Gregers Hansen and James H Sawyers. Detectability loss due to" greatest of" selection in a cell-averaging CFAR. *IEEE Transactions on Aerospace and Electronic Systems*, (1):115–118, 1980.

Kaiming He, Xiangyu Zhang, Shaoqing Ren, and Jian Sun. Spatial pyramid pooling in deep convolutional networks for visual recognition. *IEEE Transactions on Pattern Analysis and Machine Intelligence*, 37(9):1904–1916, 2015. doi: 10.1109/TPAMI.2015.2389824.

https://www.ti.com/sensors/mmwave-radar/automotive/technical documents.html. Available online.

Xu Huang, Hasnain Cheena, Abin Thomas, and Joseph KP Tsoi. Indoor detection and tracking of people using mmWave sensor. *Journal of Sensors*, 2021, 2021.

Texas Instruments. AWR1642 evaluation module (awr1642boost) single-chip mmwave sensing solution, https://www.ti.com/product/awr1642, 2018a.

Texas Instruments. AWR1642 single-chip 77-and 79-GHz FMCW radar sensor: Datasheet, 2018b.

Peiyuan Jiang, Daji Ergu, Fangyao Liu, Ying Cai, and Bo Ma. A review of YOLO algorithm developments. *Procedia Computer Science*, 199:1066–1073, 2022. ISSN 1877-0509. doi: https://doi.org/10.1016/j.procs.2022.01.135. URL `https://www.sciencedirect.com/science/article/pii/S1877050922001363`.

Feng Jin and Siyang Cao. Automotive radar interference mitigation using adaptive noise canceller. *IEEE Transactions on Vehicular Technology*, 68(4):3747–3754, 2019.

Jaehoon Jung, Sohee Lim, Byung-Kwan Kim, and Seongwook Lee. CNN-based driver monitoring using millimeter-wave radar sensor. *IEEE Sensors Letters*, 5(3):1–4, 2021.

Tulasi Saisri Kavya, GS Vandana, Pathipati Srihari, Bethi Pardhasaradhi, et al. DoA estimation for micro and nano UAV targets using AWR2243 cascaded imaging

radar. In *2022 IEEE International Symposium on Smart Electronic Systems (iSES)*, pages 528–531. IEEE, 2022.

Jin-Cheol Kim, Hwi-Gu Jeong, and Seongwook Lee. Simultaneous target classification and moving direction estimation in millimeter-wave radar system. *Sensors*, 21(15), 2021. ISSN 1424-8220. doi: 10.3390/s21155228. URL `https://www.mdpi.com/1424-8220/21/15/5228`.

Jun-Hwa Kim, Namho Kim, Yong Woon Park, and Chee Sun Won. Object detection and classification based on YOLO-V5 with improved maritime dataset. *Journal of Marine Science and Engineering*, 10(3), 2022. ISSN 2077-1312. doi: 10.3390/jmse10030377. URL `https://www.mdpi.com/2077-1312/10/3/377`.

Richard Klemm and Michael Mertens. Tracking of convoys by airborne STAP radar. In *2008 11th International Conference on Information Fusion*, pages 1–8, 2008.

Atsutake Kosuge, Satoshi Suehiro, Mototsugu Hamada, and Tadahiro Kuroda. mmWave-YOLO: A mmwave imaging radar-based real-time multiclass object recognition system for ADAS applications. *IEEE Transactions on Instrumentation and Measurement*, 71:1–10, 2022. doi: 10.1109/TIM.2022.3176014.

D. K. Kumuda, G. S. Vandana, Bethi Pardhasaradhi, B. S. Raghavendra, Pathipati Srihari, and Linga Reddy Cenkeramaddi. Multitarget detection and tracking by mitigating spot jammer attack in 77-GHz mm-Wave radars: An experimental evaluation. *IEEE Sensors Journal*, 23(5):5345–5361, 2023. doi: 10.1109/JSEN.2022.3227012.

Fabian D Lapierre, Jacques G Verly, Braham Himed, Richard Klemm, and Marc Lesturgie. Radar space-time adaptive processing, 2006.

Neal B Lawrence. Performance comparison of cell averaging and 'greatest-of' constant false alarm rate (CFAR) methods. Technical report, ARMY MISSILE COMMAND REDSTONE ARSENAL AL ADVANCED SENSORS DIRECTORATE, 1981.

Ang Li, Baoyu Zheng, and Lei Li. Intelligent transportation application and analysis for multi-sensor information fusion of internet of things. *IEEE Sensors Journal*, 21 (22):25035–25042, 2021a. doi: 10.1109/JSEN.2020.3034911.

Xinrong Li, Xiaodong Wang, Qing Yang, and Song Fu. Signal processing for TDM MIMO FMCW millimeter-wave radar sensors. *IEEE Access*, 9:167959–167971, 2021b. doi: 10.1109/ACCESS.2021.3137387.

Yu-Chien Lin and Ta-Sung Lee. Max-MUSIC: a low-complexity high-resolution direction finding method for sparse MIMO radars. *IEEE Sensors Journal*, 20(24): 14914–14923, 2020.

Jau Lin Jr, Yuan-Ping Li, Wei-Chiang Hsu, and Ta-Sung Lee. Design of an FMCW radar baseband signal processing system for automotive application. *SpringerPlus*, 5(1):1–16, 2016.

Shu Liu, Lu Qi, Haifang Qin, Jianping Shi, and Jiaya Jia. Path aggregation network for instance segmentation. In *Proceedings of the IEEE Conference on Computer Vision and Pattern Recognition (CVPR)*, June 2018.

Zhenyu Liu, Wei Lu, Jiayan Wu, Siyuan Yang, and Guangping Li. A PELT-KCN algorithm for FMCW radar interference suppression based on signal reconstruction. *IEEE Access*, 8:45108–45118, 2020.

Shun Luo, Juan Yu, Yunjiang Xi, and Xiao Liao. Aircraft target detection in remote sensing images based on improved YOLOv5. *IEEE Access*, 10:5184–5192, 2022. doi: 10.1109/ACCESS.2022.3140876.

Dongze Lv, Yanting Che, and Chaoju Li. Frequency spot jamming against FMICW. In *2019 5th International Conference on Control Science and Systems Engineering (ICCSSE)*, pages 68–72. IEEE, 2019.

Adrian Macaveiu and Andrei Câmpeanu. Automotive radar target tracking by kalman filtering. In *2013 11th International Conference on Telecommunications in Modern Satellite, Cable and Broadcasting Services (TELSIKS)*, volume 2, pages 553–556. IEEE, 2013.

PM Moo. GMTI performance of/spl sigma//spl delta/-stap for a forward-looking radar. In *Proceedings of the 2001 IEEE Radar Conference (Cat. No. 01CH37200)*, pages 258–263. IEEE, 2001.

Peter Joseph Basil Morris and KVS Hari. Detection and localization of unmanned aircraft systems using millimeter-wave automotive radar sensors. *IEEE Sensors Letters*, 5(6):1–4, 2021.

Sharef Neemat, Oleg Krasnov, and Alexander Yarovoy. An interference mitigation technique for FMCW radar using beat-frequencies interpolation in the STFT domain. *IEEE Transactions on Microwave Theory and Techniques*, 67(3):1207–1220, 2019. doi: 10.1109/TMTT.2018.2881154.

Alexandros Ninos, Jürgen Hasch, and Thomas Zwick. Real-time macro gesture recognition using efficient empirical feature extraction with millimeter-wave technology. *IEEE Sensors Journal*, 21(13):15161–15170, 2021.

Alexandros Ninos, Jürgen Hasch, Michael Heizmann, and Thomas Zwick. Radar-based robust people tracking and consumer applications. *IEEE Sensors Journal*, 2022.

Ramon Nitzberg. Constant-false-alarm-rate signal processors for several types of interference. *IEEE Transactions on Aerospace and Electronic Systems*, (1):27–34, 1972.

Daniel Padilla Carrasco, Hatem A. Rashwan, Miguel Ángel García, and Domènec Puig. T-YOLO: Tiny vehicle detection based on YOLO and multi-scale convolutional neural networks. *IEEE Access*, 11:22430–22440, 2023. doi: 10.1109/ACCESS.2021.3137638.

Bethi Pardhasaradhi and Linga Reddy Cenkeramaddi. GPS spoofing detection and mitigation for drones using distributed radar tracking and fusion. *IEEE Sensors Journal*, 22(11):11122–11134, 2022.

Prabhat Kumar Rai, Henning Idsøe, Rajesh Reddy Yakkati, Abhinav Kumar, Mohammed Zafar Ali Khan, Phaneendra K Yalavarthy, and Linga Reddy Cenkeramaddi. Localization and activity classification of unmanned aerial vehicle using mmWave FMCW radars. *IEEE Sensors Journal*, 21(14):16043–16053, 2021.

Muhammad Rameez, Mats I. Pettersson, and Mattias Dahl. Interference compression and mitigation for automotive FMCW radar systems. *IEEE Sensors Journal*, 22 (20):19739–19749, 2022. doi: 10.1109/JSEN.2022.3204505.

Joseph Redmon, Santosh Divvala, Ross Girshick, and Ali Farhadi. You Only Look Once: Unified, real-time object detection. In *Proceedings of the IEEE Conference on Computer Vision and Pattern Recognition (CVPR)*, June 2016.

Mark A Richards. *Fundamentals of radar signal processing*. McGraw-Hill Education, 2014.

Nicolae-Cătălin Ristea, Andrei Anghel, and Radu Tudor Ionescu. Fully convolutional neural networks for automotive radar interference mitigation. In *2020 IEEE 92nd Vehicular Technology Conference (VTC2020-Fall)*, pages 1–5, 2020. doi: 10.1109/VTC2020-Fall49728.2020.9348690.

Ali Rizik, Emanuele Tavanti, Hussien Chible, Daniele D. Caviglia, and Andrea Randazzo. Cost-efficient FMCW radar for multi-target classification in security gate monitoring. *IEEE Sensors Journal*, 21(18):20447–20461, 2021. doi: 10.1109/JSEN.2021.3095674.

Johanna Rock, Mate Toth, Elmar Messner, Paul Meissner, and Franz Pernkopf. Complex signal denoising and interference mitigation for automotive radar using convolutional neural networks. In *2019 22th International Conference on Information Fusion (FUSION)*, pages 1–8. IEEE, 2019.

Hermann Rohling. Radar CFAR thresholding in clutter and multiple target situations. *IEEE transactions on aerospace and electronic systems*, (4):608–621, 1983.

Adham Sakhnini. A radar signal processing study.

Abhijit Sinha, Zhen Ding, Thia Kirubarajan, and Mohamad Farooq. Track quality based multitarget tracking approach for global nearest-neighbor association. *IEEE Transactions on Aerospace and Electronic Systems*, 48(2):1179–1191, 2012.

Yan Song, Zheng Hu, Tiancheng Li, and Hongqi Fan. Performance evaluation metrics and approaches for target tracking: A survey. *Sensors*, 22(3):793, 2022.

Gunnery Srinath, H Prashantha Kumar, Pathipati Srihari, Ratnasingham Tharmarasa, and Thiagalingam Kirubarajan. Coherent radar target detection with in-band cyclostationary wireless interference. *IEEE Access*, 10:11173–11190, 2022.

Emanuele Tavanti, Ali Rizik, Alessandro Fedeli, Daniele D. Caviglia, and Andrea Randazzo. A short-range FMCW radar-based approach for multi-target human-vehicle detection. *IEEE Transactions on Geoscience and Remote Sensing*, 60:1–16, 2022. doi: 10.1109/TGRS.2021.3138687.

TI. AWR1642 single-chip 77-and 79-GHz FMCW radar sensor: Datasheet, 2018. URL `https://www.ti.com/product/AWR1642`.

Liu Ting, Zhou Baijun, Zhao Yongsheng, and Yan Shun. Ship detection algorithm based on improved YOLO V5. In *2021 6th International Conference on Automation, Control and Robotics Engineering (CACRE)*, pages 483–487, 2021. doi: 10.1109/CACRE52464.2021.9501331.

Girish Tiwari and Shalabh Gupta. An mmWave radar based real-time contactless fitness tracker using deep CNNs. *IEEE Sensors Journal*, 21(15):17262–17270, 2021.

Sriharsha Nag TS, GS Vandana, Pathipati Srihari, and Bethi Pardhasaradhi. SAR imaging with automotive radar: Range migration algorithm, experiment, and future directions in automotive vehicle. In *2022 IEEE 7th International Conference on Recent Advances and Innovations in Engineering*, pages 1–6. IEEE, 2022.

Faruk Uysal and Sasanka Sanka. Mitigation of automotive radar interference. pages 0405–0410, 04 2018. doi: 10.1109/RADAR.2018.8378593.

G S Vandana, Bethi Pardhasaradhi, and Pathipati Srihari. Intruder detection and tracking using 77GHz FMCW radar and camera data. In *2022 IEEE International Conference on Electronics, Computing and Communication Technologies (CONECCT)*, pages 1–6. IEEE, 2022.

Christian Waldschmidt, Juergen Hasch, and Wolfgang Menzel. Automotive radar from first efforts to future systems. *IEEE Journal of Microwaves*, 1(1):135–148, 2021.

Renjie Wan, Yaoliang Song, Tong Mu, and Zhonghan Wang. Moving target detection using the 2D-FFT algorithm for automotive FMCW radars. In *2019 International Conference on Communications, Information System and Computer Engineering (CISCE)*, pages 239–243. IEEE, 2019.

Hechuang Wang. Multi-sensor fusion module for perceptual target recognition for intelligent machine learning visual feature extraction. *IEEE Sensors Journal*, 21 (22):24993–25000, 2021. doi: 10.1109/JSEN.2021.3061207.

Jianping Wang. CFAR-based interference mitigation for FMCW automotive radar systems. *IEEE Transactions on Intelligent Transportation Systems*, 23(8):12229–12238, 2022. doi: 10.1109/TITS.2021.3111514.

Yi Wang, Qixun Zhang, Zhiqing Wei, Yuewei Lin, and Zhiyong Feng. Performance analysis of coordinated interference mitigation approach for automotive radar. *IEEE Internet of Things Journal*, 10(13):11683–11695, 2023. doi: 10.1109/JIOT.2023.3244566.

J. Ward. Space-time adaptive processing for airborne radar. *IET Conference Proceedings*, pages 2–2(1), January 1998. URL `https://digital-library.theiet.org/content/conferences/10.1049/ic_19980240`.

M Weiss. Analysis of some modified cell-averaging CFAR processors in multiple-target situations. *IEEE Transactions on Aerospace and Electronic Systems*, (1):102–114, 1982.

Tee Yi Wen and Siti Armiza Mohd Aris. Hybrid approach of EEG stress level classification using K-means clustering and support vector machine. *IEEE Access*, 10: 18370–18379, 2022.

L MELVIN William et al. A STAP overview. *IEEE A&E System Magazine*, 19(1): 19–35, 2004.

A. N. Wilson, Abhinav Kumar, Ajit Jha, and Linga Reddy Cenkeramaddi. Multitarget angle of arrival estimation using rotating mmWave FMCW radar and Yolov3. *IEEE Sensors Journal*, 23(3):3173–3182, 2023. doi: 10.1109/JSEN.2022.3231790.

Renjie Xu, Haifeng Lin, Kangjie Lu, Lin Cao, and Yunfei Liu. A forest fire detection system based on ensemble learning. *Forests*, 12(2), 2021. ISSN 1999-4907. doi: 10.3390/f12020217. URL `https://www.mdpi.com/1999-4907/12/2/217`.

Zhihuo Xu and Min Yuan. An interference mitigation technique for automotive millimeter wave radars in the tunable Q-factor wavelet transform domain. *IEEE Transactions on Microwave Theory and Techniques*, 69(12):5270–5283, 2021. doi: 10.1109/TMTT.2021.3121322.

Xirui Xue, Shucai Huang, Jiahao Xie, Jiashun Ma, and Ning Li. Resolvable cluster target tracking based on the DBSCAN clustering algorithm and labeled RFS. *IEEE Access*, 9:43364–43377, 2021.

Mohammad Reza Zakerhaghighi, Mohsen Mivehchy, and Mohammad Farzan Sabahi. Implementation and assessment of jamming effectiveness against an FMCW tracking radar based on a novel criterion. *IEEE Transactions on Aerospace and Electronic Systems*, 56(6):4723–4733, 2020.

Mengyuan Zhang, Shibo He, Chaoqun Yang, Jiming Chen, and Junshan Zhang. Vanet-assisted interference mitigation for millimeter-wave automotive radar sensors. *IEEE Network*, 34(2):238–245, 2020. doi: 10.1109/MNET.001.1900271.

Renyuan Zhang and Siyang Cao. Real-time human motion behavior detection via CNN using mmWave radar. *IEEE Sensors Letters*, 3(2):1–4, 2018.

Yuhong Zhang and Hong Wang. Further results of/spl sigma//spl delta/-stap approach to airborne surveillance radars. In *Proceedings of the 1997 IEEE National Radar Conference*, pages 337–342. IEEE, 1997.

Zihao Zhao, Yuying Song, Fucheng Cui, Jiang Zhu, Chunyi Song, Zhiwei Xu, and Kai Ding. Point cloud features-based kernel SVM for human vehicle classification in millimeter wave radar. *IEEE Access*, 8:26012–26021, 2020.

List of Publications

1. Kumuda D K, Vandana G S, Pardhasaradhi Bethi, B S Raghavendra, Pathipati Srihari, and Linga Reddy Cenkeramaddi, "Multi Target Detection and Tracking by Mitigating Spot Jammer Attack in 77GHz mm-Wave Radars: An Experimental Evaluation," IEEE Sensors Journal, year: 2023, volume: 23, number: 5, pages: 5345-5361, doi: 10.1109/JSEN.2022.3227012

2. Kumuda. D. K, A. K Shetty, P. Srihari, D. Sheshagiri, V. Mahajan and P. Joseph, "Multiple Target Detection using $\Sigma\Delta$-STAP in the Presence of Airborne Clutter," 2021 IEEE International Conference on Electronics, Computing and Communication Technologies (CONECCT), 2021, pp. 1-6, doi: 10.1109/CONECCT52877.2021.9622629.

3. D. K. Kumuda, P. Srihari, D. Sheshagiri, M. K. Raju and B. Pardhasaradhi, "A Mutual Interference Mitigation Algorithm for Dense On-Road Automotive Radars Scenario," 2023 IEEE International Conference on Electronics, Computing and Communication Technologies (CONECCT), Bangalore, India, 2023, pp. 1-6, doi: 10.1109/CONECCT57959.2023.10234787.

4. D. K. Kumuda, P. Srihari, D. Sheshagiri, P. R. Kumar and B. Pardhasaradhi, "Clipping and Hampel Filtering Algorithm to Mitigate Mutual Interference for Automotive Radars," 2023 IEEE International Conference on Electronics, Computing and Communication Technologies (CONECCT), Bangalore, India, 2023, pp. 1-5, doi: 10.1109/CONECCT57959.2023.10234809.

5. Kumuda. D. K, Wilson A N, Bethi Pardhasaradhi, Pathipati Srihari and Linga Reddy Cenkeramaddi "Deep Learning based (YOLO) Target Detection using Range-Doppler maps obtained from CFAR techniques" (To be communicated to IEEE journal)

CURRICULUM VITAE

Name	Kumuda D.K
Address	House no: 904, 11th cross, Gangothrinagar, Tumkur-572103 Karnataka, India
E-mail	kumudamurthy@gmail.com

Qualification	• M.Tech | Digital Communication Engineering | MSRIT, Bangalore, Karnataka • B.E | Electronics and Communication Engineering | SIET, Tumkur, Karnataka
Experience	• Assistant Professor | Siddaganga Institute of Technology, Tumkur